NUMERICAL SIMULATIONS OF ELASTIC RODS

by

Jeremy A. Warner

Thesis submitted to the Faculty of the Graduate School
of The University of Maryland in partial fulfillment
of the requirements for the degree of
Master of Arts
1997

Advisory Committee:

Professor John Maddocks, Chairman/Advisor
Professor R. Bruce Kellogg
Associate Professor Andrew Baden

NUMERICAL SIMULATIONS OF ELASTIC RODS

by

Jeremy A. Warner

Thesis submitted to the Faculty of the Graduate School
of The University of Maryland in partial fulfillment
of the requirements for the degree of
Master of Arts
1997

Advisory Committee:

Professor John Maddocks, Chairman/Advisor
Professor R. Bruce Kellogg
Associate Professor Andrew Baden

NUMERICAL SIMULATIONS OF ELASTIC RODS

by

Jeremy A. Warner

Thesis submitted to the Faculty of the Graduate School
of The University of Maryland in partial fulfillment
of the requirements for the degree of
Master of Arts
1997

Advisory Committee:

Professor John Maddocks, Chairman/Advisor
Professor R. Bruce Kellogg
Associate Professor Andrew Baden

Abstract

Title of Thesis: NUMERICAL SIMULATIONS OF ELASTIC RODS

Name of degree candidate: Jeremy A. Warner

Degree and year: Master of Arts, 1997

Thesis directed by: Professor John Maddocks
Department of Mathematics and

Motivated by a phenomenon called ratcheting that is observed in experiments, a numerical study was made of elastic rods with various physical properties (i.e., various bending stiffnesses and unstressed curvatures) when they were bent into certain deformed semi-circular configurations and then twisted at one end. The rods were modeled by a two-point boundary value problem for a 15^{th} order system of ODEs. Numerical continuation and branch switching methods were used in all computations, using the package AUTO. Qualitatively interesting behaviors were observed both in deforming the rods into the various configurations as well as when twisting the ends. A study was also made of ways to reformulate the rod equilibrium equations in an effort to make the numerical calculations more efficient. Effective speed-ups of a factor of 2.5 were achieved.

Dedication

To Stephanie, for all her patience and support in making this work a reality.

Acknowledgements

I would like to thank Dr. Maddocks for allowing me to work with and learn from him. It was a most enlightening experience. In addition I would like to thank Randy Paffenroth, Kathleen Rogers, Dr. Rob Manning, Dr. Tom Stone, and the rest of the members of the LCVM for their help with various technical problems, and also Dr. Brian Hunt for his assistance as an interlocutor with the Alpha Farm computer system managers. Dr. Brian Berg was also of great assistance in understanding the problem to be modelled. I would also like to thank the Keck Foundation, whose grant of computers was of invaluable assistance, as well as the AFOSR for their financial support and provision of computer equipment.

Table of Contents

List of Tables

List of Figures

Chapter 1

Introduction

In certain surgical procedures (e.g., angioplasty), thin elastic wires are inserted into the patient's veins or arteries for use as either guide wires or as carriers of surgical instruments. Consequently, these wires have to be very flexible in order to navigate the convoluted arterial pathways, and in many circumstances the wires have to be twisted when their ends reach the desired locations. When the surgeon twists the external end of the wire, they (and the patient) want the twisting action to be as smooth as possible, without sudden changes in the rotational response. However, with the wire contorted into a perhaps highly curved configuration, it is observed that the wire has a tendency to ratchet - that is, to undergo abrupt changes in the torque required to twist the wire.

In this thesis we attempt to model these surgical wires numerically. Specifically we aim to recreate experimental data observed by Dr. Brian Berg. These experiments involve holding the ends of the wires in a fixed location and orientation, and then measuring the torque required to twist the wire at one end. The ratcheting phenomenon is clearly observable in these experiments. In this thesis computations are used to show that, at least at a qualitative level, ratcheting can be accounted for by the presence of quite small unstressed curvatures. Such small unstressed curvatures are almost inevitable due to the wire manufacturing process and the sets (or plastic deformation) undergone during storage of wire in coils. The ultimate goal of this effort is to develop the model to the point where numerical experiments can be performed which will lead to better methods of manufacturing and storing the wires, in the hope of minimizing ratcheting.

Mathematical models of wires fall in the domain of rod theory. Accordingly, we consider a two-point boundary value problem (BVP) which models an elastic rod whose orientation is described by a set of directors $\mathbf{d}_i$ (see Fig 1.1). Boundary conditions (BCs) are imposed at the ends of the rod which enforce the relative position of the ends and also the orientation of the rod at the endpoints. The rod is described by a 15^{th} order system of ODEs which is written in the coordinate system defined by the $\mathbf{d}_i$. When written in this way, the only physical properties of the rod that enter into the equations are the unstressed curvature and the bending stiffnesses, which properties appear as parameters in the system of equations.

We solved this system of ODEs numerically for various values of the physical parameters mentioned above (provided by Dr. Berg), corresponding to different types of wires with various unstressed curvatures, and for ranges of the loading parameter. In the process of solving the problem, we discovered interesting behavior when the distance between the endpoints of the rod was changed, so we also explored this phenomenon. When twisting the end of the rod, we were specifically looking for a fold in the torque vs. angle relationship. Such folds correspond to ratcheting of a real wire. We found such folds, and the twist angle vs. torque diagrams we computed look strikingly similar to those measured in Dr. Berg's experiments. We also compared the behavior of rods with a helical unstressed shape of given curvature and varying pitch. Dr. Berg's suggestion was that for given curvature unstressed shapes with shorter pitch (greater torsion) would display less severe ratcheting. This conjecture was borne out by the computations.

The basic tools for accomplishing the numerical modeling were already in existence. The mathematical model is based upon the special Cosserat rod theory, with numerics based on a formulation exploiting Euler parameters that is described in [13]. The resulting problem is a 2-point BVP which is solved using collocation and continuation as implemented in the software package AUTO that is discussed in [6] and [7]. Visualization of the numerical results was also essential, and the software used in performing this task was developed by G. Domokos and R. Paffenroth, as is described fully in [9].

In Chapter 2 we review the derivation of the rod model, as well as the numerical methods used in solving the model. This material is not original, and we follow the presentation of [13].

In Chapter 3 we discuss numerical solutions found for the particular BVPs of interest here. We first discuss results from a secondary problem, namely the bending of the rod into the configuration from which it will be twisted. This process was also carried out using the continuation methods implemented in AUTO, and it yielded interesting results. We then discuss the results from twisting one end of the rod. For both the bending and twisting problems we consider both a perfectly straight rod and a simply curved rod whose unstressed shape is a circular arc. We also consider twisting a helically curved rod, which had the effect of reducing the ratcheting phenomenon as compared to a planar rod of the same curvature. These results are presented largely in graphical form, with discussions identifying trends in the behavior of the rod corresponding to variations in its physical properties (i.e., unstressed curvature, initial configuration, and ratio of bending stiffnesses). We conclude the chapter with a numerical demonstration of why a particular assumption previously used in interpreting experimental data is false.

In Chapter 4 we describe the dependence of our results on the choice of numerical discretization, and also discuss modifications to the mathematical formulation which produce identical final results, but which have the effect of minimizing CPU usage. These modifications include reduction of order of the governing system of equations by replacing equations with AUTO parameters, introducing integral constraints in place of BCs, and using an analytic instead of a numeric Jacobian. By making these modifications, effective reductions in CPU usage of a factor of 2.5 are found.

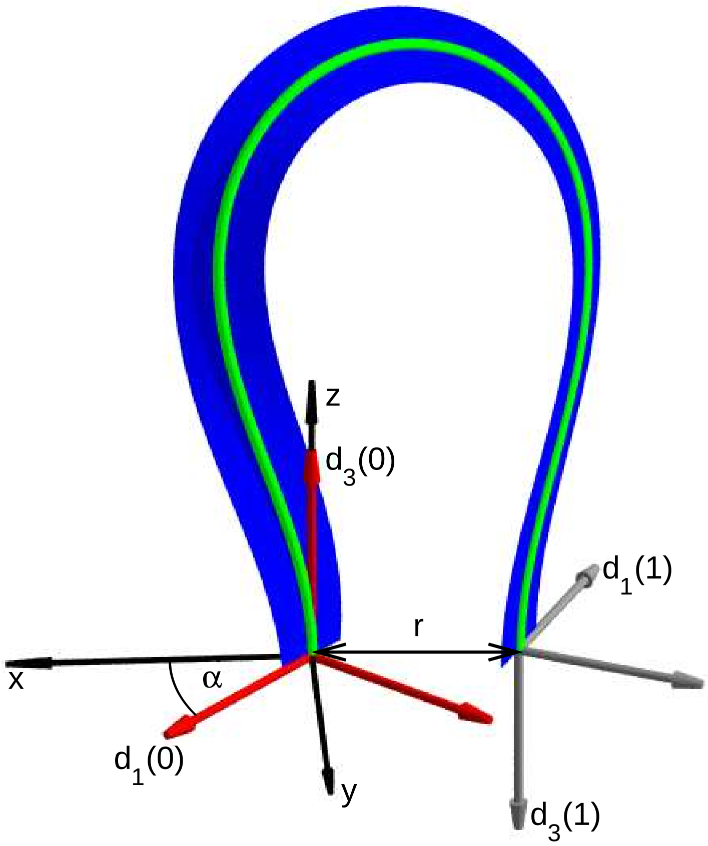

Figure 1.1: A Representative Ribbon Describing the Configuration of an Elastica The tube in the center of the ribbon represents the centerline of the rod and is parameterized by its arc-length σ. The attached ribbon illustrates twisting of the rod. The orthonormal triad of directors $\mathbf{d}_1$, $\mathbf{d}_2$ and $\mathbf{d}_3$ can be regarded as indicating the orientation of a cross-section of the rod, with $\mathbf{d}_3$ tangent to the centerline, and $\mathbf{d}_1$ tangent to the ribbon.

Finally, in Chapter 5 we reprise the results discussed in Chapters 3 & 4.

Chapter 2

Rod Model and Numerical Procedures

In this chapter we discuss the rod model that will be adopted, followed by a brief discussion of the AUTO program, which was used for numerical computations. The material on the derivation of the Hamiltonian system is taken from [13]. The discussion of the numerics is taken from [7] & [8]. Those readers interested in more information on these topics (especially collocation) should consult these references.

In Section 2.1 we give an overview of the director theory of rods. Included in this is a discussion of coordinate free equilibrium equations and constitutive relations. In Section 2.2 we discuss the equations governing the behavior of the rod. Included in this section is a discussion of a representation of the directors in terms of Euler parameters, of a variational formulation of the system, and of the integrals and symmetries inherent in the Hamiltonian system of equations. In Section 2.3 we briefly discuss the numerical simulation techniques used in the later analysis.

2.1 The Director Theory of Rods

In this section we summarize the theory of special Cosserat rods in exactly the form that will subsequently be used in our computations. Within the continuum mechanics literature, the model is considered to be a standard description of an inextensible, unshearable rod or *elastica* (cf. e.g. [1]).

2.1.1 Directors

The configuration of an elastica is described by the specification of two smooth vector functions

$$\mathbf{r}(\sigma), \;\; \mathbf{d}_1(\sigma): \quad [0,1] \to \mathbb{R}^3.$$

Here $\mathbf{r}(\sigma)$ describes the *centerline* (or *line of centroids* or *axis*) of the rod, and $\mathbf{d}_1(\sigma)$ is chosen to be a material unit vector lying in the normal cross–section at σ. The rod is assumed to be inextensible so the variable σ can, with suitable normalization, be interpreted as arc–length along the axis in any configuration.

Given $\mathbf{d}_1(\sigma)$, the orientation of the material cross–section at σ in any configuration is also specified because, by the assumption of unshearability, material normal cross-sections remain undeformed and normal to the deformed axis.

The condition of inextensibility implies that $\mathbf{r}'(\sigma)$ is a unit vector, denoted $\mathbf{d}_3(\sigma)$. (Here and throughout $'$ denotes a derivative with respect to arclength σ.) A right–handed orthonormal basis $\{\mathbf{d}_1, \mathbf{d}_2, \mathbf{d}_3\}$, called the *directors*, may then be defined, in which $\mathbf{d}_2 = \mathbf{d}_3 \times \mathbf{d}_1$. The σ-dependent orthonormal basis $\{\mathbf{d}_i(\sigma)\}$ will later be related, *via* Euler parameters, to the fixed orthonormal basis $\{\mathbf{X},\, \mathbf{Y},\, \mathbf{Z}\}$. The configuration of the rod is fully determined if the functions $\mathbf{d}_i(\sigma)$, $i = 1,\, 2,\, 3$, are specified, and *vice versa*. The function $\mathbf{r}(\sigma)$ can always be recovered from the differential equation

$$\mathbf{r}'(\sigma) = \mathbf{d}_3(\sigma), \qquad \mathbf{r}(0) = \mathbf{r}_0. \tag{2.1}$$

As σ varies the basis $\{\mathbf{d}_i(\sigma)\}$ changes smoothly relative to the fixed basis and as the directors are orthonormal the change can be expressed as

$$\mathbf{d}_i' = \mathbf{u} \times \mathbf{d}_i, \qquad i = \ 1,\, 2,\, 3, \tag{2.2}$$

where the vector $\mathbf{u}$ is often called the *Darboux* vector. The components $u_i \equiv \mathbf{u}\cdot\mathbf{d}_i$ of the vector $\mathbf{u}$ with respect to the directors $\{\mathbf{d}_i\}$ are the components of strain associated with bending and twist. The triple of coordinates is denoted

$$\mathsf{u}(\sigma) = (u_1(\sigma),\, u_2(\sigma),\, u_3(\sigma)). \tag{2.3}$$

Knowledge of $u_1(\sigma)$ and $u_2(\sigma)$ is equivalent to knowledge of the curvature and geometrical torsion of the axis regarded as a space–curve. The strain $u_3(\sigma)$ measures physical twist; it is not the geometrical torsion which is a property of the centerline only. The quantity $u_3(\sigma)$, which will here always be referred to as *twist rate*, is the same as the quantity that is often referred to as *torsion* in the engineering literature.

2.1.2 Coordinate-Free Equilibrium Equations

It happens that convenient dependent variables for our analysis will be the Euler parameters alluded to earlier. However it is illuminating first to consider coordinate–free equilibrium equations, constitutive relations and boundary conditions.

The stresses acting across each material normal cross–section are equivalent to a force and a moment applied at the centroid of the cross–section at $\mathbf{r}(\sigma)$; let $\mathbf{n}(\sigma)$ and $\mathbf{m}(\sigma)$ denote, respectively, this resultant force and moment (of the material on the side σ^+ acting on the material on the side σ^-). We will here assume that the only external loads are couples and forces applied at the ends of the rod. The equilibrium equations are

$$\mathbf{n}'(\sigma) = \mathbf{0}\,, \tag{2.4}$$

and

$$\mathbf{m}'(\sigma) + \mathbf{r}'(\sigma) \times \mathbf{n}(\sigma) = \mathbf{0}. \tag{2.5}$$

Equation (2.4) has the integral

$$\mathbf{n}(\sigma) = \mathbf{n}(0)\,, \tag{2.6}$$

so that equation (2.5) has the integral

$$\mathbf{m}\,(\sigma) \,+\, \mathbf{r}\,(\sigma) \times \mathbf{n}\,(\sigma) = \boldsymbol{\xi}\,. \tag{2.7}$$

Here $\boldsymbol{\xi}$ is a constant vector which, by choice of origin for $\mathbf{r}$, can be chosen to be parallel to $\mathbf{n}$. From (2.6) and (2.7) we have that

$$\mathbf{m}(\sigma) \cdot \mathbf{n}(\sigma) = \mathbf{m}(0) \cdot \mathbf{n}(0)\,. \tag{2.8}$$

When evaluated at $\sigma = 1$, equations (2.6) and (2.8) provide relations between the boundary conditions at $\sigma = 0$ and those at $\sigma = 1$ that are implied by the balance of external forces and moments acting on the elastica.

2.1.3 Constitutive Relations

In order to proceed further it is necessary to introduce constitutive relations between the strains and the resultant forces and moments appearing in the rod model. In point of fact, because we assume the rod to be inextensible and unshearable, the components of the resultant force $\mathbf{n}$ are basic unknowns. In contrast, the components of the bending and twist moment $\mathbf{m}$ are related to the bending and twist strains u_i, introduced in (2.3). In order to specify this constitutive relation some further notation is required. The triple of components $m_i(\sigma) \equiv \mathbf{m}(\sigma) \cdot \mathbf{d}_i(\sigma)$ will be denoted $\mathsf{m} = (m_1,\, m_2,\, m_3)$. We also allow the unstressed configuration of the rod to have intrinsic curvature and twist. The strains at this unstressed state will be denoted $\hat{\mathsf{u}}(\sigma) = (\hat{u}_1(\sigma),\, \hat{u}_2(\sigma),\, \hat{u}_3(\sigma)\,)$ with the $\hat{u}_i(\sigma)$ being prescribed functions. The unstressed configuration is straight when $\hat{u}_1(\sigma) \equiv \hat{u}_2(\sigma) \equiv 0$. If in addition $\hat{u}_3(\sigma) \equiv 0$, the unstressed state is prismatic or untwisted.

We shall only consider the case in which the rod is hyper-elastic, i.e. there exists a scalar–valued strain energy density function $W(\mathsf{u} - \hat{\mathsf{u}}, \sigma)$, dependent upon the three strain measures $u_i - \hat{u}_i$, and arc–length σ, with the property that

$$m_i = \frac{\partial W}{\partial u_i}, \qquad i = 1,\, 2,\, 3\,. \tag{2.9}$$

Following common practice, we shall assume that the function W is a strictly convex function of the three arguments $(u_i - \hat{u}_i)$, with a minimum at $W(0,\, 0,\, 0,\, \sigma)$.

For computation, a specific form of W must be chosen and we will focus here upon the case where the rod is assumed to be linearly elastic, that is, the strain energy density function is quadratic in the u_i. Explicitly

$$W(\mathsf{u} - \hat{\mathsf{u}},\, s) = \frac{1}{2}\, K_1 (u_1 - \hat{u}_1)^2 + \frac{1}{2}\, K_2 (u_2 - \hat{u}_2)^2 + \frac{1}{2}\, K_3 (u_3 - \hat{u}_3)^2, \tag{2.10}$$

with

$$m_i = \frac{\partial W}{\partial u_i} = K_i(u_i - \hat{u}_i)\,, \qquad i = 1,\, 2,\, 3\,. \tag{2.11}$$

Here the bending and twist stiffnesses $K_i(\sigma)$ are prescribed positive functions of σ, possibly constant.

Models of rod mechanics often begin with the assumption that the rod is a solid object whose diameter is small compared to its length. This is the approach taken in the theory of Kirchhoff and Clebsch, as described in [14], for example. If we adopt this point of view, and also assume that the material composing the rod is homogeneous and isotropic, then we can further interpret the elastic coefficients as $K_1 = EI_1$, $K_2 = EI_2$ and $K_3 = GI_3$, where I_i is the geometric moment of the planar cross–section about the $\mathbf{d}_i$ axis (so that $I_3 = I_1 + I_2$), E is the Young's modulus, $G = E/[2(1+\nu)]$ is the shear modulus, and ν is Poisson's ratio.

2.2 The Governing Equations

In this section we develop the Hamiltonian system of ordinary differential equations that will provide the basis for our computations. We first describe the Euler parameter description of the directors $\mathbf{d}_i$. We then introduce a variational form of the equilibrium conditions, and the associated Lagrangian and Hamiltonian forms of the governing equations. Finally we describe the symmetries and associated integrals of the governing Hamiltonian system.

2.2.1 Representation of Directors by Euler Parameters

Thus far we have not specified any particular parameterization of the directors $\{\mathbf{d}_i(\sigma)\}$. For three-dimensional equilibria, a parameterization of the directors $\{\mathbf{d}_i(\sigma)\}$ is equivalent to selecting a representation for the group of proper orthogonal transformations $SO(3)$. In mechanics there are several common choices for such a representation (cf. e.g. [11]). Euler parameters will be used here, which provides a global (i.e. singularity free), four parameter, two–to–one description of $SO(3)$. An elementary discussion of Euler parameters can be found, for example, in [11].

The components of the orthonormal triad $\{\mathbf{d}_i\}$ (with respect to the fixed space basis) in terms of a set of Euler parameters $\mathbf{q}$ are given by:

$$\mathbf{d}_1 = \begin{pmatrix} q_1^2 - q_2^2 - q_3^2 + q_4^2 \\ 2(q_1q_2 + q_3q_4) \\ 2(q_1q_3 - q_2q_4) \end{pmatrix}, \quad \mathbf{d}_2 = \begin{pmatrix} 2(q_1q_2 - q_3q_4) \\ -q_1^2 + q_2^2 - q_3^2 + q_4^2 \\ 2(q_2q_3 + q_1q_4) \end{pmatrix}, \tag{2.12}$$

$$\mathbf{d}_3 = \begin{pmatrix} 2(q_1q_3 + q_2q_4) \\ 2(q_2q_3 - q_1q_4) \\ -q_1^2 - q_2^2 + q_3^2 + q_4^2 \end{pmatrix}. \tag{2.13}$$

The strains u_i appearing in equations (2.2) are given in terms of the Euler parameters by (see, for example, Dichmann [5] or Kane [12])

$$u_i = \frac{2\mathbf{q}' \cdot \mathbf{B}_i\mathbf{q}}{|\mathbf{q}|^2}, \qquad i = 1,\ 2,\ 3. \tag{2.14}$$

Here the $\mathbf{B}_i$ are 4×4 skew–symmetric matrices:

$$\mathbf{B}_1 = \begin{pmatrix} 0 & 0 & 0 & 1 \\ 0 & 0 & 1 & 0 \\ 0 & -1 & 0 & 0 \\ -1 & 0 & 0 & 0 \end{pmatrix}, \quad \mathbf{B}_2 = \begin{pmatrix} 0 & 0 & -1 & 0 \\ 0 & 0 & 0 & 1 \\ 1 & 0 & 0 & 0 \\ 0 & -1 & 0 & 0 \end{pmatrix}$$

$$\mathbf{B}_3 = \begin{pmatrix} 0 & 1 & 0 & 0 \\ -1 & 0 & 0 & 0 \\ 0 & 0 & 0 & 1 \\ 0 & 0 & -1 & 0 \end{pmatrix}$$

For any set of Euler parameters the vectors $\{\mathbf{B}_i\mathbf{q}\}$, together with $\mathbf{q}$, form an orthonormal basis for $\mathbb{R}^4$. Geometrically, the vector $\mathbf{B}_i\mathbf{q}$ acts as the infinitesimal generator of rotation about the ith director $\mathbf{d}_i$.

2.2.2 Variational Formulations

Using equation (2.14) to eliminate the strains, the strain energy density function can be written in terms of the Euler parameters and their derivatives

$$W(\mathsf{u} - \hat{\mathsf{u}},\ \sigma) = W\left(\frac{2\mathbf{q}' \cdot \mathbf{B}_i\mathbf{q}}{|\mathbf{q}|^2} - \hat{u}_i,\ \sigma\right). \tag{2.15}$$

The equilibrium configurations can then be characterized as constrained critical points of the energy functional

$$\int_0^1 W\left(\frac{2\mathbf{q}' \cdot \mathbf{B}_i\mathbf{q}}{|\mathbf{q}|^2} - \hat{u}_i,\ \sigma\right) d\sigma\,, \tag{2.16}$$

subject to the constraints,

$$\mathbf{r}'(\sigma) = \mathbf{d}_3(\mathbf{q}(\sigma)) \qquad \text{and} \qquad \mathbf{q}(\sigma) \cdot \mathbf{q}'(\sigma) = 0\,, \tag{2.17}$$

and appropriate boundary conditions, including the requirement that the Euler parameters have unit norm at one end point. Here $\mathbf{d}_3(\mathbf{q}(\sigma))$ denotes the vector of quadratic functions of q_i defined in (2.13). By introducing Lagrange multiplier functions $\boldsymbol{\lambda}(\sigma) \in \mathbb{R}^3$ and $\nu(\sigma) \in \mathbb{R}$ associated with the pointwise constraints (2.17), the equilibrium configurations can be characterized as unconstrained critical points of the Lagrangian

$$\mathcal{L}(\mathbf{q}, \mathbf{q}', \mathbf{r}', \boldsymbol{\lambda}, \nu, \sigma) = W\left(\frac{2\mathbf{q}' \cdot \mathbf{B}_i \mathbf{q}}{|\mathbf{q}|^2} - \hat{u}_i,\, \sigma\right) + \boldsymbol{\lambda} \cdot (\mathbf{r}' - \mathbf{d}_3) + \nu\, \mathbf{q} \cdot \mathbf{q}' \,. \tag{2.18}$$

For our numerical treatment it is convenient to write the governing equations in the form of a first order system, and for the sake of analysis it is convenient to take the first-order system to be Hamiltonian. So we can define the conjugate variable

$$\boldsymbol{\mu} \equiv \frac{\partial \mathcal{L}}{\partial \mathbf{q}'} = \frac{2}{|\mathbf{q}|^2} \sum_i W_{u_i} \mathbf{B}_i \mathbf{q} + \nu \mathbf{q}. \tag{2.19}$$

The Hamiltonian system involves the (standard) Legendre transform $W^*(\mathsf{v},\, s)$ of the constitutive function $W(\mathsf{w},\, s)$ introduced in (2.9). We assume that

$$\frac{\partial W}{\partial \mathsf{w}}(0) = 0, \tag{2.20}$$

and that W is a strictly convex function of w. Then the variables v conjugate to w are defined by

$$\mathsf{v} = \frac{\partial W}{\partial \mathsf{w}}(\mathsf{w})\,. \tag{2.21}$$

By the strict convexity assumption we can invert to solve for w, to get

$$\mathsf{w} = \phi(\mathsf{v})\,. \tag{2.22}$$

The Legendre transform is then defined to be

$$W^*(\mathsf{v}) = \mathsf{v} \cdot \phi(\mathsf{v}) - W(\phi(\mathsf{v})). \tag{2.23}$$

In the special case of a pure quadratic W,

$$W(\mathsf{w}) = \frac{1}{2} \sum_i K_i\, w_i^2\,, \tag{2.24}$$

the conjugate variables are $v_i = K_i\, w_i$, and the Legendre transform is

$$W^*(\mathsf{v}) = \frac{1}{2} \sum_i \frac{v_i^2}{K_i}. \tag{2.25}$$

We claim that the Hamiltonian leading to the equations governing the equilibria of an elastica can now be written in the form

$$H(\mathbf{r}, \mathbf{q}, \mathbf{n}, \boldsymbol{\mu}, \sigma) = W^*(\mathsf{m}, \sigma) + \mathsf{m} \cdot \hat{\mathsf{u}}(\sigma) + \mathbf{n} \cdot \mathbf{d}_3. \tag{2.26}$$

The phase space variables in this Hamiltonian formulation are the axis $\mathbf{r}$, the force $\mathbf{n}$ which is conjugate to $\mathbf{r}$, the Euler parameters $\mathbf{q}$, and their conjugate variable, namely $\boldsymbol{\mu}$. The right hand side of (2.26) can be written in terms of the phase variables by substituting the expression (2.13) for $\mathbf{d}_3(\mathbf{q})$ and by using the relations

$$m_i = \frac{1}{2}\boldsymbol{\mu} \cdot \mathbf{B}_i\mathbf{q} \,(= W_{u_i}(\mathsf{u} - \hat{\mathsf{u}})) \qquad i = 1, 2, 3, \tag{2.27}$$

which follow from the hyper-elastic constitutive relation (2.9) and the components of the definition (2.19) of $\boldsymbol{\mu}$ in the directions $\mathbf{B}_i\mathbf{q}$. The second equation in (2.27) can itself be further inverted using the implicitly defined inverse function ϕ introduced in equations (2.21) and (2.22), leading to the expression

$$\mathsf{u} = \hat{\mathsf{u}} + \phi\left(\frac{\boldsymbol{\mu} \cdot \mathbf{B}_1\mathbf{q}}{2}, \frac{\boldsymbol{\mu} \cdot \mathbf{B}_2\mathbf{q}}{2}, \frac{\boldsymbol{\mu} \cdot \mathbf{B}_3\mathbf{q}}{2}\right) \tag{2.28}$$

for the strains. In the particular case of linear elasticity, (2.28) simplifies to

$$u_i = \hat{u}_i + \frac{\boldsymbol{\mu} \cdot \mathbf{B}_i\mathbf{q}}{2\,K_i}, \qquad i = 1,\ 2,\ 3, \tag{2.29}$$

and the Hamiltonian takes the explicit form

$$H(\mathbf{r}, \mathbf{q}, \mathbf{n}, \boldsymbol{\mu}) = \sum_{i=1}^{3}\left(\frac{m_i^2}{2\,K_i} + \hat{u}_i m_i\right) + \mathbf{n} \cdot \mathbf{d}_3. \tag{2.30}$$

The Hamiltonian system of equations governing equilibria is of the form

$$\left\{\begin{aligned}
\mathbf{r}' &= \frac{\partial H}{\partial \mathbf{n}} = \mathbf{d}_3,\\
\mathbf{q}' &= \frac{\partial H}{\partial \boldsymbol{\mu}} = \frac{1}{2}\sum_{i=1}^{3} u_i\,\mathbf{B}_i\mathbf{q},\\
\mathbf{n}' &= -\frac{\partial H}{\partial \mathbf{r}} = 0,\\
\boldsymbol{\mu}' &= -\frac{\partial H}{\partial \mathbf{q}} = \frac{1}{2}\sum_{i=1}^{3} u_i\,\mathbf{B}_i\boldsymbol{\mu} - \frac{\partial \mathbf{d}_3}{\partial \mathbf{q}}^T \mathbf{n},
\end{aligned}\right. \tag{2.31}$$

where again $\mathbf{d}_3(\mathbf{q})$ is defined by the formula (2.13), so that

$$\frac{\partial \mathbf{d}_3}{\partial \mathbf{q}} = 2\begin{pmatrix} q_3 & q_4 & q_1 & q_2 \\ -q_4 & q_3 & q_2 & -q_1 \\ -q_1 & -q_2 & q_3 & q_4 \end{pmatrix},$$

and the u_i are written in terms of the phase variables $\mathbf{q}$ and $\boldsymbol{\mu}$ using relation (2.28), or in the case of linear elasticity the explicit form (2.29).

2.2.3 Analysis of Integrals and Symmetries

We next detail the integrals or conserved quantities of the Hamiltonian system (2.31), i.e., functions of the phase variables that are independent of arc–length σ. We will later see the usefulness of these integrals in the choice of boundary conditions.

Six integrals are obtained immediately from equations (2.6) and (2.7). The three components of force $\mathbf{n}$ are constant due to the translational symmetry of the Hamiltonian system in space. Similarly the three components of $\mathbf{m} + \mathbf{r} \times \mathbf{n}$ are invariant as a consequence of rotational symmetry about the three inertial axes. To see that these expressions provide integrals of (2.31), we merely need to write them as functions of the phase variables. Components of $\mathbf{n}$ and $\mathbf{r}$ with respect to the fixed basis are trivially phase variables, and it can be verified that the components $\overline{m}_i$ of $\mathbf{m}$ with respect to the fixed space basis can be written as (cf. [5])

$$\overline{m}_i = \frac{1}{2}\boldsymbol{\mu} \cdot \mathbf{F}_i \mathbf{q}, \qquad i = 1, 2, 3, \tag{2.32}$$

where

$$\mathbf{F}_1 = \begin{pmatrix} 0 & 0 & 0 & 1 \\ 0 & 0 & -1 & 0 \\ 0 & 1 & 0 & 0 \\ -1 & 0 & 0 & 0 \end{pmatrix}, \quad \mathbf{F}_2 = \begin{pmatrix} 0 & 0 & 1 & 0 \\ 0 & 0 & 0 & 1 \\ -1 & 0 & 0 & 0 \\ 0 & -1 & 0 & 0 \end{pmatrix},$$

$$\mathbf{F}_3 = \begin{pmatrix} 0 & -1 & 0 & 0 \\ 1 & 0 & 0 & 0 \\ 0 & 0 & 0 & 1 \\ 0 & 0 & -1 & 0 \end{pmatrix}.$$

In addition to the integrals listed above which have physical interpretations, there are two integrals which arise from the representation of $SO(3)$ by the four Euler parameters, rather than by a three parameter description. By construction, the second equation of (2.31) implies

$$\mathbf{q} \cdot \mathbf{q}' = \frac{1}{2}\sum_{i=1}^{3} u_i \, \mathbf{q} \cdot \mathbf{B}_i \mathbf{q} = 0,$$

so that $|\mathbf{q}|^2$ is a seventh integral.

Next consider the quantity $\boldsymbol{\mu} \cdot \mathbf{q} + 2\mathbf{r} \cdot \mathbf{n}$. By virtue of (2.31), we find

$$\begin{aligned} \frac{d}{d\sigma}(\boldsymbol{\mu} \cdot \mathbf{q} + 2\mathbf{r} \cdot \mathbf{n}) = \; & -\mathbf{n} \cdot \frac{\partial \mathbf{d}_3}{\partial \mathbf{q}}\mathbf{q} + \frac{1}{2}\sum_{i=1}^{3} u_i \mathbf{q} \cdot \mathbf{B}_i \boldsymbol{\mu} \\ & + \frac{1}{2}\sum_{i=1}^{3} u_i \boldsymbol{\mu} \cdot \mathbf{B}_i \mathbf{q} + 2\mathbf{d}_3 \cdot \mathbf{n}. \end{aligned} \tag{2.33}$$

Euler's Theorem for homogeneous functions implies that $2\mathbf{d}_3 = \dfrac{\partial \mathbf{d}_3}{\partial \mathbf{q}}\mathbf{q}$. Moreover the matrices $\mathbf{B}_i$ are skew symmetric, so it follows that (2.33) vanishes and

$$\boldsymbol{\mu} \cdot \mathbf{q} + 2\mathbf{r} \cdot \mathbf{n} \tag{2.34}$$

is an eighth integral of the system. The integral (2.34) is associated with invariance of the Hamiltonian under the (variational) symmetry in which $\mathbf{q}$ is replaced by $(1+\epsilon)\mathbf{q}$, $\boldsymbol{\mu}$ is replaced by $(1+\epsilon)^{-1}\boldsymbol{\mu}$, $\mathbf{r}$ is replaced by $(1+\epsilon)^2\mathbf{r}$ and $\mathbf{n}$ is replaced by $(1+\epsilon)^{-2}\mathbf{n}$. Specification of the value of the integral (2.34) merely eliminates the gauge freedom in $\boldsymbol{\mu}$.

The above integrals arise for all constitutive laws. There are two additional, constitutive dependent, integrals that arise in each of the cases of an *isotropic* rod, and a *uniform* rod. The tangential component of bending moment is

$$m_3(\sigma) \equiv \mathbf{m} \cdot \mathbf{d}_3 = \frac{\boldsymbol{\mu} \cdot \mathbf{B}_3 \mathbf{q}}{2}$$

A straightforward computation, using (2.29), (2.31) and properties of the $\mathbf{B}_i$ matrices, reveals that

$$\begin{aligned} 2\frac{d}{d\sigma}m_3(\sigma) &= (\boldsymbol{\mu} \cdot \mathbf{B}_3\mathbf{q}' + \boldsymbol{\mu}' \cdot \mathbf{B}_3\mathbf{q}) = -u_1\boldsymbol{\mu} \cdot \mathbf{B}_2\mathbf{q} + u_2\boldsymbol{\mu} \cdot \mathbf{B}_1\mathbf{q} \\ &= (\boldsymbol{\mu} \cdot \mathbf{B}_1\mathbf{q})(\boldsymbol{\mu} \cdot \mathbf{B}_2\mathbf{q})\left(\frac{1}{K_2} - \frac{1}{K_1}\right) - \hat{u}_1\boldsymbol{\mu} \cdot \mathbf{B}_2\mathbf{q} + \hat{u}_2\boldsymbol{\mu} \cdot \mathbf{B}_1\mathbf{q}\,. \end{aligned}$$

Accordingly, if $K_1(\sigma) \equiv K_2(\sigma)$ and $\hat{u}_1 \equiv \hat{u}_2 \equiv 0$, then $m_3(\sigma) = \boldsymbol{\mu} \cdot \mathbf{B}_3\mathbf{q}/2$ provides a ninth integral. This case will be described as a *transversely isotropic* or just *isotropic* rod. The symmetry associated with the twist integral is a rotation of the rod about its own centerline.

The second constitutive dependent symmetry is uniformity. If the constitutive function W has no explicit σ dependence, which in the linearly elastic case means the stiffnesses K_i and the unstressed strains $\hat{u}_i$ are all constant, then the Hamiltonian $\mathcal{H}$ (2.26) has no explicit σ dependence, and therefore represents a tenth integral of the system. The associated symmetry is translation in the arc-length σ, or relabeling of the material point corresponding to $\sigma = 0$.

In summary the Hamiltonian system always has at least eight integrals, namely $\mathbf{n}$, $|\mathbf{q}|^2$, $\mathbf{m} + \mathbf{r} \times \mathbf{n}$, and $\boldsymbol{\mu} \cdot \mathbf{q} + 2\mathbf{r} \cdot \mathbf{n}$. If the rod is isotropic m_3 provides an additional integral, and if the rod is uniform then the Hamiltonian $\mathcal{H}$ (2.26) provides a tenth integral.

2.3 Numerical Discretization Implemented in the AUTO Package

The problems discussed in this thesis are nonlinear two-point boundary value problems. There exist a number of software packages for boundary value problems, see for example [2], [4]. The software we used in our computations is called

AUTO. This software package was written specially for continuation and bifurcation problems in ordinary differential equations. The discretization scheme adopted in AUTO is the so–called collocation method. In this section we give a brief description about this method and some theoretical results related to it. For more detailed information see [6], [7], and [8].

Consider the first order system of ordinary differential equations of the form

$$\dot{\mathbf{u}}(\sigma) = \mathbf{f}(\mathbf{u}(\sigma),\, \lambda), \qquad \sigma \in [0,\ 1], \qquad \mathbf{u}(\,\cdot\,), \mathbf{f}(\,\cdot\,,\ \cdot\,) \in \mathbb{R}^{n}\,, \qquad \boldsymbol{\lambda} \in \mathbb{R}^{n_\lambda}, \tag{2.35}$$

subject to general, possibly nonlinear or non–separated, boundary conditions

$$B_i(\,\mathbf{u}\,(0)\,,\,\mathbf{u}\,(1)\,,\,\boldsymbol{\lambda}\,) \,=\, 0\,, \qquad\qquad i \,=\, 1\,,2\,,\cdots,n_b\,, \tag{2.36}$$

where $\boldsymbol{\lambda}$ is the continuation parameter vector. In order for problem (2.35) $\sim$ (2.36) to be formally well posed we require that $n_\lambda = n_b - n + 1$. This implies that there will always be one free parameter, so that the equations will normally yield curves of solutions, i.e., we are concerned with a continuation problem. For example, for our rod problem we have $n = 15$, $n_b = 15$ and one free parameter $n_\lambda = 1$.

In AUTO the differential equation (2.35) is approximated by the method of collocation at m Gauss points with piecewise polynomials that belong to the class $C\,[\,0\,,\,1\,]$, where m is an integer between 2 and 7 . This approach is equivalent to an implicit Runge Kutta method (cf. [16]). More precisely, define a mesh

$$\{\,0 = \sigma_0 \,<\, \sigma_1 \,<\, \cdots \,<\, \sigma_N = 1\,\}\,, \qquad \Delta\sigma_j \equiv \sigma_{j+1} - \sigma_j\,, \quad (\,0 \,\le\, j \,\le\, N-1\,)\,,$$

and for each j introduce the Lagrange basis polynomials

$$\{\,\omega_{j,i}\,(\sigma)\,\}\,, \qquad j \,=\, 0\,,1\,,\cdots,N-1\,, \qquad i \,=\, 0\,,1\,,\cdots,m\,,$$

defined by

$$\omega_{j,i}\,(\sigma) \,=\, \prod_{k=0,\,k\neq i}^{m} \frac{\sigma \,-\, \sigma_{j+\frac{k}{m}}}{\sigma_{j+\frac{i}{m}} - \sigma_{j+\frac{k}{m}}}\,, \qquad\qquad \sigma_{j+\frac{i}{m}} \,\equiv\, \sigma_j + \frac{i}{m}\,\Delta\sigma_j\,.$$

The collocation method now consists of finding

$$\mathbf{p}_j\,(\sigma) \,=\, \sum_{i=0}^{m} \omega_{j,i}\,(\sigma)\,\mathbf{u}_{j+\frac{i}{m}}\,, \qquad\qquad j \,=\, 0\,,1\,,\cdots,N-1\,,$$

such that

$$\dot{\mathbf{p}}_j(z_{j,i}) = \mathbf{f}(\mathbf{p}_j(z_{j,i}), \boldsymbol{\lambda}), \qquad i = 1, 2, \cdots, m, \qquad j = 0, 1, \cdots, N-1, \tag{2.37}$$

where in each subinterval $[\sigma_{j-1}, \sigma_j]$ the points $\{z_{j,i}\}_{i=1}^{m}$ are the zeros of the mth degree Legendre polynomial relative to that subinterval. With the above choice of basis, $\mathbf{u}_j$ and $\mathbf{u}_{j+\frac{i}{m}}$ are to approximate the solution $\mathbf{u}(\sigma)$ of the continuous problem at σ_j and $\sigma_{j+\frac{i}{m}}$ respectively.

The discrete boundary conditions are $B_i(\mathbf{p}_1(0), \mathbf{p}_N(1), \boldsymbol{\lambda}) = 0$, $i = 1, 2, \cdots, n_b$, i.e.,

$$B_i(\mathbf{u}_0, \mathbf{u}_N, \boldsymbol{\lambda}) = 0, \qquad i = 1, 2, \cdots, n_b. \tag{2.38}$$

There is extensive literature on the relation between the solutions of the discrete approximations and the continuous problem (see for example [2], [3], [10] & [15]), and we shall not deal with this subject here. We only mention the following error estimate. Assuming that the problem (2.35), (2.36) is sufficiently smooth, the local behavior of the error for $\sigma \in [\sigma_j, \sigma_{j+1})$ is

$$\|u_l(\sigma) - v_l(\sigma)\|_{(i)} = c_l |u_l^{m+1}(\sigma_i)| h_i^m + O(h_i^{m+1}), \;\; l = 1, 2, \cdots, n, \;\; h_i = \sigma_{i+1} - \sigma_i,$$

where c_l are known constants, m is the number of collocation points per subinterval, $\mathbf{v}(\sigma)$ is the collocation solution, and for any appropriate function ψ,

$$\|\psi\|_{(i)} = \max_{\sigma \in [\sigma_i, \sigma_{i+1})} |\psi(\sigma)|.$$

If the mesh is uniform, we then have

$$\|u_l(\sigma) - v_l(\sigma)\|_{L^\infty([0,1])} = O(h^{m+1}).$$

In particular, at the mesh points σ_i we have the super-convergence result

$$\max_{0 \le i \le N} |u_l(\sigma_i) - v_l(\sigma_i)| = O(h^{2m}), \qquad l = 1, 2, \cdots, n,$$

with $h = \max\limits_{1 \le j \le N} h_j$.

Chapter 3

Numerical Results

In this chapter we discuss the numerical experiments performed in support of this thesis. In Section 3.1 we discuss the experiment we are modeling, and the BVP we use to describe the experiment mathematically. In Section 3.2 we discuss the numerical solutions to the BVP for an ideal rod (i.e., perfectly straight and uniform). In Section 3.3 we discuss the numerical solutions to the BVP for an imperfect rod. The behavior is discussed in terms of two different parameter continuations: the change of position of the free end of the rod with respect to the fixed end, and the twisting of the fixed end of the rod. In Section 3.4 we discuss the numerical simulation of twisting a rod with a helical curvature. And finally in Section 3.5 we discuss numerical simulations carried out when allowing the free end of the rod to slide as well as turn (i.e., to lengthen or shorten the loop of rod connecting the two endpoints).

3.1 The Boundary Value Problem

In this section we lay out our particular BVP. First we will describe the experiment we are modeling and discuss the appropriate BCs. We then discuss the continuation parameters used in performing the numerical calculations, and also the continuation strategy we employed.

3.1.1 Boundary Conditions

The experiments being modeled were carried out by Dr. Brian Berg. Briefly, the experiments were as follows:

A thin wire of arbitrary length is placed in an apparatus such that one end is fixed at the origin and pointing in the positive $\mathbf{r}_3$ direction, and the other end is bent around the u_2 direction (i.e., bent around the r_2-axis), until it returns to the r_1-axis with the wire directed in the negative $\mathbf{r}_3$ direction (see Figure 1.1). By definition, the wire returns to the r_1-axis at the coordinate ρ. Once the wire is placed in this configuration, the end of the wire fixed at the origin is twisted through several complete revolutions, and the torque required to twist the wire is measured as a function of the angle θ.

The BCs for this problem are as follows:

$$\boldsymbol{r}(0) = \mathbf{0} \tag{3.1}$$

$$\boldsymbol{r}(1) = (\rho, 0, 0)^T \tag{3.2}$$

$$\boldsymbol{q}(0) = (0, 0, \sin(\theta/2), \cos(\theta/2))^T \tag{3.3}$$

$$\boldsymbol{q}(0) \cdot \boldsymbol{\mu}(0) = 0 \tag{3.4}$$

$$m_3(1) = 0 \tag{3.5}$$

$$2(q_1(1)q_3(1) - q_2(1)q_4(1)) = 0 \tag{3.6}$$

$$2(q_2(1)q_3(1) - q_1(1)q_4(1)) = 0 \tag{3.7}$$

$$s(0) = 0 \tag{3.8}$$

The first six BCs (Eqs. (3.1) & (3.2)) arise from fixing the coordinates of the ends of the rod, and the next four BCs (Eq. (3.3)) come from the orientation of the rod at the origin. The next BC (Eq. (3.4)) is introduced to eliminate a gauge freedom induced by symmetries in the Hamiltonian system caused by describing a 3-D group (SO(3)) with the four dimensional Euler parameters (cf. [13]). Then we have Eq. (3.5), which mandates that at $\sigma = 1$ the rod is free to spin (i.e., the tangential torque m_3 at $\sigma = 1$ must vanish). Eqs. (3.6) & (3.7) restrict the orientation of the free end of the rod to be in the $-r_3$ direction. The final BC (Eq. (3.8)) stems simply from including the arc-length parameter explicitly as a dependent variable in the problem. This was done in concordance with the procedures implemented in AUTO that allow coefficients such as $\hat{\mathbf{u}}$ to be a function of σ, a situation which will be discussed in §3.4.

The experiment calls for an arbitrary length of wire, but in AUTO $\sigma \in [0, 1]$ by definition. So in the mathematical formulation we use the length of the wire as a length scale.

In the original experiment it was thought that the free end of the wire was not only free to turn, but was also free to slide. This condition leads to an additional boundary condition, viz $n_3(1) = 0$, and an additional parameter, namely the physical length of the loop, which ensures that there is no tangential component of the force pulling or pushing on the free end of the rod. The numerical modeling found that this assumption is problematic. This issue is further discussed in §3.5.

3.1.2 Continuation Parameters

To model this problem using AUTO we take into account various values of two different physical parameters of the rod (namely $\hat{\mathbf{u}}$ and K_3/K_1). We also have two configuration parameters, namely ρ (which governs the distance between the ends of the rod), and θ (which represents the angle through which we have twisted the end of the rod fixed at the origin). This make a total of four continuation parameters.

For most of the discussions we leave $\hat{u}_1 = \hat{u}_3 = 0$ and vary $\hat{u}_2$ directly as its own parameter. In §3.4 however, when we consider a helical rod, we use $|\hat{\mathbf{u}}|$ as our continuation parameter. In the discussion in the following section, we assume the continuation parameter to be $|\hat{\mathbf{u}}|$ for convenience, though all statements hold for continuation in $\hat{u}_2$ as well.

3.1.3 Continuation Strategy

To get AUTO started it needs a known initial solution at some parameter values in either analytic or numeric form. For most of the AUTO runs, continuing from various values of different parameters and traversing different branches, we used a numeric solution calculated by AUTO itself as the starting point. However, for the very first run an analytic solution is necessary.

This solution was arrived at by using a perfectly straight rod (i.e., $\hat{\boldsymbol{u}} \equiv \mathbf{0}$), and bending it into a perfect semi-circle. It is easy to check that the following solution of the equilibrium equations matches the BCs specified by Eqs. (3.1) - (3.8).

$$\boldsymbol{r}(\sigma) = (1 - \cos(\sigma\pi))/\pi, 0, \sin(\sigma\pi)/\pi)^T \tag{3.9}$$

$$\boldsymbol{q}(\sigma) = (0, \sin(\sigma\pi/2), 0, \cos(\sigma\pi/2))^T \tag{3.10}$$

$$\boldsymbol{n}(\sigma) = (0, 0, 0)^T \tag{3.11}$$

$$\boldsymbol{\mu}(\sigma) = (0, K_2\pi\cos(\sigma\pi/2), 0, 2K_2\pi\sin(\sigma\pi/2))^T \tag{3.12}$$

$$s(\sigma) = \sigma \tag{3.13}$$

Here, again, s is our explicit arc-length parameter, included only to be able to handle the non-constant $\hat{\boldsymbol{u}}$ situation. In this notation, σ is the arc-length parameter used by AUTO.

Once we have this initial analytic solution, we can begin our continuation steps. We first perform continuation in ρ, pulling the free end of the rod away from the origin. We did this because the analytic starting solution is for a rod held in a semi-circular shape, but we wished to include in our region of study rods with the ends farther apart than this, and pulling the ends apart first was the most efficient way to do this.

Once this expansion has been carried out, we determine a variety of K_3/K_1 values by performing continuation in K_3 and leaving K_1 fixed, using as our initial solution the numeric solution provided by AUTO after the first continuation. Numerical solutions were saved for K_3/K_1 at the following values: 0.4, 0.6, 0.8, 1.0, 1.2, 1.4, and 1.5. These values were chosen to cover the ranges of K_3/K_1 ratios provided by Dr. Berg for both Nitinol and stainless steel wires (which are the wires most commonly used in the surgical procedures mentioned in Chapter 1). We take $K_1 = K_2$ because, according to Dr. Berg, the manufactured wires are very nearly isotropic.

After continuing in K_3/K_1, we continue each of the seven saved solutions in $|\hat{\mathbf{u}}|$, again saving numerical solutions for a variety of values of $|\hat{\mathbf{u}}|$ (for each target K_3/K_1 value). Solutions were garnered for the following values of $|\hat{\mathbf{u}}|$: 0, 0.01, 0.03, 0.05, 0.1, 0.2, 0.4, and 0.6. These values were chosen to look carefully at nearly straight rods, but to also sample rods with a significantly larger radii of curvature in their unstressed form. A comparison of rods with these different

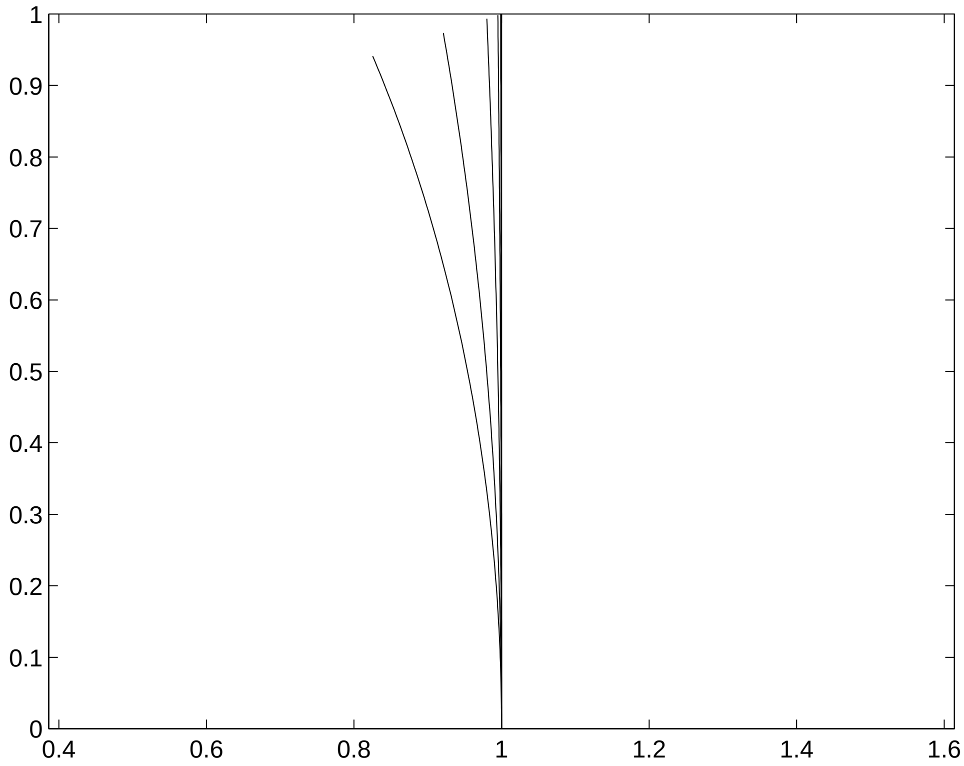

Figure 3.1: Comparison of Rod Shapes
This diagram compares rods of the radii of curvature used in this study. Each line in the diagram follows the path of a rod of length 1 with a different radius of curvature. To the accuracy of this diagram, the values of $|\hat{\mathbf{u}}| = 0, 0.01, 0.03$, and 0.05 all overlay one another, and are represented by the vertical line. The line with the largest deviation from the vertical is for $|\hat{\mathbf{u}}| = 0.6$. The first rod that visibly deviates from the vertical has $|\hat{\mathbf{u}}| = 0.1$.

radii of curvature can be found in Figure 3.1. Since the wires are nearly straight when they are manufactured, the concern is for any unstressed curvature induced in the storage of the wires, and since the wires are stored in large hoops, it is a reasonable approximation to assume that all the unstressed curvature lies in a single orientation.

At this point we have a 2-D grid of solutions with a total of 56 starting points. We next take each of these saved solutions and continue in ρ, again saving solutions for a variety of values of ρ. The standard values of ρ from which solutions were saved were 0.8, $2/\pi$, 0.6, 0.4, 0.2, 0, -0.2, -0.4, -0.6, $-2/\pi$, and -0.8. During this step we also encountered many bifurcation points, so we also generated bifurcation diagrams for the ρ continuations. These diagrams are discussed in detail in §3.2 and §3.3.

At this point there were a total of $7 \times 8 \times 11 = 616$ saved numerical solutions, each of which needed to be twisted to determine its behavior. Each of the saved solutions was continued in θ for two complete revolutions (to assure periodicity of the solution) in order to determine the behavior of the rod under twisting of one end.

3.2 The Idealized Problem

In this context, the idealized (or "perfect") problem is defined as modeling a perfectly straight, uniform rod, in the way described in the previous section. Clearly the continuation step in $|\hat{\mathbf{u}}|$ does not apply here, and in point of fact the behavior of the rod is identical for all values of K_3/K_1 as long as $\hat{\mathbf{u}} \equiv \mathbf{0}$, so the K_3/K_1 continuation also does not apply to this case. Accordingly we need only consider the problems of performing the continuation in ρ and θ. In this section we first consider continuation in ρ, which we refer to as Sliding, and then we consider continuation in θ, which we call Twisting.

3.2.1 Sliding

When we perform the Sliding continuation step, we move the free end of the rod along the line connecting the ends (i.e., the r_1-axis) while keeping the other end fixed. We start with the ends of the rod pulled apart, and slide the free end of the rod until it passes through the fixed end and moves some distance beyond (i.e., so that $\rho < 0$). When we perform this continuation on an ideal rod, we find a bifurcation point at $\rho = 0$. By continuing along this bifurcating branch, and along any other branches we encounter during this process, we were able to generate the bifurcation diagram depicted in Figure 3.2.

In this diagram, the Top and Bottom branches of the diagram correspond to configurations of the rod where the rod lies in the $r_1 - r_3$ plane, while the Middle branch corresponds a rigid body rotation of the rod about the r_3-axis. The rod remains in a planar configuration while traversing the Middle Branch, even though it is not in the $r_1 - r_3$ plane. The Top branch is the original deformation, while the Bottom branch is an analogous continuation where the rod has been turned around by an angle of exactly π.

The color of the diagram was chosen to depict the value of n_3 to illustrate the fact that $n_3 = 0$ only in the event that the wire is in a planar configuration. Later we will see that if the wire becomes non-planar, then $n_3 \neq 0$. The importance of this point will be discussed in §3.5.

A typical physical configuration of the rod on each of the three branches is shown in Figures 3.3 - 3.5

3.2.2 Twisting

After generating the Sliding bifurcation diagram of the rod, we choose certain points on the diagram (i.e., certain values of ρ) and twist the fixed end of the rod while observing its behavior. In particular we are looking for the ratcheting phenomenon exhibited by physical rods which was discussed in Chapter 1.

At any point on the planar branches of this diagram the rod can be twisted, and at all of these points the rod will remain planar (see Figure 3.6). In addition,

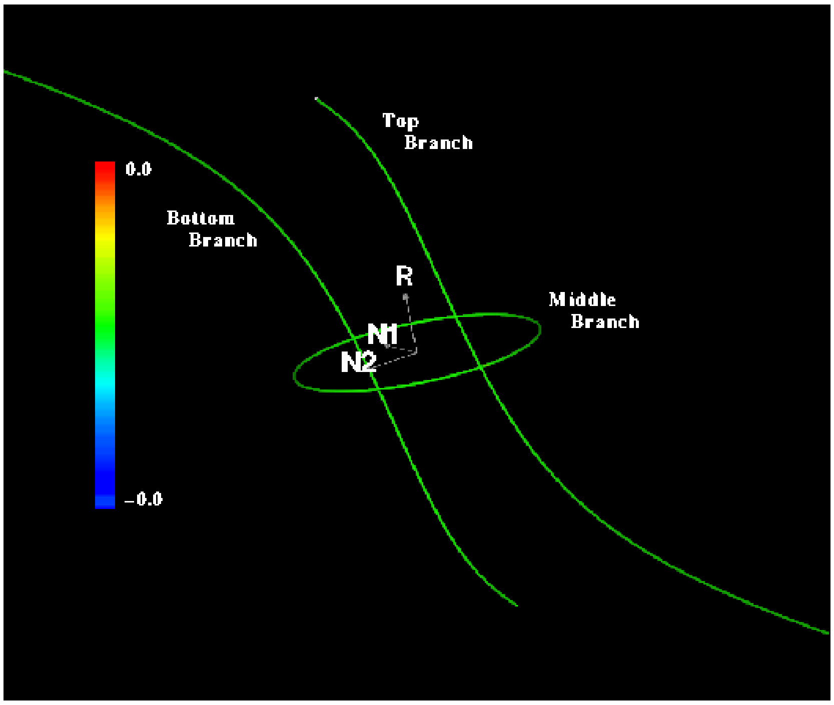

Figure 3.2: Idealized Problem Bifurcation Diagram
In this diagram, color represents n_3. The color suggests that the value of n_3 is zero throughout the entire diagram, and this is in fact the case to the accuracy of the numerics. The Middle Branch connects to the Top Branch at the intersection point furthest to the right in the diagram, while it connects to the Bottom Branch at the intersection point furthest to the left. The other two apparent intersections are due to the projection of a three dimensional space onto a two dimensional image, and are in fact not intersections at all.

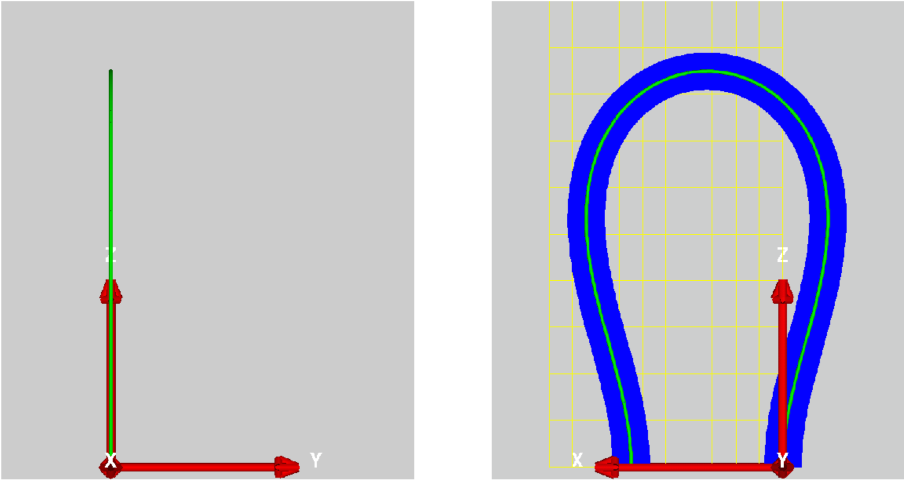

Figure 3.3: Physical Configuration on the Top Branch
This figure shows the actual shape of the rod for $\rho > 0$ along the Top Branch of Figure 3.2. The view on the left is taken looking down the x-axis, while the view on the right is rotated 90 degrees and looking down the y-axis. The rod lies in the x-z plane, and from the ribbon one can see the rod is unrotated.

all twisting motions will be smooth (i.e., no ratcheting is exhibited when the rod is perfectly straight). In fact, the rod rotates with zero torque, as can be seen in Figure 3.7. So in this sense, this truly is the perfect problem.

This problem serves as a starting point for further discussions in this chapter. The Sliding and Twisting problems discussed below can be considered as perturbations of this problem, with changes in the Twisting and Sliding behavior being tied directly to changes in the $|\hat{\mathbf{u}}|$ parameter controlling the unstressed shape. As soon as $|\hat{\mathbf{u}}|$ deviates from zero, however, the K_3/K_1 ratio becomes important as well, as we shall see.

3.3 Imperfect Problem

As in §3.2, we first discuss the effects of sliding the free end of the rod, followed by a description of the behavior of the rod while it is being twisted. Here we only consider rods with unstressed curvature of the form $\hat{\mathbf{u}} = (0, \hat{u}_2, 0)^T$, where $\hat{u}_2$ is constant.

3.3.1 Sliding

Several effects were observed when deforming the rod from a semi-circular configuration by moving the free end of the rod along the line connecting it to the

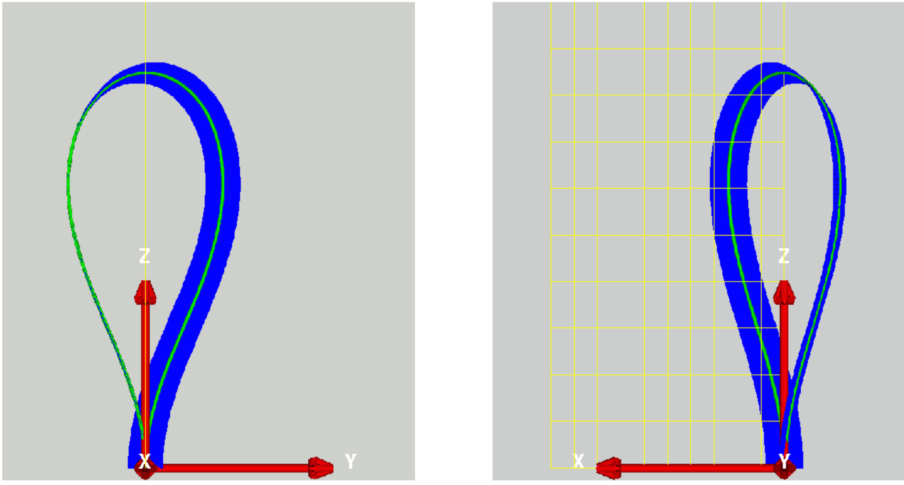

Figure 3.4: Physical Configuration on the Middle Branch
This figure shows the actual shape of the rod approximately half-way between the bifurcation points along the Middle Branch of Figure 3.2. The view on the left is taken looking down the x-axis, while the view on the right is rotated 90 degrees and looking down the y-axis. The rod has spun out of the x-z plane, and from the ribbon one can see the induced rotation.

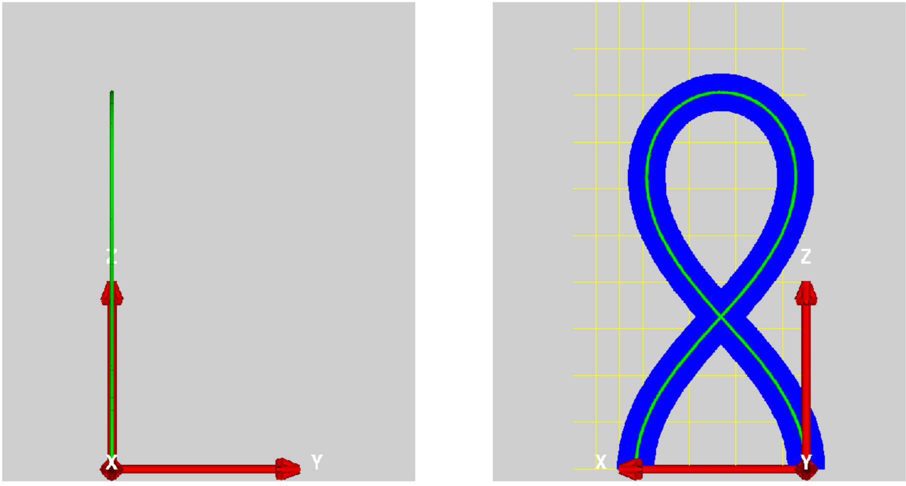

Figure 3.5: Physical Configuration on the Bottom Branch
This figure shows the actual shape of the rod for $\rho > 0$ along the Bottom Branch of Figure 3.2. The view on the left is taken looking down the x-axis, while the view on the right is rotated 90 degrees and looking down the y-axis. The rod lies in the x-z plane, and from the ribbon one can see the rod is unrotated.

fixed end. With the distance between the ends of the rod denoted by ρ, the numerics exhibited bifurcation points at various values of ρ. The locations of these bifurcation points in the phase space were highly dependent on values of $\hat{u}_2$ and K_3/K_1. A typical bifurcation diagram can be seen in Figure 3.8.

Notice that in this figure, there are four branches. The Top Branch, derived from the initial deformation, runs along the top-right of the diagram. It should be noted that the rod remains in a planar configuration for this entire branch, residing in the r_1-r_3 plane. We see that there is a bifurcation point near $\rho = 0$. When we move along this new branch (the Middle Branch) we find that the rod twists out of the plane (see Figure 3.9), and in fact the rod spins all the way around while traversing this branch. Exactly half way around this branch the rod is again in a planar configuration, and it is at this point that we encounter a second bifurcation point. We find that this third branch (the Bottom Branch) running along the bottom-left of Figure 3.8, is also a planar solution, and is in fact a mirror image of the Top Branch. The rod has spun exactly half-way around, and so the configuration of the rod as ρ increases looks exactly like the configuration of the rod with ρ decreasing along the Top Branch (see Figures 3.10 and 3.11). This configuration corresponds to performing the same initial deformation, but using a value of $\hat{u}_2$ that is equal in magnitude but opposite in sign to the original $\hat{u}_2$ value.

There is, however, a certain asymmetry between the Top and Bottom Branches. First we notice that these branches intersect the Middle Branch at different values

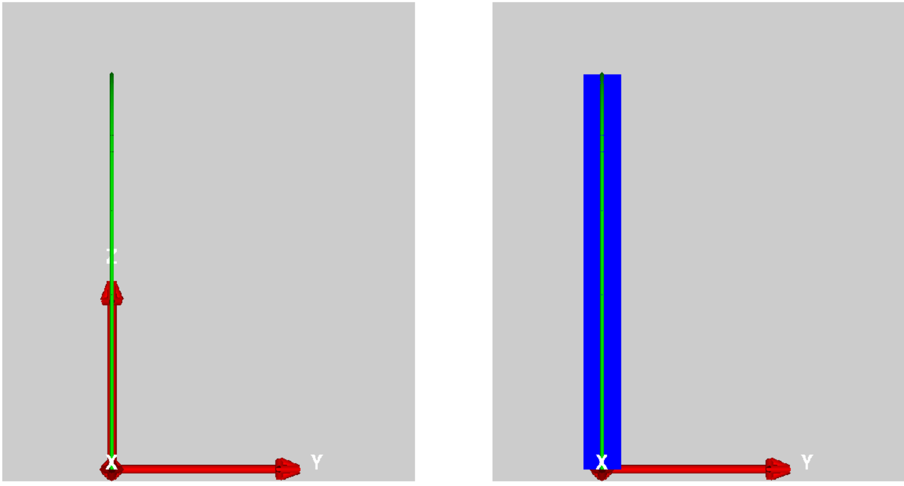

Figure 3.6: Physical Configuration of a Rotation from the Top Branch
This figure shows the actual shape of the rod for $\rho > 0$ along the Top Branch of Figure 3.2. Both views are taken looking down the x-axis. The view on the left is with $\theta = 0$, while the view on the right is with $\theta \approx \pi/2$. In both cases the rod lies in the x-z plane, and from the ribbon one can see the effect of the rotation.

of ρ. Of more interest, however, is that the Bottom Branch exhibits an additional bifurcation as ρ gets large, leading to the Trailing Branch, a phenomenon which is not seen on the Top Branch for this value of $\hat{u}_2$. In this situation, downward stresses on the rod are such that the loop of rod tips out of the plane (see Figure 3.12). This situation is analogous to the buckling of a strut when stress applied to one end reaches a critical level. The Trailing Branch can appear on the Top Branch, but only for higher values of $\hat{u}_2$, and in point of fact the value of ρ at which this bifurcation takes place is very dependent on the values of $\hat{u}_2$ and K_3/K_1.

The other thing to notice in Figure 3.8 is that the value of n_3 (denoted by color) deviates from 0 whenever the rod becomes non-planar. We will see this phenomenon again, and it will be discussed in §3.5.

The Middle branch described above, however, does not necessarily have to behave in this manner. When $\hat{u}_2$ grows large, the nearly circular shape of this branch exhibited in Figure 3.2 becomes quite elongated (see Figure 3.13), and at some point the second bifurcation point slides off the diagram entirely, leaving instead of one circular branch two detached branches, as in Figure 3.14. As one goes further and further out these branches, the solution to the rod approaches a planar configuration (notice how $n_3 \to 0$ as one moves further out the branch), but this planar condition is never actually reached. This suggests that if we extended the solution out further, eventually the rod would become planar again. This makes intuitive sense physically, as further extending ρ in the negative

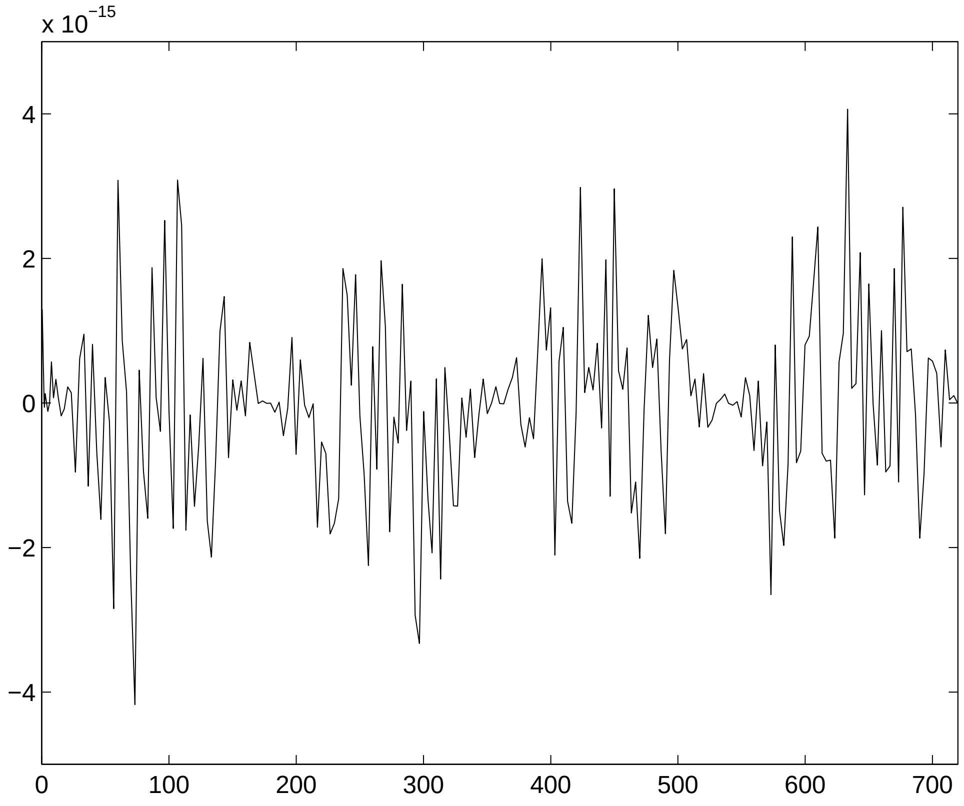

Figure 3.7: Twist Angle vs m_3 for $\hat{u}_2 = 0$
This diagram shows the behavior of a perfectly straight rod while it is being twisted from the fixed end. The x-axis of the graph represents θ, while the left axis represents $m_3(0)$. To the accuracy of the numerics, $m_3(0) = 0$ throughout the twisting process (notice the scale of the diagram).

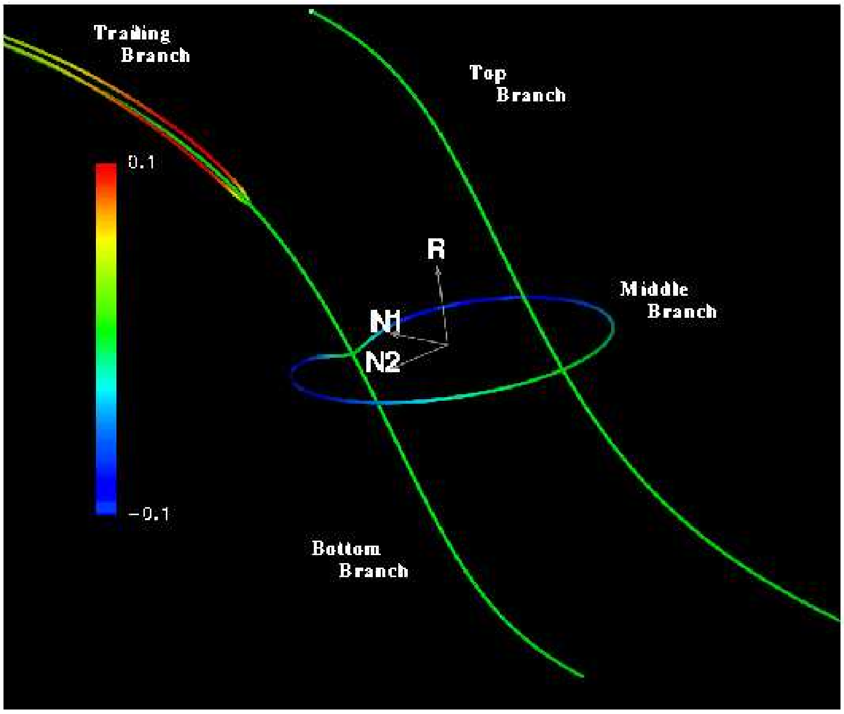

Figure 3.8: Bifurcation Diagram with Non-zero $\hat{u}_2$

In this figure $\hat{u}_2 = 0.2$. Color represents n_3. We notice four separate bifurcating branches in this diagram. Also notice that the Middle Branch is noticeably perturbed from the nice circular shape seen in Figure 3.2. Notice that whenever the rod deviates from a planar configuration, $n_3 \neq 0$.

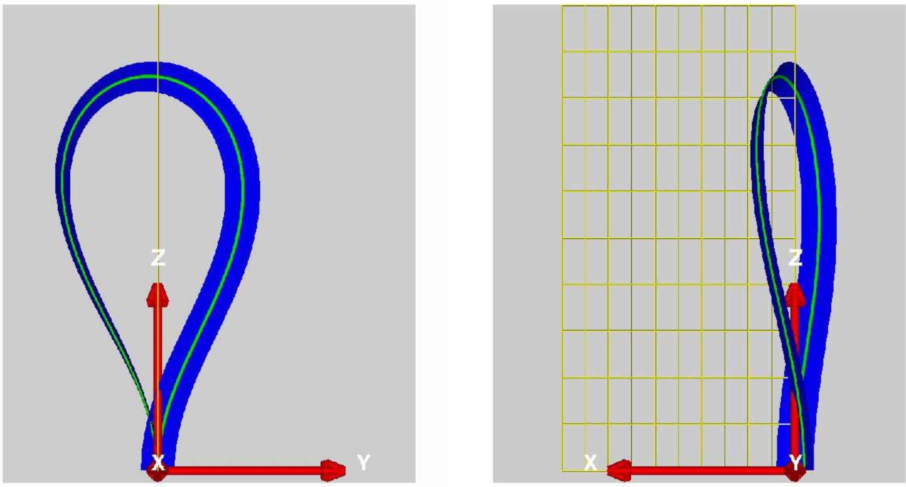

Figure 3.9: Physical Configuration on Middle Branch
This figure shows the actual shape of the rod approximately half-way between the bifurcation points along the Middle Branch of Figure 3.8. The view on the left is taken looking down the x-axis, while the view on the right is rotated 90 degrees and looking down the y-axis. The rod is non-planar, and from the ribbon one can see the rotation induced in the rod.

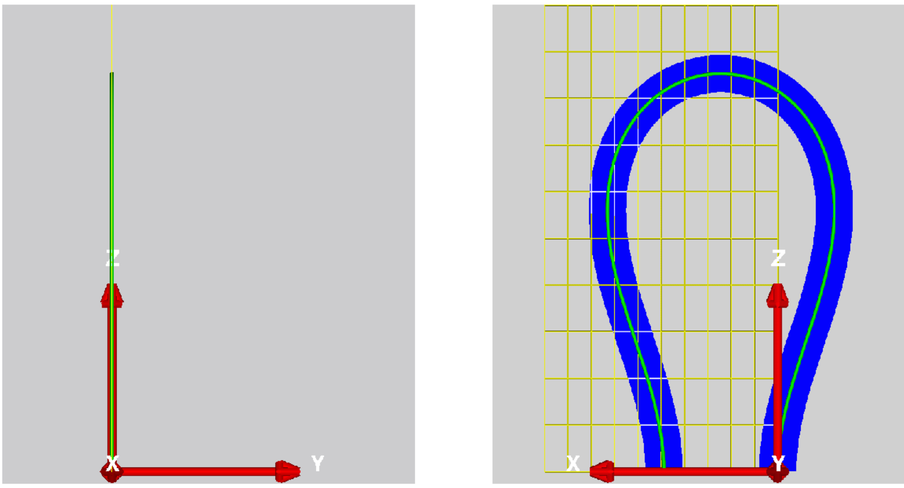

Figure 3.10: Physical Configuration on Top Branch
This figure shows the actual shape of the rod at a point along the Top Branch of Figure 3.8. The view on the left is taken looking down the x-axis, while the view on the right is rotated 90 degrees and looking down the y-axis. The rod lies in the x-z plane.

direction imposes greater stress on the rod, which will work against the tendency of the rod to move out of the plane. Further, in the most extreme case where $\rho = -1$, we see that the rod (which is of length 1) must in fact be planar, because physically it must lie in a line.

To get a clearer picture of what happens to the figure when $\hat{u}_2$ changes, we can put a series of diagrams together, each with a different value of $\hat{u}_2$ (see Figure 3.15). Notice how increasing the value of $\hat{u}_2$ changes the shape of the bifurcation diagram. The Top and Bottom Branches of the figure overlay each other, regardless of the values of $\hat{u}_2$. However, the location of the central bifurcation point goes more negative in ρ as the value of $\hat{u}_2$ increases. In addition, as was described above, the Middle Branch of the diagram perturbs from the circle in the $\hat{u}_2 = 0$ case, becoming elongated as it moves towards the Bottom Branch. When $\hat{u}_2$ becomes large enough, the connection with the Bottom Branch slides off of this diagram entirely. Figure 3.16 shows the physical configuration of the rod at a point on the Bottom Branch of this diagram, and from the right side of this figure we see that the Bottom Branch is in fact planar. Figure 3.17 shows the physical configuration at a point near the end of one of the disconnected branches. From this figure we see that the rod is approaching planar, lending further credence to the assertion that the perturbations introduced into the rod have simply slid the connection to the Bottom Branch off the diagram.

Similarly, we also can put together a series of pictures with varying K_3/K_1 ratio but constant $\hat{u}_2$ in order to see the effect of changing the K_3/K_1 ratio more

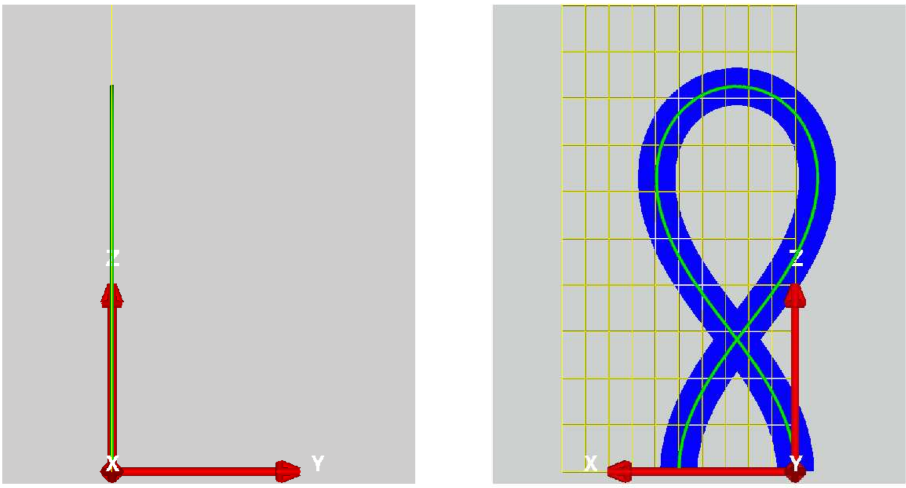

Figure 3.11: Physical Configuration on Bottom Branch
This figure shows the actual shape of the rod at a point along the Bottom Branch of Figure 3.8. The value of ρ is approximately the same as in Figure 3.10. The view on the left is taken looking down the x-axis, while the view on the right is rotated 90 degrees and looking down the y-axis. The rod lies in the x-z plane, and from the shape of the rod and from the ribbon one can see that a half-twist has been induced in the rod while traveling along the Middle Branch.

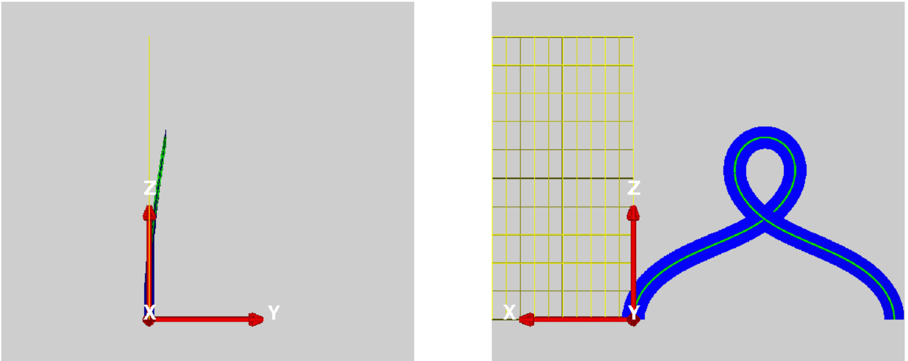

Figure 3.12: Physical Configuration on Trailing Branch
This figure shows the actual shape of the rod at a point along the Trailing Branch of Figure 3.8. The view on the left is taken looking down the x-axis, while the view on the right is rotated 90 degrees and looking down the y-axis. The loop of rod is tipped out of the x-z plane.

clearly. This diagram can be seen in Figure 3.19. Notice how increasing the value of K_3/K_1 mollifies the effects induced by the value of $\hat{u}_2$ (i.e., the shape of the bifurcation diagram approaches that in Figure 3.2). Indeed, these two parameters seem to work at odds with one another, with a higher K_3/K_1 circularizing the Middle Branch and forcing ρ to ever higher (negative) values before we see the tipping of the loop out of the plane (i.e., before we see the Trailing Branch bifurcation), effects that are exactly contrary to the effects of increasing $\hat{u}_2$ we noted earlier.

Figures 3.15 and 3.19 have another interesting feature, namely what we call the Fourth Branch. This appears to be another bifurcation from the Top and Bottom Branches of the diagram. However, AUTO does not recognize the sudden change in direction of the diagram as a bifurcation. Another interesting feature of this phenomenon is that it occurs at a constant value of $\rho = \pm 0.21888$ for all values of $\hat{u}_2 > 0$, and for all values of K_3/K_1 covered in this survey.

Figure 3.19 is very complicated in the vicinity of the Fourth Branch coming off the Bottom Branch. A closer view of this region, depicted in Figure 3.20, reveals the details nicely. Here we see that for some values of K_3/K_1, the Fourth Branch is the only branch for increasing ρ. As we increase K_3/K_1 to the maximum value (i.e., $K_3/K_1 = 1.5$), we find that the Fourth Branch does not even appear, but instead we see a complete Bottom Branch.

We also notice that some of the diagrams stop for the value of ρ where the Fourth Branch begins, neither going along the Fourth Branch nor continuing

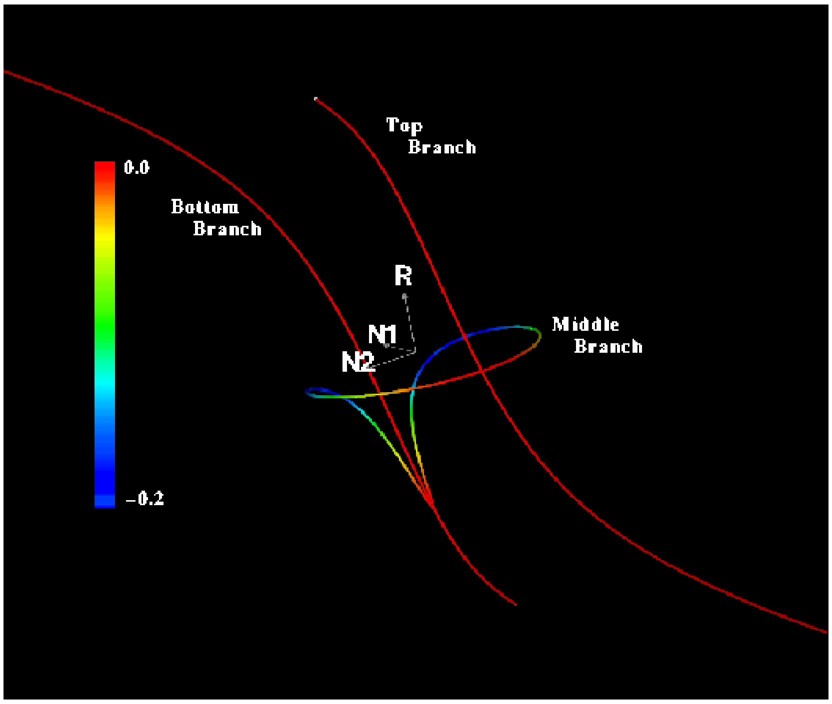

Figure 3.13: Bifurcation Diagram with Elongated Middle Branch
In this figure we see that for a relatively high value of $\hat{u}_2$, the Middle Branch is very perturbed from that seen in Figure 3.2.

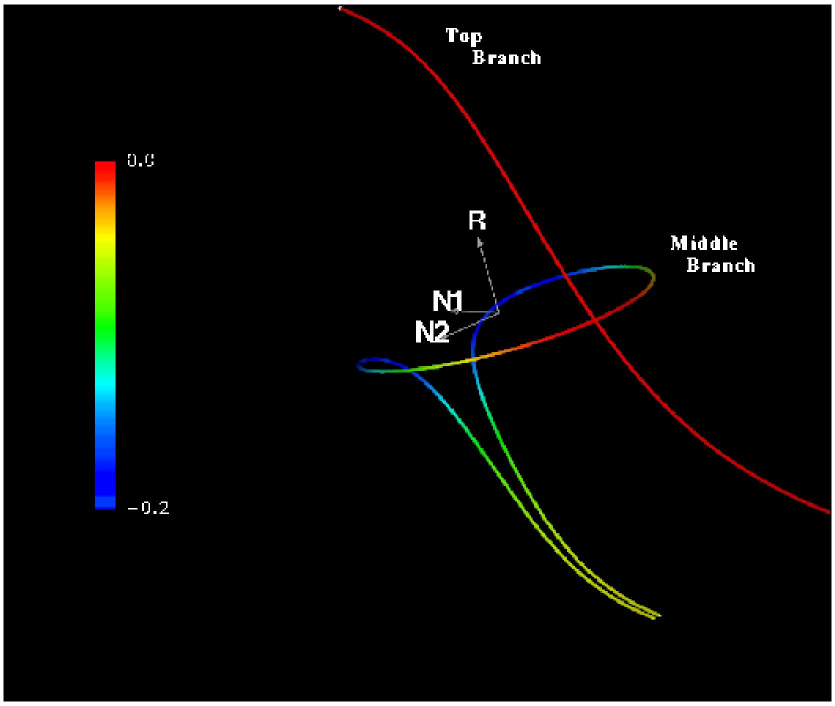

Figure 3.14: Bifurcation Diagram with Disconnected Middle Branch
Here we see that the bifurcation diagram is significantly perturbed from the Perfect Problem diagram. The bifurcation point connecting the Middle and Bottom Branches seen on other diagrams has moved off this diagram entirely, leaving the two ends of the Middle Branch disconnected. The Bottom Branch should still exist here, running between the arms of the Middle Branch with the connecting bifurcation point running far out in the negative direction.

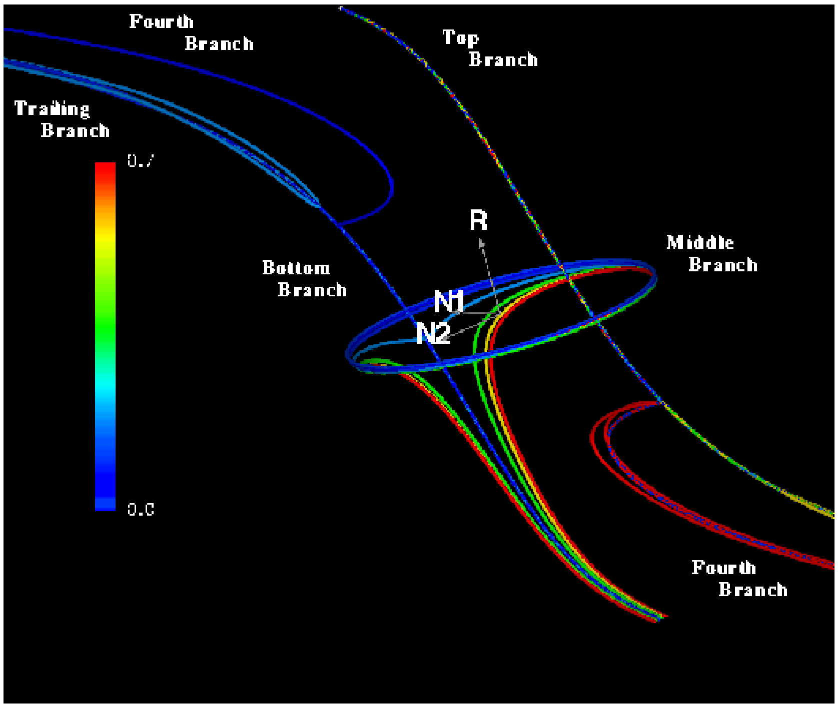

Figure 3.15: Bifurcation Diagram with Varying $\hat{u}_2$

This diagram shows how the ρ bifurcation diagrams change as a function of varying $\hat{u}_2$. The value of $\hat{u}_2$ is denoted by color, with bluer denoting lower values of $\hat{u}_2$ and redder denoting higher values of $\hat{u}_2$. The speckling of the Top Branch indicates that the branch is multi-covered in this projection. It should be noted that the Bottom Branch is also multi-covered, but all of the paths that cover it are for low values of $\hat{u}_2$ and thus the all have approximately the same color. Notice that even the green Middle Branch in this diagram is disconnected.

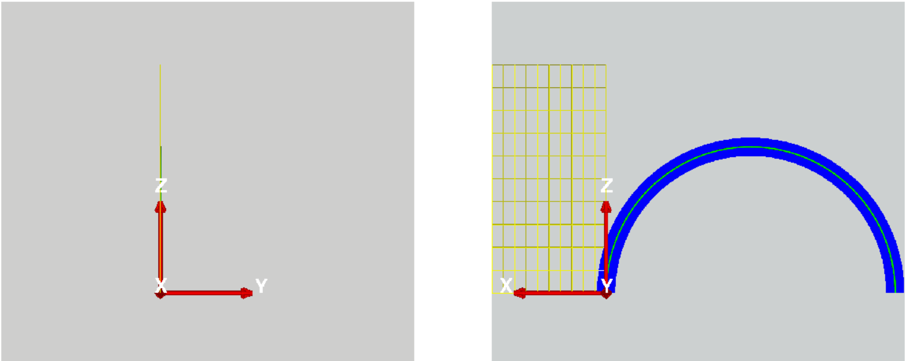

Figure 3.16: Physical Configuration on Bottom Branch
This figure shows the actual shape of the rod far out the Bottom Branch in the $\rho < 0$ direction. The view on the left is taken looking down the x-axis, while the view on the right is rotated 90 degrees and looking down the y-axis. The rod lies in the x-z plane

along the Bottom Branch. Numerically, it turns out that this is a particularly difficult region of the diagram. In fact, AUTO often gets stuck at this point and can find no other solutions, although some AUTO parameters can be altered to help it find the correct path. However, this remedy does not work in all cases, as can be seen by the omissions in the figure. Again, a physical solution must exist for all values of K_3/K_1 in this region of the diagram, but the numerics simply cannot find it.

The most striking features of Figure 3.20 are the blue and yellow bifurcations off of the Bottom Branch and the Fourth Branch, respectively, especially the oddly shaped blue bifurcating branches. We see, however, that these blue branches are simply a case of the Trailing Branch which bifurcates before the Fourth Branch bifurcation point. In this case, the bifurcating branches follow along with the Fourth Branch. The yellow branches are also Trailing Branches, but which have bifurcated after the jump to the Fourth Branch. Figure 3.21 compares the physical configurations of the rod at nearby points on the yellow and blue branches. As can be seen, the rod exhibits very similar behavior along these two branches.

3.3.2 Twisting

Now leaving aside the Sliding problem, let us consider the problem of twisting the rod at one end after the Sliding has occurred (which was the original experimental

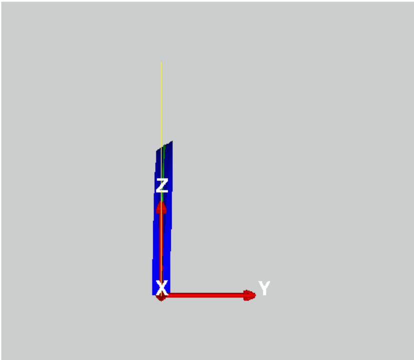

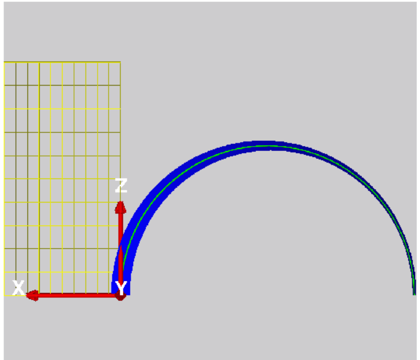

Figure 3.17: Physical Configuration on Disconnected Branch
This figure shows the actual shape of the rod far out on the disconnected Middle Branch, where it is approaching the Bottom Branch. The view on the left is taken looking down the x-axis, while the view on the right is rotated 90 degrees and looking down the y-axis. The rod is slightly out of the x-z plane.

problem we wished to model). We are interested in examining the torque applied to the $s = 0$ end of the rod as we twist the rod, and seeing how the torque changes as a function of the properties of the rod and the rod's configuration. When we look at this problem, we again notice a set of trends based on the values of K_3/K_1 and $\hat{u}_2$, and in this case also on ρ (as would be expected).

As we stated in §3.2, with $\hat{u}_2 = 0$ we have a perfectly smooth twisting torque. However, if $\hat{u}_2 \neq 0$ we observe deviations from this ideal state. As $\hat{u}_2$ grows, these deviations become larger and larger, until a fold is introduced in the solution. This fold corresponds to the ratcheting effect seen in the physical experiments. The reasoning is as follows: if one were to twist a wire that behaved like the numerics imply, then as one twisted the wire the torque required to keep twisting would follow the curve depicted in Figure 3.22. The torque would reach a maximum value and then begin to decrease, but when one reached the fold point (the angle represented by the vertical line), then suddenly there is no nearby solution as one increases the angle. If one keeps twisting the wire beyond that point, the torque undergoes a sudden jump in value down to where the vertical line intersects the curve again. This sudden jump is the ratcheting effect. An example of the effect of $\hat{u}_2$ on the twisting is shown in Figure 3.23.

This is all very nice, but the real question now is how do the twisting diagrams compare to the experimental data taken on the real wires? Figure 3.24 shows data from actual experiments carried out by Dr. Berg. Here we see the torque gradually increasing, peaking and slowly dropping, and then suddenly jumping

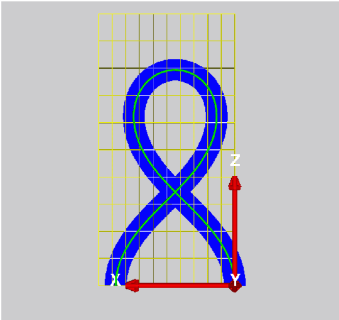

Figure 3.18a

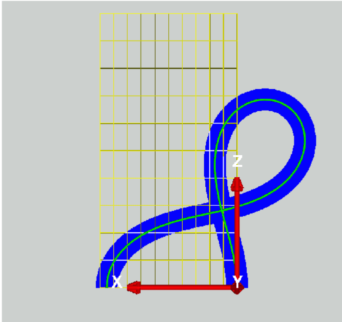

Figure 3.18b

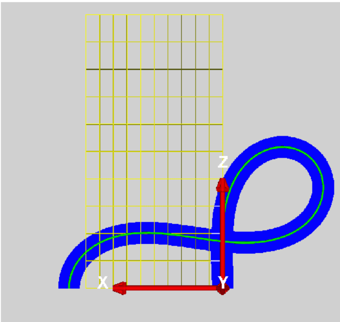

Figure 3.18c

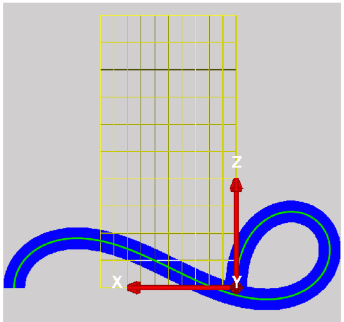

Figure 3.18d

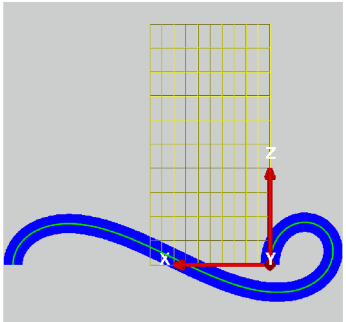

Figure 3.18e

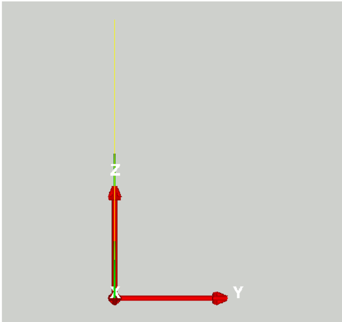

Figure 3.18f

Figure 3.18: Physical Configuration on Fourth Branch

This figure shows the evolution of the physical configuration as we move along the Fourth Branch of the bifurcation diagram. Sub-figures a-e show the collapsing if the rod from the upright position, while sub-figure f shows that the rod remains in a planar configuration as we move along this branch.

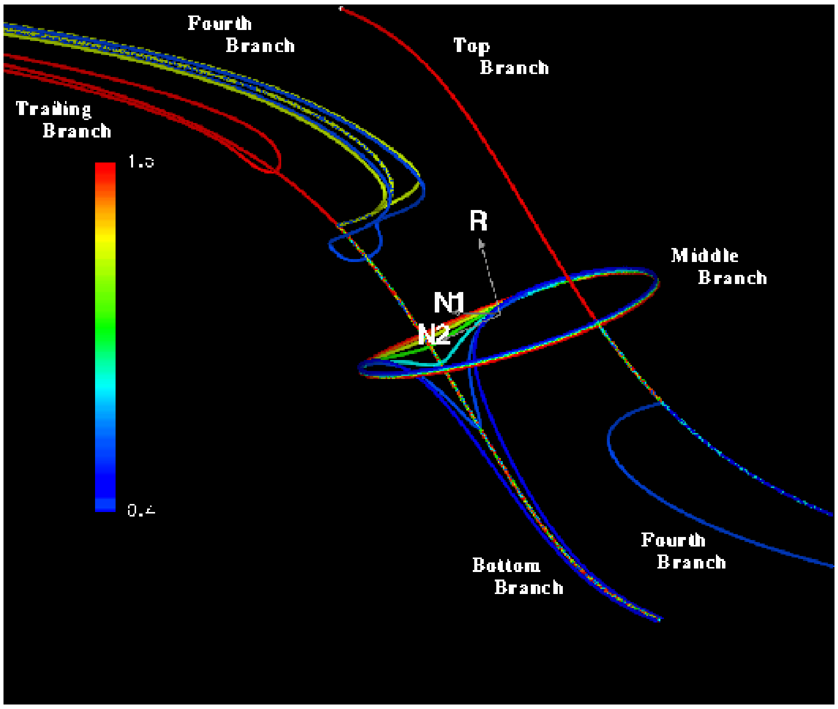

Figure 3.19: Bifurcation Diagram with Varying K_3/K_1

This diagram shows how the ρ bifurcation diagrams change as a function of varying K_3/K_1. The value of K_3/K_1 is denoted by color, with bluer denoting lower values of K_3/K_1 and redder denoting higher values of K_3/K_1. We have $\hat{u}_2 = 0.4$ in this diagram.

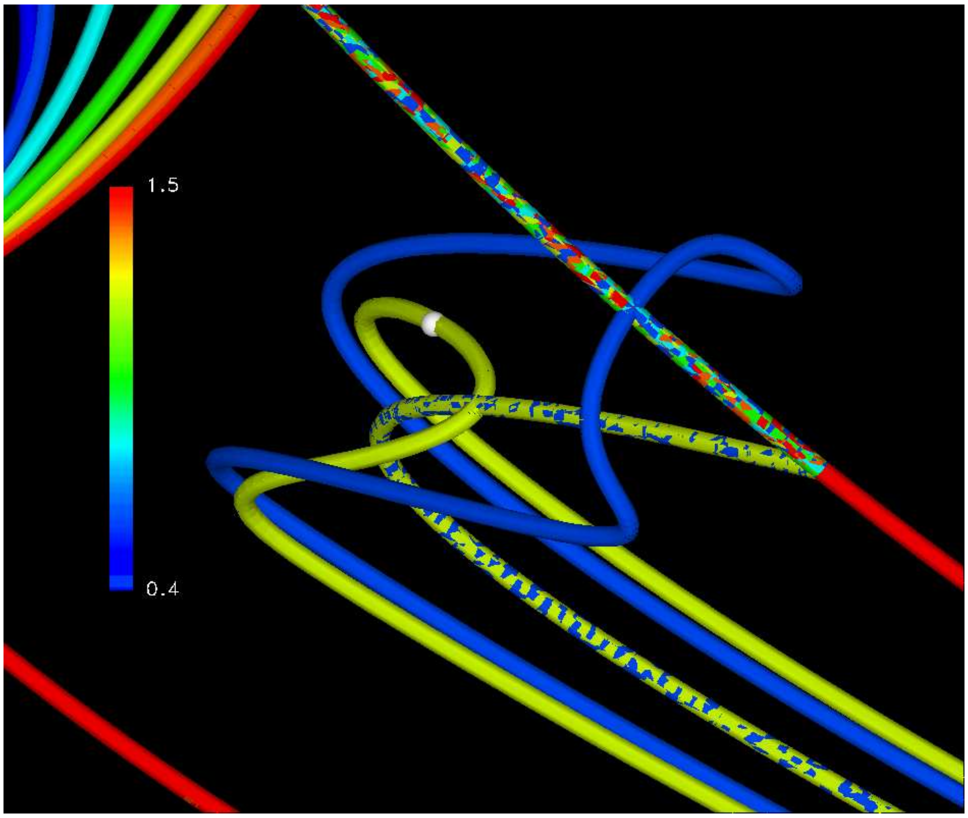

Figure 3.20: Closeup of the Fourth Branch
This diagram shows a closeup of where the Fourth Branch bifurcates from the Bottom Branch in Figure 3.19. The blue branch is for $K_3/K_1 = 0.4$, while the yellow branch is for $K_3/K_1 = 1.2$. The red branch has $K_3/K_1 = 1.5$

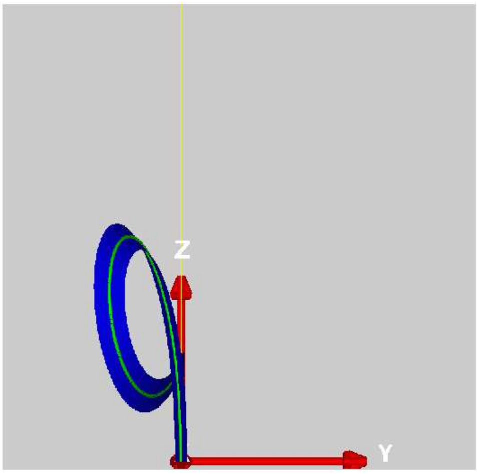

Figure 3.21a

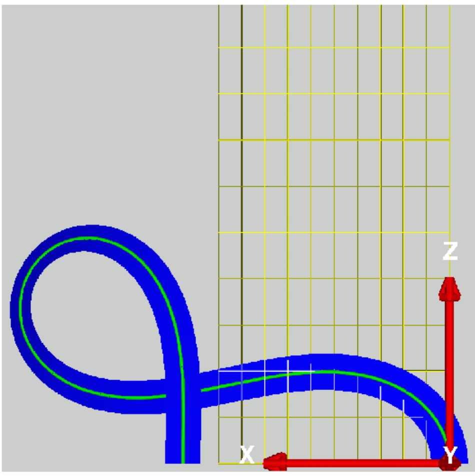

Figure 3.21b

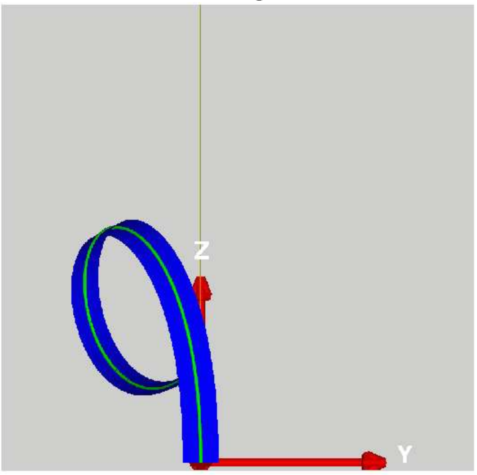

Figure 3.21c

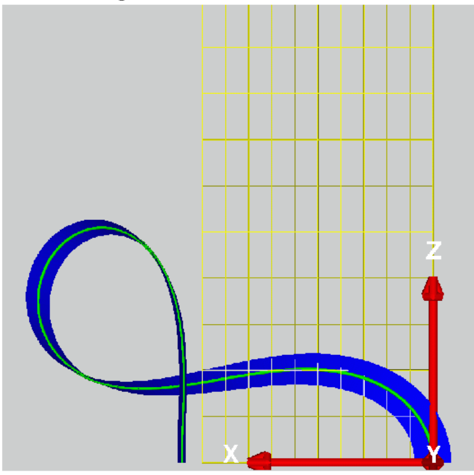

Figure 3.21d

Figure 3.21: Comparison of Physical Configurations of Different Fourth Branch Bifurcations
This figure shows the physical configuration as we move from a point on the yellow branch to a nearby point on the blue branch in Figure 3.20. Sub-figures a and b show the configuration on the yellow branch, while sub-figures c and d show the configuration on the blue branch.

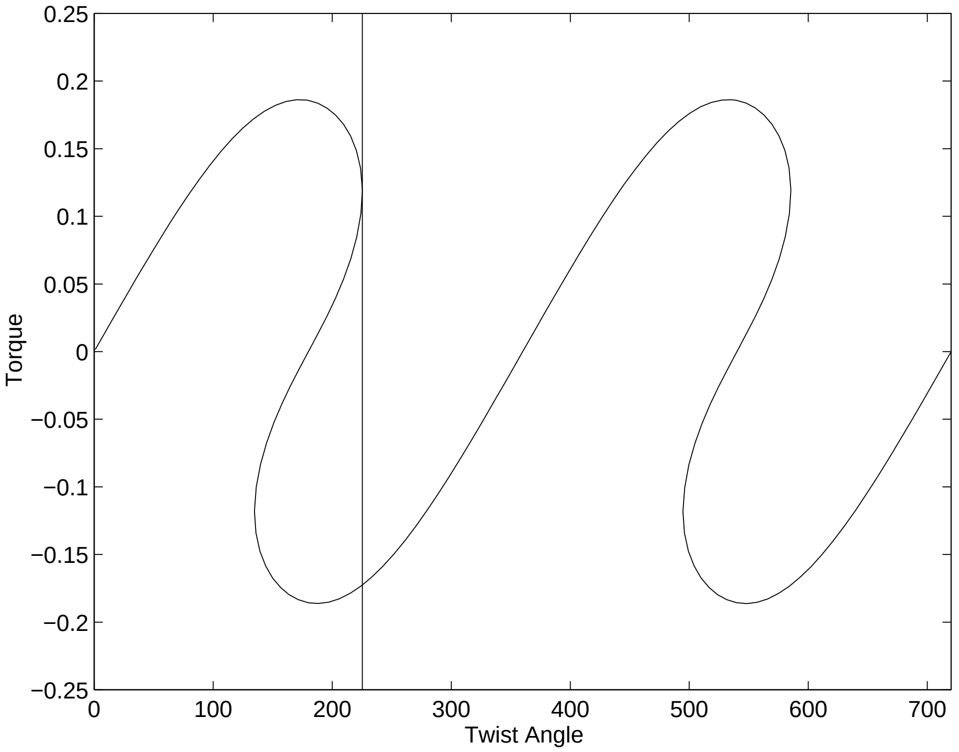

Figure 3.22: Demonstration of Ratcheting Effect
This diagram shows the behavior of the rod as it is twisted for $\rho = 0.6$, $K_3/K_1 = 0.4$, and $\hat{u}_2 = 0.6$. The vertical line lies tangent to the curve just at the point of the fold.

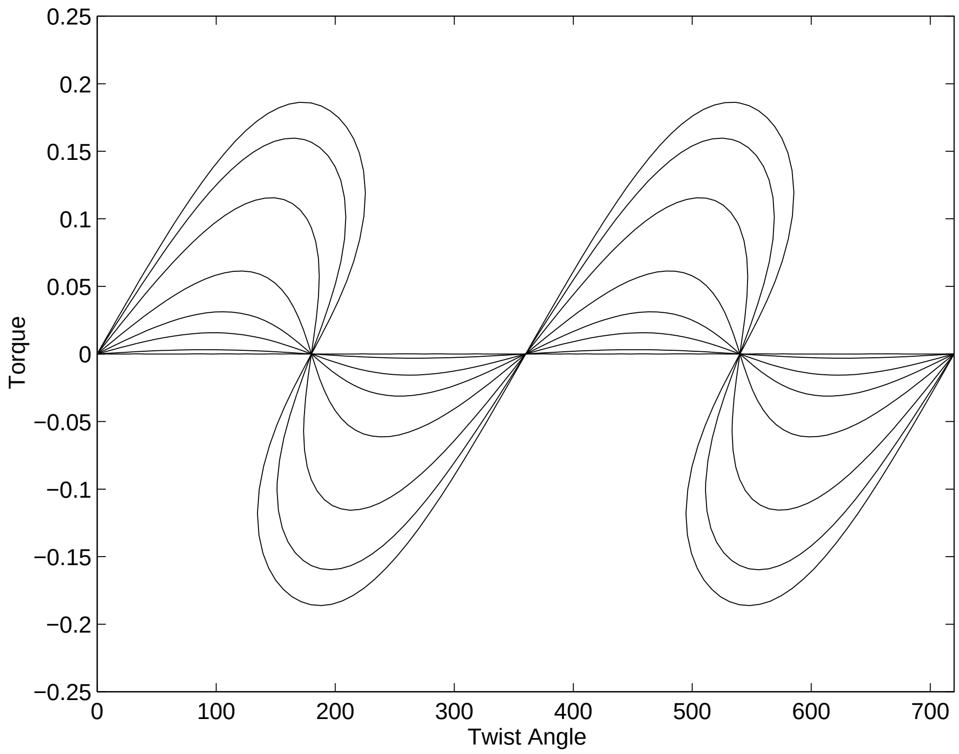

Figure 3.23: Twist Angle vs m_3 for $\rho = 0.4$, $K_3/K_1 = 0.4$

This diagram shows the behavior of the rod as it is twisted for $\hat{u}_2 = 0, 0.01, 0.03, 0.05, 0.1, 0.2, 0.4,$ and 0.6. Each curve represents the behavior at a different value of $\hat{u}_2$, with deviations from zero torque growing as the value of $\hat{u}_2$ grows. Notice that the folds, which correspond to ratcheting, appear and become more pronounced as $\hat{u}_2$ increases (the curves for $\hat{u}_2 = 0.01$ and $\hat{u}_2 = 0$ are almost indistinguishable).

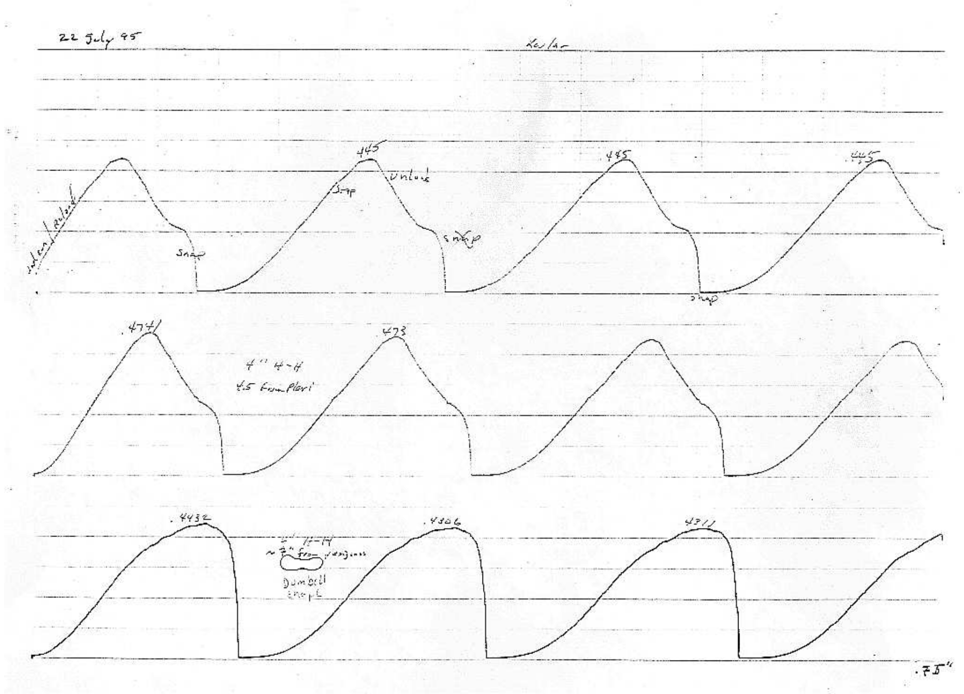

Figure 3.24: Experimental Data
This is a copy of actual experimental data collected by Dr. Berg. As with the computed data, the plots are of twist angle vs torque. This data was collected for a wire bent into a full circle, with orientation and position BCs enforced in the center of the rod as well as the ends. The experiment also could not measure a negative torque, so the encounter with a fold is analogous to the jump down in the torque followed by a flat stretch. The three separate plots represent different unstressed configurations of the wire.

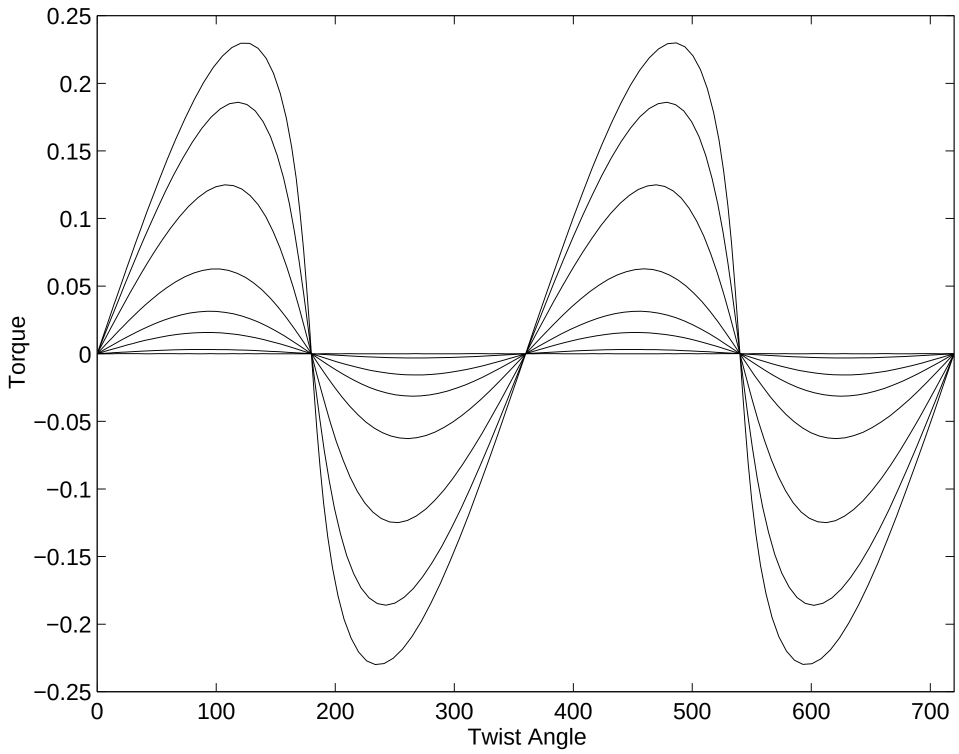

Figure 3.25: Twist Angle vs m_3 for $\rho = 0.4$, $K_3/K_1 = 1.4$
This diagram shows the behavior of the rod as it is twisted for $\hat{u}_2 = 0, 0.01, 0.03, 0.05, 0.1, 0.2, 0.4$, and 0.6. Notice the folds are almost entirely absent from this diagram (the highest value of $\hat{u}_2$ does exhibit a small fold, which is imperceptible to the resolution of this diagram). Even so, it does exhibit an extremely steep slope, which represents a very rapid change in the torque as the rod is twisted near the angle $\pi/2$.

to 0 (i.e., ratcheting). The experimental design was only able to detect positive torques, so we see the torque remaining fixed at 0 for a stretch before it builds up again, repeating the pattern. The experimental data looks strikingly similar to the numerical results, and gives us good reason to believe that we are modeling the experiments correctly.

As with the deformation process, we find that the effects of increasing $\hat{u}_2$ are somewhat mollified by a larger K_3/K_1 ratio, to the point where, for even the largest values of $\hat{u}_2$ used in this survey, the largest K_3/K_1 all but eliminates the fold. This mollification is demonstrated in Figure 3.25 as compared to Figure 3.23.

Now, however, the picture is complicated by the addition of the ρ parameter. In this instance, we have the situation where $\rho = 2/\pi$ (i.e., when the rod is in a semi-circular configuration) is the value which produces the most gentle twisting torque for given values of $\hat{u}_2$ and K_3/K_1. Deformation from this configuration leads rapidly to much more wild behavior of the twisting motion, and much larger folds in the diagrams. The effects of changing ρ for a constant $\hat{u}_2$ and K_3/K_1 can

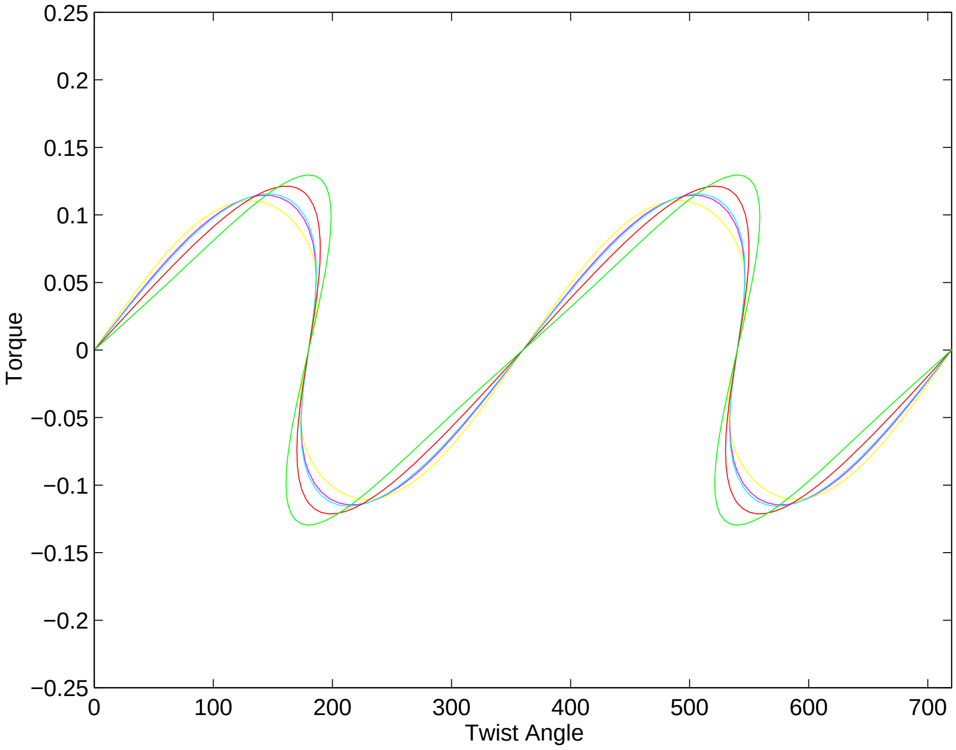

Figure 3.26: Twist Angle vs m_3 for $\hat{u}_2 = 0.4$, $K_3/K_1 = 0.4$

This diagram was made for values of $\rho = 0.8, 2/\pi, 0.6, 0.4$, and 0.2. The ordering of the lines is yellow, magenta, light blue, red, and green, which corresponds directly to the stated values of ρ. Notice how, as the value of ρ decreases (i.e., more stress is placed on the rod), the maximum torques become larger and the folds become deeper.

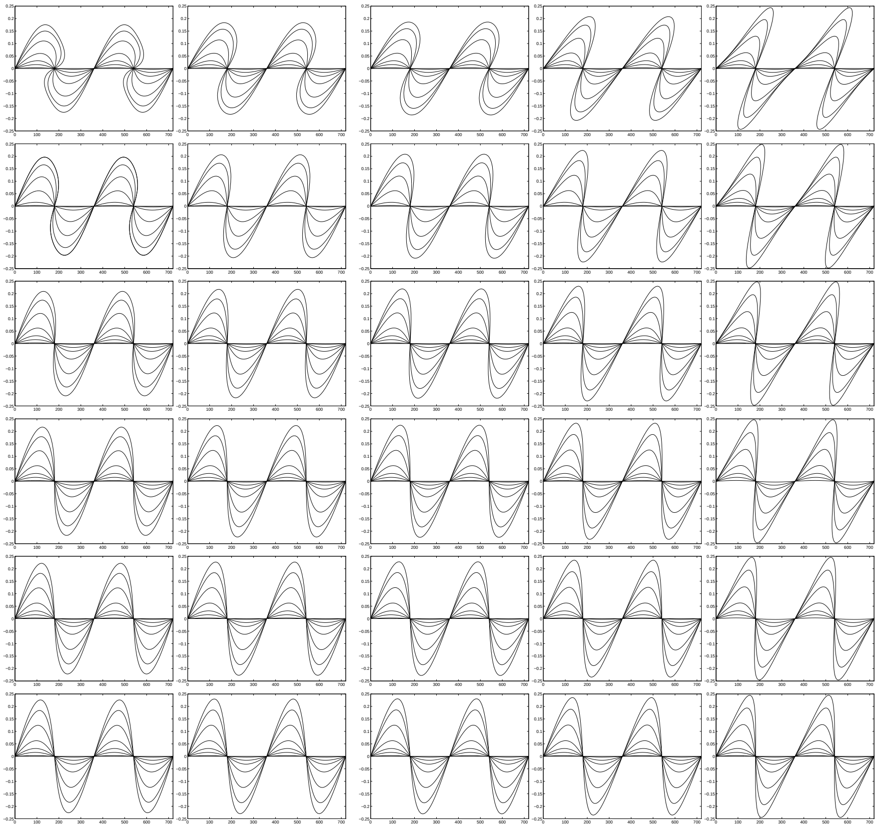

Figure 3.27: Survey of Torque Diagrams
These diagrams show how the torque changes with ρ, K_3/K_1, and $\hat{u}_2$. Each individual diagram shows the behavior of the torque for the various values of $\hat{u}_2 = 0, 0.01, 0.03, 0.05, 0.1, 0.2, 0.4$, and 0.6. As the diagrams go across from left to right, the value of ρ changes, covering values of $\rho = 0.8, 2/\pi(\approx 0.6366), 0.6, 0.4$, and 0.2. As the diagrams go down the value of K_3/K_1 changes, encompassing values of $K_3/K_1 = 0.4, 0.6, 0.8, 1.0, 1.2$, and 1.4.

be seen in Figure 3.26.

To more clearly see the dependency of the torque on ρ, θ, $\hat{u}_2$, and K_3/K_1, all of the torque diagrams (for this survey) have been compiled in to a single diagram (see Figure 3.27). Within each diagram in Figure 3.27, we see the behavior becoming more wild as the value of $\hat{u}_2$ increases. In addition, viewing successive diagrams from left to right, we see the the behavior of the rod also becoming more extreme as more stress is placed on the rod (i.e., as the value of ρ decreases). Working against these trends, viewing successive diagrams from top to bottom, we see the effects of increased $\hat{u}_2$ and ρ somewhat mollified by the increasing value of K_3/K_1. Full sized versions of all of these diagrams can be found in Appendix B.

3.4 Helical Rod

The ultimate intent of the experimentation was to show that a wire with a helical rest configuration would behave in a way that was more conducive to the surgical procedures for which it would be used (i.e., ratcheting for a given curvature $|\hat{\mathbf{u}}|$ would be less if the unstressed shape of rod is helical instead of an arc of a circle). Accordingly, the form of the unstressed curvature was assumed to be

$$\hat{\mathbf{u}} = (\kappa \sin(s\tau\pi), \kappa \cos(s\tau\pi), 0)^T, \tag{3.14}$$

where κ is the curvature, τ is the torsion, and s is the arc-length parameter. Note that $\kappa = |\hat{\mathbf{u}}|$. This form was chosen so that, as $\tau \to 0$, the unstressed shape of the rod would go to the circular arc discussed above. Therefor we can think of this as a perturbation of the non-helical problem.

The main property we were interested in investigating was smoothness of the torque needed to twist the rod. We saw above that the rod turns perfectly smoothly when $\hat{\mathbf{u}} = \mathbf{0}$, and the twisting motion is nearly smooth when this ideal condition is approximated. But in practice the rod is stored is loops, so the rod takes a set in storage and thus is not straight. If the rod is untwisted when it is stored the set will be planar, but if the rod is twisted when it is stored then the set will be helical.

We saw in §3.3.2 that large discontinuities can arise when twisting a rod with nonzero $|\hat{\mathbf{u}}|$. However, when we introduce a $\hat{\mathbf{u}}$ with a helical form (see Figure 3.28), rather than the form of a simple semicircular unstressed curvature, we find that the deviations from smooth twisting can be reduced. In Figure 3.29 we see that by making the rod helical, we can significantly reduce the range from maximum to minimum torque. However, even though we have reduced this range, we have not managed to eliminate the ratcheting phenomenon altogether, although the size of the jump has been reduced. We also note that a minimum in the smoothing has been reached in this diagram. We see that the deviation from zero torque for the second red line ($\tau = 2.0$) are larger than those for the second light-blue line ($\tau = 1.5$). This implies that simply increasing the value of τ ad infinitum will not reduce the torque to zero.

Complementing this result on ratcheting, we have Figure 3.30, which shows the effects of having a helical shape in a situation when there is no ratcheting. In this diagram, we see that having a rod with helical unstressed shape can dramatically reduce the torque required to twist the wire.

In light of this very modest survey, we see that using a helically curved wire for the surgical procedures could be beneficial. Some benefit could be derived by giving the wire some helical curvature, with reductions in the variability of the torque required to twist the wire. However, so far as this survey is concerned, the ratcheting phenomenon would not be eliminated.

3.5 Free End Problem

In the initial description of the experiment, the $\sigma = 1$ end of the wire was thought to be not only free to rotate, but also free to slide (i.e., the wire could feed through,

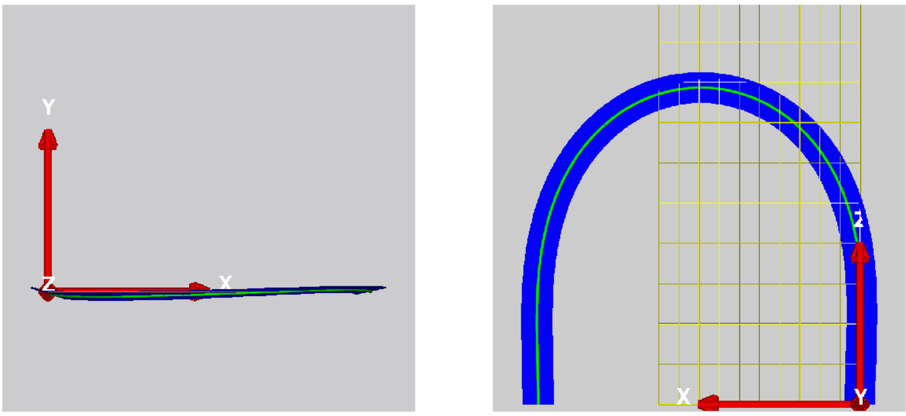

Figure 3.28: Helical $\hat{\mathbf{u}}$ Physical Configuration
This diagram shows the physical configuration of a rod with helical $\hat{\mathbf{u}}$. Here $\tau = 2$. The figure on the left is the view looking down the z-axis on the rod, while the figure of the right is looking down the y-axis. The rod is slightly non-planar.

either lengthening or shortening between the places of fixed orientation) until it reached an equilibrium configuration (i.e., when $n_3 = 0$).

For anything but a straight rod, however, this proved to be infeasible numerically, as $n_3 \neq 0$ unless the rod was planar (see e.g. Figure 3.31). As with the torque survey, we find that the magnitude of n_3 grows as varying ρ moves the physical shape of the rod away from a semi-circle (Figure 3.32), and also as $\hat{u}_2$ increases (Figure 3.33), but is reduced as K_3/K_1 becomes large (Figure 3.34).

One can get a better feel for how the force changes with ρ by looking at a diagram in which twisting is performed much more frequently (say, at every tenth point of the continuation in ρ). Such a diagram is shown in Figure 3.35. In this diagram one can see the folds, and the gradual changes in the twisting action as ρ changes can be seen to form a surface in this space. Another interesting fact emerges when we look at this diagram. Recalling the discussion from §3.3.1, we see that the only equilibria with $n_3 = 0$ are planar solutions.

When we try to do the continuation in twist angle in the free end case, we find that the problem has non-isolated planar solutions corresponding to changes in length. Hence the linearization of the system is singular, and we have no guarantee that the continuation can be achieved in an arbitrary parameter (e.g., twist angle). The numerics indicate that indeed continuation in twist angle is not possible. The fact that in all computations of the fixed problem the only solutions with $n_3 = 0$ were planar also lends credence to the inappropriateness of the free-end model.

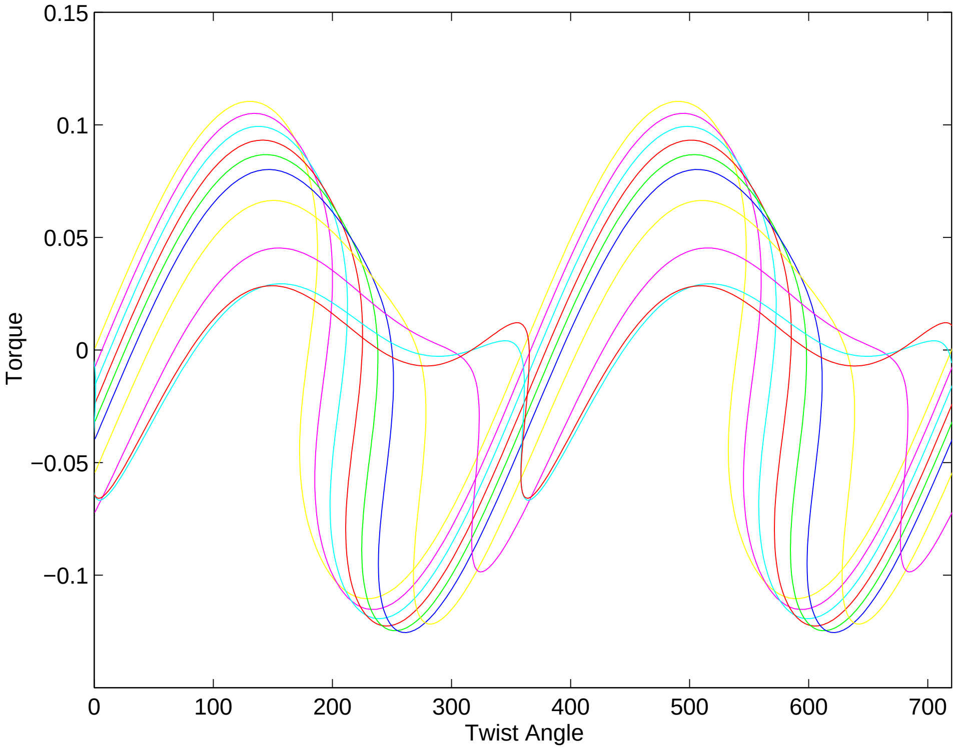

Figure 3.29: Helical $\hat{\mathbf{u}}$ Twisting Diagram with Ratcheting

This diagram shows the torques needed to twist rods with values of $\tau = 0, 0.1, 0.2, 0.3, 0.4, 0.5, 0.7, 1.0, 1.5,$ and 2.0. The other pertinent values are $\rho = 0.8$, $\hat{u}_2 = 0.4$, and $K_3/K_1 = 0.4$. The path with the largest deviation from 0 is for $\tau = 0$ (i.e., for a simply-curved rod). The lines repeatedly cycle through the colors yellow, magenta, light blue, red, green, and violet. The colors correspond directly to the stated values of τ.

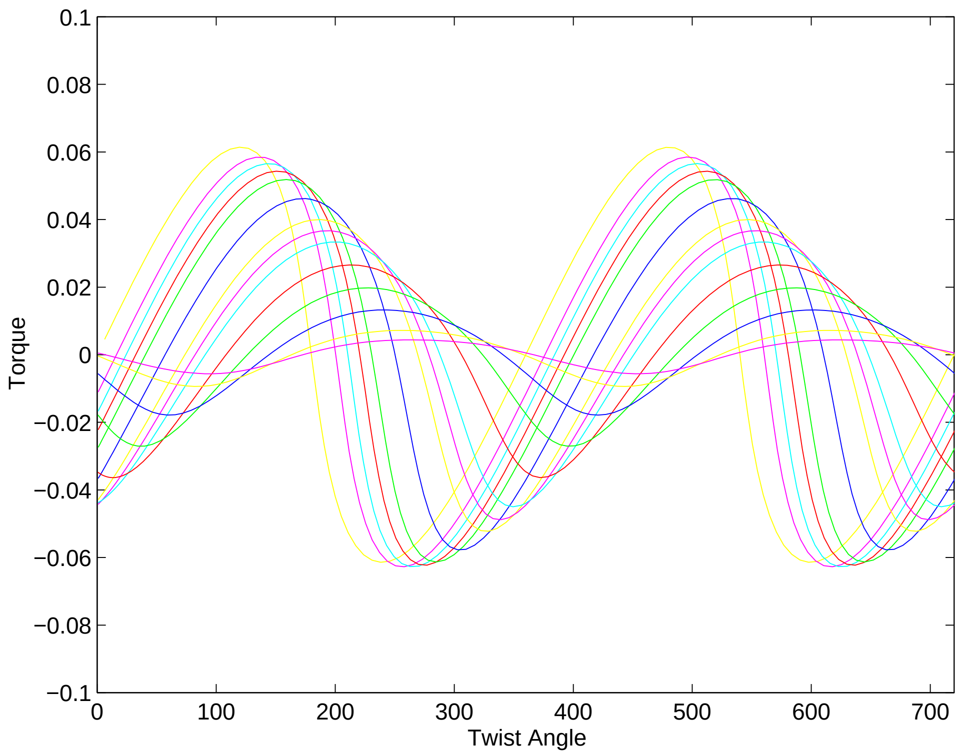

Figure 3.30: Helical $\hat{\mathbf{u}}$ Twisting Diagram without Ratcheting
This diagram shows the torques needed to twist rods with values of $\tau = 0, 0.2, 0.3, 0.4, 0.5, 0.7, 0.9, 1.0, 1.1, 1.3, 1.5, 1.7, 1.9,$ and 2.0. The other pertinent values are $\rho = 0.6$, $\hat{u}_2 = 0.2$, and $K_3/K_1 = 0.4$. The path with the largest deviation from 0 is for $\tau = 0$ (i.e., for a simply-curved rod). The lines repeatedly cycle through the colors yellow, magenta, light blue, red, green, and violet. The colors correspond directly to the stated values of τ.

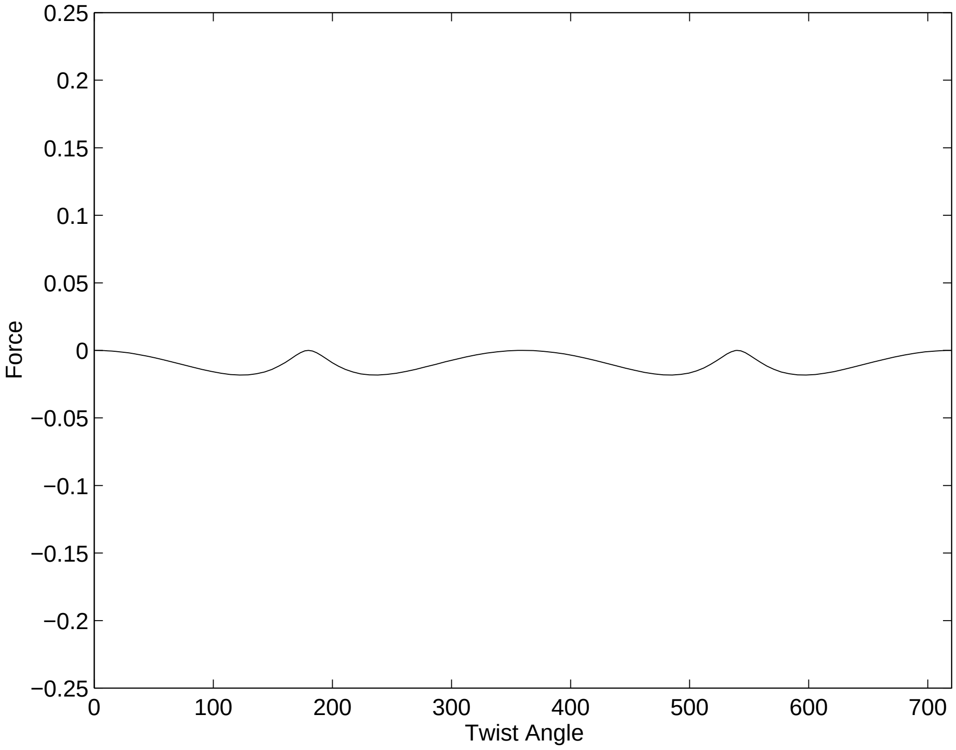

Figure 3.31: Twist Angle vs n_3 for $\hat{u}_2 = 0.1$, $K_3/K_1 = 0.4$, $\rho = 2/\pi$

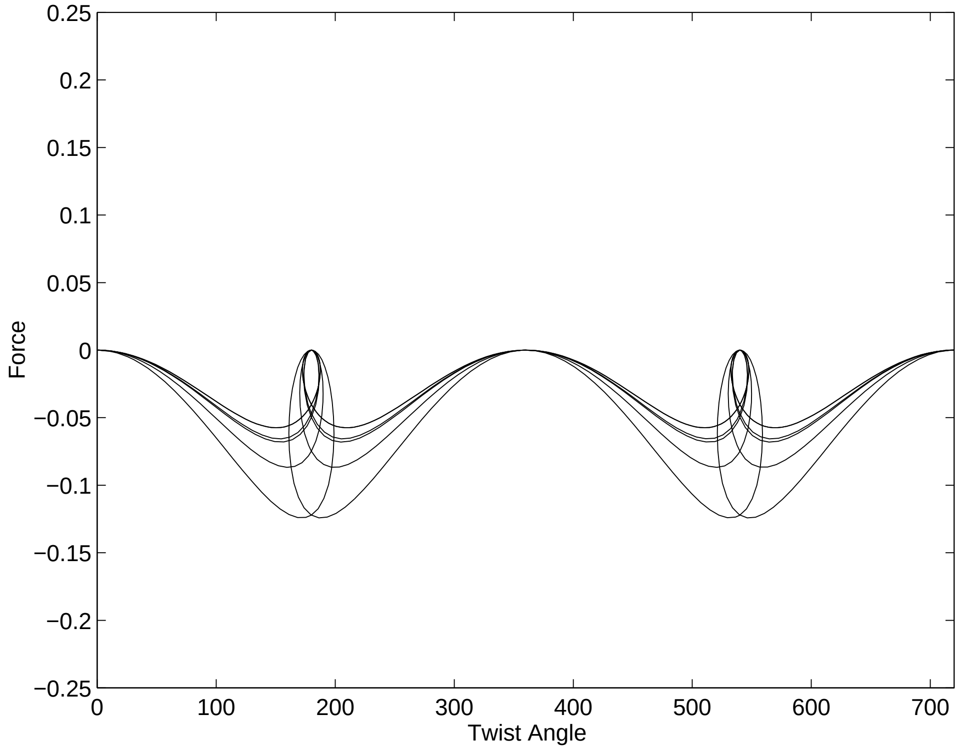

Figure 3.32: Twist Angle vs n_3 for Varying ρ
This plot is taken with $\hat{u}_2 = 0.4$ and $K_3/K_1 = 0.4$. Here the deviation of the curves from $n_3 = 0$ increases as ρ decreases.

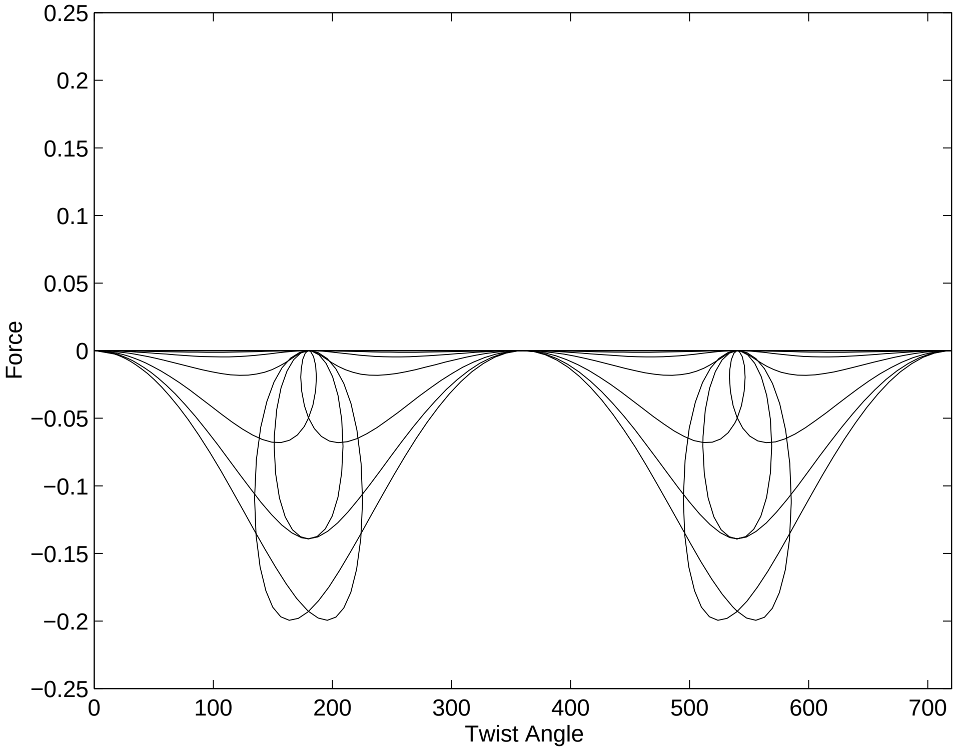

Figure 3.33: Twist Angle vs n_3 for Varying $\hat{u}_2$
This plot is taken with $\rho = 0.2$ and $K_3/K_1 = 0.4$. Here the deviation of the curves from from $n_3 = 0$ increases as $\hat{u}_2$ increases. Notice how n_3 varies much more wildly as $\hat{u}_2$ increases, much as was the case when looking at m_3.

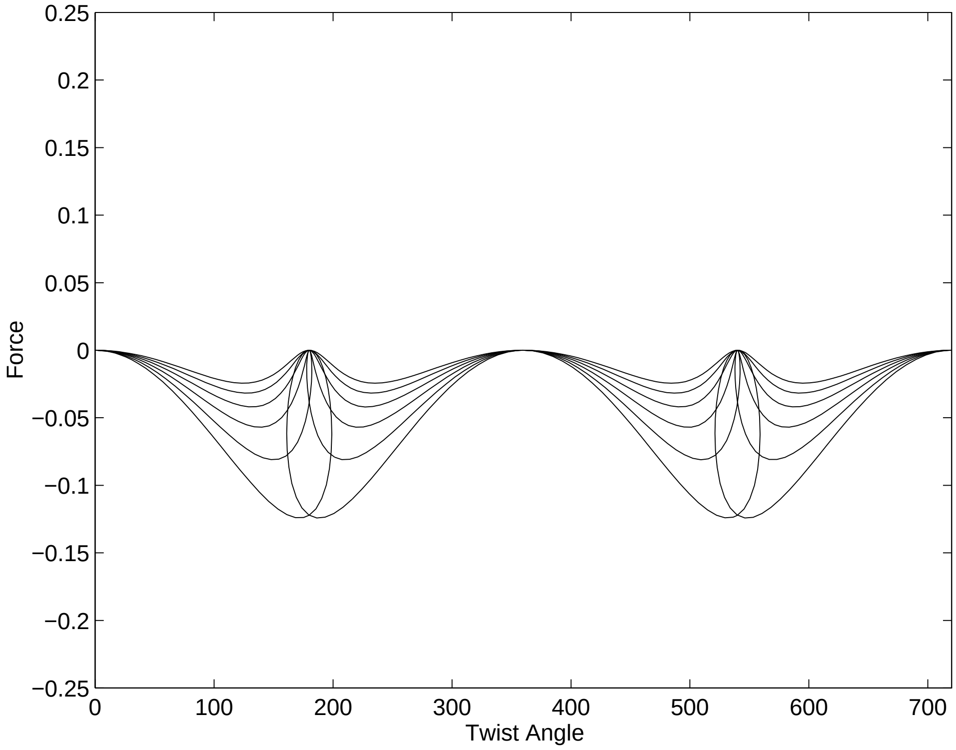

Figure 3.34: Twist Angle vs n_3 for Varying K_3/K_1
This plot is taken with $\rho = 0.2$ and $\hat{u}_2 = 0.4$. Here the deviation of the curves from from $n_3 = 0$ increases as K_3/K_1 decreases. Notice the mollifying effect increasing K_3/K_1 has on n_3 when the rod is twisted, again much like the case when looking at m_3.

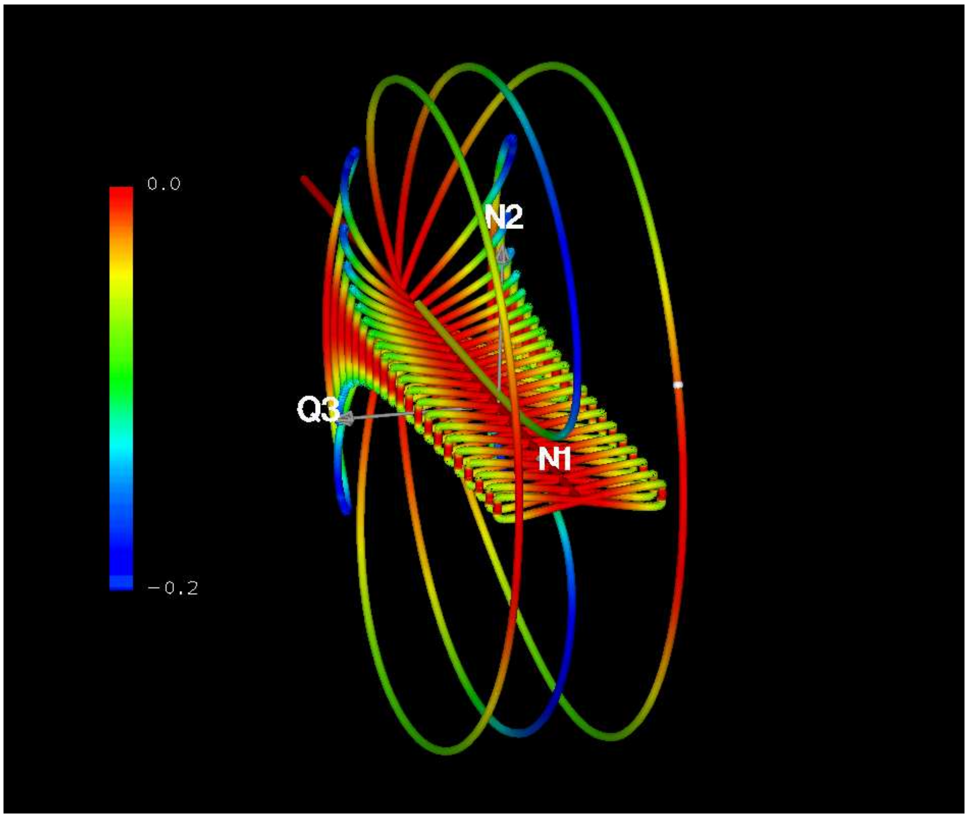

Figure 3.35: Twisted Bifurcation Diagram Mapping n_3
Bifurcation diagram for ρ with $\hat{u}_2 = 0.4$ and $K_3/K_1 = 0.4$, where twisting has been performed at every 10^{th} continuation step in ρ. In this diagram, the color represents n_3, where bluer denotes a more negative value of n_3 and redder denotes a less negative value of n_3. n_3 approaches 0 only as the rod approaches a planar configuration.

Chapter 4

Numerical Accuracy and Alternative Numerical Formulations

This chapter is concerned with the properties of the numerical approximation to Eqs. (2.31). Consequently, in Section 4.1 we discuss a convergence study, in which we explore the reasonableness of the numerical parameters we chose for our approximation. In Section 4.2 we discuss rewriting Eqs. (2.31) in a different form to make the numerical computations more efficient. In Section 4.3 we discuss using an Analytic Jacobian in place of the Numeric Jacobian calculated by AUTO, as a way to further speed up the computations. And finally in Section 4.4 we compare the different computation methods, both in terms of results and in terms of efficiency (i.e., CPU usage).

4.1 Numerical Accuracy

When performing any numeric calculation of this sort, one needs to be sure that the algorithm is converging. The way we did that here was a multi-step process. First we reduced the collocation step-size (i.e., we increased the number of Gauss points from 4 to 6) and then checked to make sure the results were the same as when fewer collocation points were used. We then increased the number of mesh intervals (from 30 to 60), and again compared the results. Finally, we increased both the number of Gauss points and the number of mesh intervals and again compared the results. In each case we checked the results numerical results at 6 to 8 points, and in all cases we found the numeric results to match to within 6 decimal places.

This study convinced us of the appropriateness of our numerical parameters, and gave us confidence that the numerical results had converged to within the assumed tolerances.

4.2 Alternative Formulations

In this section we first discuss methods for reducing the order of Eqs. (2.31), first by parameterizing the $\mathbf{n}$ variables and then by removing the $\mathbf{r}$ variables and replacing their associated BCs with Integral Constraints. Following that, we discuss a method for replacing the Integral Constraints themselves with other BCs based on integrals of the system.

4.2.1 Reduction of Order

The order of Eqs. (2.31) is 15, but we notice that some of the equations lend themselves quite readily to parameterization. Since $\mathbf{n}$ is constant for any given configuration, its components can clearly be replaced by parameters as long as 15 BCs can be found which are not conditions on $\mathbf{n}$ itself. As it turns out, none of the BCs are conditions on $\mathbf{n}$, so all the original BCs can be retained.

Thus the system can be easily reduced to the following 12 differential equations, with the 15 BCs originally noted in §3.1 (Eqs. (3.1) - (3.8)) and three free parameters. In our notation, we replace n_i with $\mathcal{N}_i$ to denote the switch of $\mathbf{n}$ from an s-dependent variable to a parameter.

$$\mathbf{r}_\sigma = \mathbf{d}_3 \tag{4.1}$$

$$\mathbf{q}_\sigma = (K_j^{-1} m_j + \hat{u}_j)\frac{1}{2}\mathbf{B}_j\mathbf{q} \tag{4.2}$$

$$\boldsymbol{\mu}_\sigma = (\mathrm{K}_\mathrm{j}^{-1}\mathrm{m}_\mathrm{j} + \hat{\mathrm{u}}_\mathrm{j})\frac{1}{2}\mathbf{B}_\mathrm{j}\boldsymbol{\mu} - \mathbf{D}_3[\mathbf{q}]\mathcal{N} \tag{4.3}$$

$$s_\sigma = 1 \tag{4.4}$$

Once this is done, we see that we can reduce the order further by removing the $\mathbf{r}_\sigma$ equations because none of the other equation right hand sides involve $\mathbf{r}$. However, six of the BCs do involve the r_i. The three BCs $\mathbf{r}(0) = \mathbf{0}$ can simply be associated with the removed $\mathbf{r}_\sigma$ equations, but the $\mathbf{r}(1) = (\rho, 0, 0)^T$ must be associated with the remaining system in order that it be well-posed.

Thus we must determine three new constraints on the reduced system of equations. As AUTO can accommodate integral constraints, the most expedient thing to do is to use the pointwise constraint.

First we note that $\mathbf{r}_\sigma = \mathbf{d}_3$ to write

$$\mathbf{r}(1) - \mathbf{r}(0) = \int_0^1 \mathbf{r}_\sigma = \int_0^1 \mathbf{d}_3. \tag{4.5}$$

Further, we have that the $\mathbf{d}_3$ are expressed in terms of $\mathbf{q}$. So the boundary condition $\mathbf{r}(1) - \mathbf{r}(0) = (\rho, 0, 0)^T$ can be rewritten in the form

$$r_1(1) - r_1(0) = \rho = \int_0^1 (q_1q_3 + q_2q_4)d\sigma \tag{4.6}$$

$$r_2(1) - r_2(0) = 0 = \int_0^1 (q_2q_3 - q_1q_4)d\sigma \tag{4.7}$$

$$r_3(1) - r_3(0) = 0 = \int_0^1 (-q_1^2 - q_2^2 + q_3^2 + q_4^2)d\sigma \tag{4.8}$$

The first integral constraint can be rewritten

$$0 = \int_0^1 (q_1q_3 + q_2q_4 - \rho)d\sigma. \tag{4.9}$$

And so we are left with the following system of nine equations in nine variables and three free parameters, with nine BCs and three Integral Constraints:

$$\mathbf{q}_\sigma = (K_j^{-1} m_j + \hat{u}_j)\frac{1}{2}\mathbf{B}_j\mathbf{q} \tag{4.10}$$

$$\boldsymbol{\mu}_\sigma = (K_j^{-1} m_j + \hat{u}_j)\frac{1}{2}\mathbf{B}_j\boldsymbol{\mu} - \mathbf{D}_3[\mathbf{q}]\mathcal{N} \tag{4.11}$$

$$s_\sigma = 1 \tag{4.12}$$

The integral constraints are as in Eqs. (4.7), (4.8), and (4.9), and the nine BCs are as in Eqs. (3.3) - (3.8).

4.2.2 Rewriting Integrals as Boundary Conditions

A further modification to the system can be made by noticing that the Integral Constraints discussed in the previous section can be replaced by additional BCs, thus eliminating the necessity of computing the Integral Constraints. This is done in the following way:

We know from the discussion in §2.2.3 that the quantities $\mathbf{m} + \mathbf{r} \times \mathcal{N}$ and $\boldsymbol{\mu} \cdot \mathbf{q} + 2\mathbf{r} \cdot \mathcal{N}$ are constants of the motion. Taking the vector product of the first expression with $\mathcal{N}$, we get

$$(\mathcal{N} \cdot \mathcal{N})\mathbf{r} + (\mathbf{r} \cdot \mathcal{N})\mathcal{N} + \mathcal{N} \times \mathbf{m} = \mathbf{C}, \tag{4.13}$$

with $\mathbf{C}$ a constant vector. Solving $\boldsymbol{\mu} \cdot \mathbf{q} + 2\mathbf{r} \cdot \mathcal{N} = \mathbf{const}$ for $\mathbf{r} \cdot \mathcal{N}$ and substituting into (4.13), we are left with

$$(\mathcal{N} \cdot \mathcal{N})\mathbf{r} + \frac{1}{2}(\mathbf{q} \cdot \boldsymbol{\mu})\mathcal{N} + \mathcal{N} \times \mathbf{m} = \mathbf{C} \tag{4.14}$$

Evaluating at the endpoints, we get

$$\left[(\mathcal{N} \cdot \mathcal{N})\mathbf{r} + \frac{1}{2}(\mathbf{q} \cdot \boldsymbol{\mu})\mathcal{N} + \mathcal{N} \times \mathbf{m}\right]_0^1 = \mathbf{0}. \tag{4.15}$$

But we know from our original BCs that $\mathbf{r}(0) = \mathbf{0}$ and $(\mathbf{q} \cdot \boldsymbol{\mu})(0) = \mathbf{0}$, so this reduces our equation to

$$(\mathcal{N} \cdot \mathcal{N})\mathbf{r}\Big|_1 + \frac{1}{2}(\mathbf{q} \cdot \boldsymbol{\mu})\mathcal{N}\Big|_1 + \mathcal{N} \times \mathbf{m}\Big|_0^1 = \mathbf{0}. \tag{4.16}$$

Also recall that $\mathbf{r}(1) = (\rho, 0, 0)^T$. With this, we get that Eq. (4.16) provides the following set of three boundary conditions:

$$\mathcal{N} \cdot \mathcal{N}\rho + \frac{1}{2}(\mathbf{q} \cdot \boldsymbol{\mu})(1)\mathcal{N}_1 + (\mathcal{N}_2 m_3 - \mathcal{N}_3 m_2)\Big|_0^1 = 0 \tag{4.17}$$

$$\frac{1}{2}(\mathbf{q} \cdot \boldsymbol{\mu})(1)\mathcal{N}_2 + (\mathcal{N}_3 m_1 - \mathcal{N}_1 m_3)\Big|_0^1 = 0 \tag{4.18}$$

$$\frac{1}{2}(\mathbf{q} \cdot \boldsymbol{\mu})(1)\mathcal{N}_3 + (\mathcal{N}_1 m_2 - \mathcal{N}_2 m_1)\Big|_0^1 = 0 \tag{4.19}$$

Additionally, recall that we have the BC that $m_3(1) = 0$, which further simplifies Eqs. (4.17) - (4.19). So the original Hamiltonian system is equivalent to the 9^{th} order system from the previous section, but without the Integral Constraints and with the Eqs. (4.17) - (4.19) as additional BCs.

4.3 Analytic Jacobian

Finally, the efficiency of the numerics can be improved by replacing the Numeric Jacobian by an Analytic Jacobian. AUTO also requires that the derivatives of the equations be calculated for each parameter (regardless of whether it is being modified by AUTO or not) and also derivatives of all BCs and integral constraints, for all variables and parameters. For the BCs, these derivatives must be calculated at both end points.

The calculation of the Jacobian is straight forward, as is the calculation of the derivatives of the BCs and Integral Constraints. In Appendix A is a listing of the AUTO code for the 15^{th} Order System and also for the 9^{th} Order System with Integral Constraints. The code provided there contains the Jacobian and other derivatives written out in a way which AUTO can understand. For an explanation of how this code works, see [6].

The analytic Jacobian for the smaller systems are appropriate subsets of the full modifications.

4.4 Comparisons of Different Methods

Comparison runs were made between the full system, the 12^{th} order system, the 9^{th} order system with Integral Constraints, and the 9^{th} order system without Integral Constraints. Each of the four systems were compared with both Analytic and Numeric Jacobian. All computations for timing comparisons were carried out on a 166 MHz AlphaStation 200 workstation.

The differences in CPU usage between the various formulations are displayed in Tables 4.1 and 4.2. As can be seen from the data, the 9^{th} order system is by far the most efficient, running in less than 36% of the time taken for the standard, 15^{th} order system with the Numeric Jacobian.

Interestingly, the difference between the Analytic and Numeric Jacobian were relatively minor. In fact, when comparing the Analytic and Numeric Jacobian more carefully, on a point-by-point basis, it was found that the time to compute a generic continuation step was virtually the same for the different types of Jacobian. The only real differences between the two Jacobians came at special points (e.g., folds) and at startup (the numeric Jacobian method takes a few seconds longer to compute the first continuation step than it takes to compute a single step in the middle of a run, while the analytic Jacobian method is as fast on the first step as on any other).

The next question to ask is, are all these systems truly the same? This question is a little difficult to answer, because we could not do a direct comparison on all the data as the continuation step-sizes between the different formulations were different. However there is one place where we can look, and that is to see if all the fold points are the same. Twisting through two revolutions entails encountering a total of four folds for the configuration used, and indeed, each system encountered the folds at the same points, with the same values for the data at those points (accurate to seven decimal places). From this, we conclude

Table 4.1: Comparison of CPU Usage in Various Formulations and Problem Sizes, Part I

Mesh Points	Order of System	Time for Numeric Jacobian	Time for Analytic Jacobian
30	15	522.9 (1.0000)	492.7 (0.9422)
	12	323.9 (0.6194)	301.7 (0.5770)
	9 + 3 ICs	212.6 (0.4066)	186.9 (0.3574)
	9	188.4 (0.3603)	179.0 (0.3423)
60	15	1018 (1.0000)	959.1 (0.9421)
	12	651.5 (0.6400)	613.3 (0.6025)
	9 + 3 ICs	438.7 (0.4309)	389.8 (0.3829)
	9	395.1 (0.3881)	358.8 (0.3525)
120	15	2001 (1.0000)	1881 (0.9400)
	12	1314 (0.6567)	1220 (0.6097)
	9 + 3 ICs	883.6 (0.4416)	787.6 (0.3936)
	9	803.8 (0.4017)	719.4 (0.3595)

This table lists the number of mesh points, the order of the system, the time (in CPU seconds) which the run took while using the Numeric Jacobian, and the time (in CPU seconds) for which the run took while using the Analytic Jacobian. For ease of comparison, the times have also been scaled (to the 15^{th} order system with the numeric Jacobian), with the scaled run times appearing in parentheses next to the total run times. Times for problems with differing number of mesh points have been scaled separately. All runs were performed on twisting a rod through two full revolutions. The system of order "9 + 3 ICs" refers to the 9^{th} order system with 3 Integral Constraints. All of these runs were made with 4 Gauss collocation points per mesh interval.

Table 4.2: Comparison of CPU Usage in Various Formulations and Problem Sizes, Part II

Mesh Points	Order of System	Time for Numeric Jacobian	Time for Analytic Jacobian
30	15	1141 (1.0000)	1094 (0.9588)
	12	720.3 (0.6313)	680.8 (0.5967)
	9 + 3 ICs	458.7 (0.4020)	422.9 (0.3705)
	9	414.0 (0.3628)	391.1 (0.3428)
60	15	2244 (1.0000)	2145 (0.9559)
	12	1434 (0.6390)	1367 (0.6092)
	9 + 3 ICs	921.0 (0.4104)	853.5 (0.3803)
	9	829.4 (0.3696)	782.9 (0.3489)
120	15	4449 (1.0000)	4267 (0.9591)
	12	2854 (0.6415)	2725 (0.6125)
	9 + 3 ICs	1839 (0.4127)	1699 (0.3819)
	9	1663 (0.3738)	1562 (0.3511)

This table is the same as Table 4.1, except that all of these runs were made with 6 Gauss collocation points per mesh interval.

that the various formulations of the Hamiltonian system are identical as far as the numerics are concerned.

Increasing the number of mesh intervals and collocation points has the effect of increasing the size of the problem to be solved. In doing this and then comparing the timing runs, we find that the benefits seen by reducing the order of the problem are slowly eroded (as a percentage of the 15^{th} order system run-time) as the problem gets larger, but this erosion is gradual. For example, for the smallest problem (30 mesh intervals, 4 collocation points per interval), the 9^{th} order system ran in 34.2% of the time needed for the 15^{th} order system, whereas for the largest problem (60 mesh intervals, 6 collocation points per interval), the 9^{th} order system ran in 35.1% of the time needed for the 15^{th} order system, a small but perceptible difference, but one that is not really of any consequence.

Chapter 5

Summary

In this chapter we summarize the conclusions reached in this thesis. In Section 5.1 we reprise the implications of the numerical experiments, and in Section 5.2 we discuss the findings of our survey of computational efficiency and related topics.

5.1 Numerical Results

In this subsection we first consider the sliding problem, and then go on to discuss twisting of a simply curved rod, the twisting of helical rods, and finally the free-end problem.

5.1.1 Sliding

The behavior of the simple rod while deforming its configuration proved to be of some interest in its own right. It was discovered that this deformation process was actually reasonably complicated, leading to bifurcation diagrams which were highly dependent on the values of $|\hat{\mathbf{u}}|$ and K_3/K_1.

In particular the Fourth Branch of the bifurcation diagram was discovered. This branch bifurcated at the value of $\rho = \pm 0.21888$ for all non-zero values of $|\hat{\mathbf{u}}|$ and for all values of K_3/K_1 for which it was observed. This bifurcation point appears to be a numerically ill-conditioned part of the solution set, as AUTO yielded inconsistent results when passing through this point, either simply stopping at $\rho = \pm 0.21888$, or going along the Fourth Branch, or missing the Fourth Branch entirely and proceeding down the main branch of the diagram. The behavior at this point warrants further study, but is outside the scope of this thesis.

5.1.2 Twisting

The numerical computations gave the expected results for the twisting behavior of the rods, giving good qualitative comparison with the experimental data. The ratcheting effect was observed for sufficiently high values of $|\hat{\mathbf{u}}|$. We found that the ratcheting increased markedly as more stress was placed on the rod (in the form of decreasing or increasing ρ from the value of $2/\pi$, which corresponds to a semi-circular shape), while it was reduced by increasing the value of K_3/K_1.

5.1.3 Helical Rods

The computations support Dr. Berg's original assertion that rods with a helical unstressed shape of given curvature should exhibit less ratcheting than rods with a planar unstressed shape of the same curvature. For moderate values of $|\hat{\mathbf{u}}|$ we found a marked decrease in the variability of torque while the wire was twisted as the torsion of the unstressed helix was increased, and a similar decrease in the ratcheting effect. In other words, a rod with moderately helical unstressed shape should have a much smoother twisting action than a rod of the same unstressed curvature but with a planar shape.

5.1.4 Free-end Problem

Our numerical results did suggest a deficiency in the experimental model. Dr. Berg had assumed that the $\sigma = 1$ end of the wire was free to slide through the experimental apparatus, thus changing the length of the loop of wire. Correspondingly the tangential component of force should vanish. When this condition was enforced numerically (i.e., $n_3 = 0$), we found no non-planar solution, and continuation in twist angle was not possible.

The problem appears to be related to the fact that, with $n_3(1) = 0$ as an additional BC and allowing the length of the rod to change, the system exhibits non-isolated solutions when in a planar configuration (that is, we can change the length continuously and still satisfy the system of equations). This non-isolation of solutions implies that the linearization of the system is singular for planar solutions. Since the continuation method used by AUTO relies on non-singularity of the linearized system at starting points, we see that numerical computations of this sort cannot be done with this package. Moreover, there is no guarantee that continuation in twist angle would be possible using any method.

In particular, for all non-planar solutions found in this thesis, we have found that $n_3(1) \neq 0$, which suggests that the $n_3(1) = 0$ boundary condition may never be possible on a non-planar solution. Since, when observing the experiments directly, we noted that the centerline of the wire was generally non-planar, we believe that the assumption $n_3(1) = 0$ is inappropriate, and that small frictional effects in the experimental apparatus play a significant role.

5.2 Computational Efficiency

Significant advantages can be gained by modifying the formulation of the problem. By reducing the amount of CPU time needed to make a single run by a factor of nearly three, the amount of computer resources needed to numerically explore the phenomena associated with this problem becomes more manageable. For example, a typical run for continuation in θ using the largest system took approximately 300 CPU seconds. To do the complete mapping of a single bifurcation diagram took on the order of 1000 runs, or well over 3 CPU days. Thus a factor of three is a significant time savings.

The time savings in the reformulations of the rod equilibrium conditions described here also have implications in interactive multi-parameter continuation packages currently being developed, where speed is of the essence.

Appendix A

AUTO Files

In this Appendix we give two samples of AUTO programs and input files which were used to to generate data for this thesis. The first program is for the 15^{th} Order System, and included the Analytic Jacobian, followed by the AUTO input file used to control the run. We then give the AUTO program for the 9^{th} Order System with 3 Integral Constraints, again followed by the AUTO input file used to control that run.

A.1 15^{th} Order System

A.1.1 Software

```
C----------------------------------------------------------------
C----------------------------------------------------------------
C  AUTRING : A Semicircle with Bifurcations.
C----------------------------------------------------------------
C----------------------------------------------------------------

      DOUBLE PRECISION FUNCTION smu1(s)
      IMPLICIT DOUBLE PRECISION (A-H,O-Z)
      COMMON /BLBCN/ NDIM,IPS,IRS,ILP,ICP(20),PAR(20)
      uhat1 = 0.0D0
      smu1 = PAR(3)*uhat1
      END

      DOUBLE PRECISION FUNCTION smu2(s)
      IMPLICIT DOUBLE PRECISION (A-H,O-Z)
      COMMON /BLBCN/ NDIM,IPS,IRS,ILP,ICP(20),PAR(20)
      uhat2 = 0.0D0
      smu2 = PAR(3)*uhat2
      END

      DOUBLE PRECISION FUNCTION smu3(s)
      IMPLICIT DOUBLE PRECISION (A-H,O-Z)
      COMMON /BLBCN/ NDIM,IPS,IRS,ILP,ICP(20),PAR(20)
```

```
      smu3 = 0.0D0
      END

      SUBROUTINE FUNC(NDIM,U,ICP,PAR,IJAC,F,DFDU,DFDP)
C     ---------- ----

      IMPLICIT DOUBLE PRECISION (A-H,O-Z)
      DOUBLE PRECISION I1,I2,I3

      DIMENSION U(NDIM),PAR(20),F(NDIM),DFDU(NDIM,NDIM)
      DIMENSION FOO(16), d3qn(4), DFDP(NDIM,20)
      DOUBLE PRECISION m(3), k(3), mu(3), kappa, alpha, beta
      DOUBLE PRECISION fact1, fact2, fact3

      kappa = 0.0D0
      alpha = 0.0D0
      beta  = 0.0D0

C     Calculate some subexpressions which will be used a lot

      mu(1) = 0.0
      mu(2) = PAR(3)
      mu(3) = beta

      m(1) = (u(7)*u(8) + u(6)*u(9) - u(5)*u(10) - u(4)*u(11))/2
      m(2) = (-u(6)*u(8) + u(7)*u(9) + u(4)*u(10) - u(5)*u(11))/2
      m(3) = (u(5)*u(8) - u(4)*u(9) + u(7)*u(10) - u(6)*u(11))/2

      d3qn(1) =  -2.0D0*(u(6)*U(12) - u(7)*U(13) - U(4)*u(14))
      d3qn(2) =  -2.0D0*(u(7)*U(12) + u(6)*U(13) - U(5)*u(14))
      d3qn(3) =  -2.0D0*(u(4)*U(12) + u(5)*U(13) + U(6)*u(14))
      d3qn(4) =  -2.0D0*(u(5)*U(12) - u(4)*U(13) + U(7)*u(14))

      k(1) = 0.1D0
      k(2) = 0.1D0
      k(3) = k(1)*par(4)

      a = (m(1)/k(1) + mu(1))/2
      b = (m(2)/k(2) + mu(2))/2
      c = (m(3)/k(3) + mu(3))/2

c     Now calculate the right hand sides

      F(1) = 2*(u(4)*u(6) + u(5)*u(7))
      F(2) = 2*(u(5)*u(6) - u(4)*u(7))
      F(3) = -u(4)*u(4) - u(5)*u(5) + u(6)*u(6) + u(7)*u(7)
```

```
      F(4) = a*u(7) - b*u(6) + c*u(5)
      F(5) = a*u(6) + b*u(7) - c*u(4)
      F(6) = -a*u(5) + b*u(4) + c*u(7)
      F(7) = -a*u(4) - b*u(5) - c*u(6)

      F(12) = 0.0D0
      F(13) = 0.0D0
      F(14) = 0.0D0

      F(8) = a*u(11) - b*u(10) + c*u(9) + d3qn(1)
      F(9) = a*u(10) + b*u(11) - c*u(8) + d3qn(2)
      F(10) = -a*u(9) + b*u(8) + c*u(11) + d3qn(3)
      F(11) = -a*u(8) - b*u(9) - c*u(10) + d3qn(4)

      F(15) = 1.0D0

      IF(IJAC.EQ.0) RETURN
C
      fact1 = 1/(4*k(1))
      fact2 = 1/(4*k(2))
      fact3 = 1/(4*k(3))
C
C     Here is the Jacobian ... and it's big
C
C     F( 1)
C
      DFDU( 1, 1) = 0.0D0
      DFDU( 1, 2) = 0.0D0
      DFDU( 1, 3) = 0.0D0
      DFDU( 1, 4) = 2*U(6)
      DFDU( 1, 5) = 2*U(7)
      DFDU( 1, 6) = 2*U(4)
      DFDU( 1, 7) = 2*U(5)
      DFDU( 1, 8) = 0.0D0
      DFDU( 1, 9) = 0.0D0
      DFDU( 1,10) = 0.0D0
      DFDU( 1,11) = 0.0D0
      DFDU( 1,12) = 0.0D0
      DFDU( 1,13) = 0.0D0
      DFDU( 1,14) = 0.0D0
      DFDU( 1,15) = 0.0D0
C
C     F( 2)
C
      DFDU( 2, 1) = 0.0D0
```

```
      DFDU( 2, 2) = 0.0D0
      DFDU( 2, 3) = 0.0D0
      DFDU( 2, 4) = -2*U(7)
      DFDU( 2, 5) =  2*U(6)
      DFDU( 2, 6) =  2*U(5)
      DFDU( 2, 7) = -2*U(4)
      DFDU( 2, 8) = 0.0D0
      DFDU( 2, 9) = 0.0D0
      DFDU( 2,10) = 0.0D0
      DFDU( 2,11) = 0.0D0
      DFDU( 2,12) = 0.0D0
      DFDU( 2,13) = 0.0D0
      DFDU( 2,14) = 0.0D0
      DFDU( 2,15) = 0.0D0
C
C     F( 3)
C
      DFDU( 3, 1) = 0.0D0
      DFDU( 3, 2) = 0.0D0
      DFDU( 3, 3) = 0.0D0
      DFDU( 3, 4) = -2*U(4)
      DFDU( 3, 5) = -2*U(5)
      DFDU( 3, 6) =  2*U(6)
      DFDU( 3, 7) =  2*U(7)
      DFDU( 3, 8) = 0.0D0
      DFDU( 3, 9) = 0.0D0
      DFDU( 3,10) = 0.0D0
      DFDU( 3,11) = 0.0D0
      DFDU( 3,12) = 0.0D0
      DFDU( 3,13) = 0.0D0
      DFDU( 3,14) = 0.0D0
      DFDU( 3,15) = 0.0D0
C
C     F( 4)
C
      DFDU( 4, 1) = 0.0D0
      DFDU( 4, 2) = 0.0D0
      DFDU( 4, 3) = 0.0D0
      DFDU( 4, 4) =    - fact1*U(7)*U(11) - fact2*U(6)*U(10) -
     *              fact3*U(5)*U( 9)
      DFDU( 4, 5) =  c - fact1*U(7)*U(10) + fact2*U(6)*U(11) +
     *              fact3*U(5)*U( 8)
      DFDU( 4, 6) = -b + fact1*U(7)*U( 9) + fact2*U(6)*U( 8) -
     *              fact3*U(5)*U(11)
      DFDU( 4, 7) =  a + fact1*U(7)*U( 8) - fact2*U(6)*U( 9) +
     *              fact3*U(5)*U(10)
```

```
      DFDU( 4, 8) =  fact1*U(7)*U(7) + fact2*U(6)*U(6) +
     *              fact3*U(5)*U(5)
      DFDU( 4, 9) =  fact1*U(6)*U(7) - fact2*U(7)*U(6) -
     *              fact3*U(4)*U(5)
      DFDU( 4,10) = -fact1*U(5)*U(7) - fact2*U(4)*U(6) +
     *              fact3*U(7)*U(5)
      DFDU( 4,11) = -fact1*U(4)*U(7) + fact2*U(5)*U(6) -
     *              fact3*U(6)*U(5)
      DFDU( 4,12) = 0.0D0
      DFDU( 4,13) = 0.0D0
      DFDU( 4,14) = 0.0D0
      DFDU( 4,15) = 0.0D0
C
C     F( 5)
C
      DFDU( 5, 1) = 0.0D0
      DFDU( 5, 2) = 0.0D0
      DFDU( 5, 3) = 0.0D0
      DFDU( 5, 4) = -c - fact1*U(6)*U(11) + fact2*U(7)*U(10) +
     *              fact3*U(4)*U( 9)
      DFDU( 5, 5) =    - fact1*U(6)*U(10) - fact2*U(7)*U(11) -
     *              fact3*U(4)*U( 8)
      DFDU( 5, 6) =  a + fact1*U(6)*U( 9) - fact2*U(7)*U( 8) +
     *              fact3*U(4)*U(11)
      DFDU( 5, 7) =  b + fact1*U(6)*U( 8) + fact2*U(7)*U( 9) -
     *              fact3*U(4)*U(10)
      DFDU( 5, 8) =  fact1*U(7)*U(6) - fact2*U(6)*U(7) -
     *              fact3*U(5)*U(4)
      DFDU( 5, 9) =  fact1*U(6)*U(6) + fact2*U(7)*U(7) +
     *              fact3*U(4)*U(4)
      DFDU( 5,10) = -fact1*U(5)*U(6) + fact2*U(4)*U(7) -
     *              fact3*U(7)*U(4)
      DFDU( 5,11) = -fact1*U(4)*U(6) - fact2*U(5)*U(7) +
     *              fact3*U(6)*U(4)
      DFDU( 5,12) = 0.0D0
      DFDU( 5,13) = 0.0D0
      DFDU( 5,14) = 0.0D0
      DFDU( 5,15) = 0.0D0
C
C     F( 6)
C
      DFDU( 6, 1) = 0.0D0
      DFDU( 6, 2) = 0.0D0
      DFDU( 6, 3) = 0.0D0
      DFDU( 6, 4) =  b + fact1*U(5)*U(11) + fact2*U(4)*U(10) -
     *              fact3*U(7)*U( 9)
```

```
      DFDU( 6, 5) = -a + fact1*U(5)*U(10) - fact2*U(4)*U(11) +
     *             fact3*U(7)*U( 8)
      DFDU( 6, 6) =    - fact1*U(5)*U( 9) - fact2*U(4)*U( 8) -
     *             fact3*U(7)*U(11)
      DFDU( 6, 7) =  c - fact1*U(5)*U( 8) + fact2*U(4)*U( 9) +
     *             fact3*U(7)*U(10)
      DFDU( 6, 8) = -fact1*U(7)*U(5) - fact2*U(6)*U(4) +
     *             fact3*U(5)*U(7)
      DFDU( 6, 9) = -fact1*U(6)*U(5) + fact2*U(7)*U(4) -
     *             fact3*U(4)*U(7)
      DFDU( 6,10) =  fact1*U(5)*U(5) + fact2*U(4)*U(4) +
     *             fact3*U(7)*U(7)
      DFDU( 6,11) =  fact1*U(4)*U(5) - fact2*U(5)*U(4) -
     *             fact3*U(6)*U(7)
      DFDU( 6,12) = 0.0D0
      DFDU( 6,13) = 0.0D0
      DFDU( 6,14) = 0.0D0
      DFDU( 6,15) = 0.0D0
C
C     F( 7)
C
      DFDU( 7, 1) = 0.0D0
      DFDU( 7, 2) = 0.0D0
      DFDU( 7, 3) = 0.0D0
      DFDU( 7, 4) = -a + fact1*U(4)*U(11) - fact2*U(5)*U(10) +
     *             fact3*U(6)*U( 9)
      DFDU( 7, 5) = -b + fact1*U(4)*U(10) + fact2*U(5)*U(11) -
     *             fact3*U(6)*U( 8)
      DFDU( 7, 6) = -c - fact1*U(4)*U( 9) + fact2*U(5)*U( 8) +
     *             fact3*U(6)*U(11)
      DFDU( 7, 7) =    - fact1*U(4)*U( 8) - fact2*U(5)*U( 9) -
     *             fact3*U(6)*U(10)
      DFDU( 7, 8) = -fact1*U(7)*U(4) + fact2*U(6)*U(5) -
     *             fact3*U(5)*U(6)
      DFDU( 7, 9) = -fact1*U(6)*U(4) - fact2*U(7)*U(5) +
     *             fact3*U(4)*U(6)
      DFDU( 7,10) =  fact1*U(5)*U(4) - fact2*U(4)*U(5) -
     *             fact3*U(7)*U(6)
      DFDU( 7,11) =  fact1*U(4)*U(4) + fact2*U(5)*U(5) +
     *             fact3*U(6)*U(6)
      DFDU( 7,12) = 0.0D0
      DFDU( 7,13) = 0.0D0
      DFDU( 7,14) = 0.0D0
      DFDU( 7,15) = 0.0D0
C
C     F( 8)
```

```
C
      DFDU( 8, 1) = 0.0D0
      DFDU( 8, 2) = 0.0D0
      DFDU( 8, 3) = 0.0D0
      DFDU( 8, 4) =  2*U(14) - fact1*U(11)*U(11) -
     *             fact2*U(10)*U(10) - fact3*U( 9)*U( 9)
      DFDU( 8, 5) =          - fact1*U(10)*U(11) +
     *             fact2*U(11)*U(10) + fact3*U( 8)*U( 9)
      DFDU( 8, 6) = -2*U(12) + fact1*U( 9)*U(11) +
     *             fact2*U( 8)*U(10) - fact3*U(11)*U( 9)
      DFDU( 8, 7) =  2*U(13) + fact1*U( 8)*U(11) -
     *             fact2*U( 9)*U(10) + fact3*U(10)*U( 9)
      DFDU( 8, 8) =      fact1*U(7)*U(11) + fact2*U(6)*U(10) +
     *             fact3*U(5)*U( 9)
      DFDU( 8, 9) =  c + fact1*U(6)*U(11) - fact2*U(7)*U(10) -
     *             fact3*U(4)*U( 9)
      DFDU( 8,10) = -b - fact1*U(5)*U(11) - fact2*U(4)*U(10) +
     *             fact3*U(7)*U( 9)
      DFDU( 8,11) =  a - fact1*U(4)*U(11) + fact2*U(5)*U(10) -
     *             fact3*U(6)*U( 9)
      DFDU( 8,12) = -2*U(6)
      DFDU( 8,13) =  2*U(7)
      DFDU( 8,14) =  2*U(4)
      DFDU( 8,15) = 0.0D0
C
C     F( 9)
C
      DFDU( 9, 1) = 0.0D0
      DFDU( 9, 2) = 0.0D0
      DFDU( 9, 3) = 0.0D0
      DFDU( 9, 4) =          - fact1*U(11)*U(10) +
     *             fact2*U(10)*U(11) + fact3*U( 9)*U( 8)
      DFDU( 9, 5) =  2*U(14) - fact1*U(10)*U(10) -
     *             fact2*U(11)*U(11) - fact3*U( 8)*U( 8)
      DFDU( 9, 6) = -2*U(13) + fact1*U( 9)*U(10) -
     *             fact2*U( 8)*U(11) + fact3*U(11)*U( 8)
      DFDU( 9, 7) = -2*U(12) + fact1*U( 8)*U(10) +
     *             fact2*U( 9)*U(11) - fact3*U(10)*U( 8)
      DFDU( 9, 8) = -c + fact1*U(7)*U(10) - fact2*U(6)*U(11) -
     *             fact3*U(5)*U( 8)
      DFDU( 9, 9) =      fact1*U(6)*U(10) + fact2*U(7)*U(11) +
     *             fact3*U(4)*U( 8)
      DFDU( 9,10) =  a - fact1*U(5)*U(10) + fact2*U(4)*U(11) -
     *             fact3*U(7)*U( 8)
      DFDU( 9,11) =  b - fact1*U(4)*U(10) - fact2*U(5)*U(11) +
     *             fact3*U(6)*U( 8)
```

```
      DFDU( 9,12) = -2*U(7)
      DFDU( 9,13) = -2*U(6)
      DFDU( 9,14) =  2*U(5)
      DFDU( 9,15) = 0.0D0
C
C     F(10)
C
      DFDU(10, 1) = 0.0D0
      DFDU(10, 2) = 0.0D0
      DFDU(10, 3) = 0.0D0
      DFDU(10, 4) = -2*U(12) + fact1*U(11)*U( 9) +
     *             fact2*U(10)*U( 8) - fact3*U( 9)*U(11)
      DFDU(10, 5) = -2*U(13) + fact1*U(10)*U( 9) -
     *             fact2*U(11)*U( 8) + fact3*U( 8)*U(11)
      DFDU(10, 6) = -2*U(14) - fact1*U( 9)*U( 9) -
     *             fact2*U( 8)*U( 8) - fact3*U(11)*U(11)
      DFDU(10, 7) =          - fact1*U( 8)*U( 9) +
     *             fact2*U( 9)*U( 8) + fact3*U(10)*U(11)
      DFDU(10, 8) =  b - fact1*U(7)*U( 9) - fact2*U(6)*U( 8) +
     *             fact3*U(5)*U(11)
      DFDU(10, 9) = -a - fact1*U(6)*U( 9) + fact2*U(7)*U( 8) -
     *             fact3*U(4)*U(11)
      DFDU(10,10) =      fact1*U(5)*U( 9) + fact2*U(4)*U( 8) +
     *             fact3*U(7)*U(11)
      DFDU(10,11) =  c + fact1*U(4)*U( 9) - fact2*U(5)*U( 8) -
     *             fact3*U(6)*U(11)
      DFDU(10,12) = -2*U(4)
      DFDU(10,13) = -2*U(5)
      DFDU(10,14) = -2*U(6)
      DFDU(10,15) = 0.0D0
C
C     F(11)
C
      DFDU(11, 1) = 0.0D0
      DFDU(11, 2) = 0.0D0
      DFDU(11, 3) = 0.0D0
      DFDU(11, 4) =  2*U(13) + fact1*U(11)*U( 8) -
     *             fact2*U(10)*U( 9) + fact3*U( 9)*U(10)
      DFDU(11, 5) = -2*U(12) + fact1*U(10)*U( 8) +
     *             fact2*U(11)*U( 9) - fact3*U( 8)*U(10)
      DFDU(11, 6) =          - fact1*U( 9)*U( 8) +
     *             fact2*U( 8)*U( 9) + fact3*U(11)*U(10)
      DFDU(11, 7) = -2*U(14) - fact1*U( 8)*U( 8) -
     *             fact2*U( 9)*U( 9) - fact3*U(10)*U(10)
      DFDU(11, 8) = -a - fact1*U(7)*U( 8) + fact2*U(6)*U( 9) -
     *             fact3*U(5)*U(10)
```

```
      DFDU(11, 9) = -b - fact1*U(6)*U( 8) - fact2*U(7)*U( 9) +
     *             fact3*U(4)*U(10)
      DFDU(11,10) = -c + fact1*U(5)*U( 8) - fact2*U(4)*U( 9) -
     *             fact3*U(7)*U(10)
      DFDU(11,11) =      fact1*U(4)*U( 8) + fact2*U(5)*U( 9) +
     *             fact3*U(6)*U(10)
      DFDU(11,12) = -2*U(5)
      DFDU(11,13) =  2*U(4)
      DFDU(11,14) = -2*U(7)
      DFDU(11,15) = 0.0D0
C
C     F(12)
C
      DFDU(12, 1) = 0.0D0
      DFDU(12, 2) = 0.0D0
      DFDU(12, 3) = 0.0D0
      DFDU(12, 4) = 0.0D0
      DFDU(12, 5) = 0.0D0
      DFDU(12, 6) = 0.0D0
      DFDU(12, 7) = 0.0D0
      DFDU(12, 8) = 0.0D0
      DFDU(12, 9) = 0.0D0
      DFDU(12,10) = 0.0D0
      DFDU(12,11) = 0.0D0
      DFDU(12,12) = 0.0D0
      DFDU(12,13) = 0.0D0
      DFDU(12,14) = 0.0D0
      DFDU(12,15) = 0.0D0
C
C     F(13)
C
      DFDU(13, 1) = 0.0D0
      DFDU(13, 2) = 0.0D0
      DFDU(13, 3) = 0.0D0
      DFDU(13, 4) = 0.0D0
      DFDU(13, 5) = 0.0D0
      DFDU(13, 6) = 0.0D0
      DFDU(13, 7) = 0.0D0
      DFDU(13, 8) = 0.0D0
      DFDU(13, 9) = 0.0D0
      DFDU(13,10) = 0.0D0
      DFDU(13,11) = 0.0D0
      DFDU(13,12) = 0.0D0
      DFDU(13,13) = 0.0D0
      DFDU(13,14) = 0.0D0
      DFDU(13,15) = 0.0D0
```

```
C
C     F(14)
C
      DFDU(14, 1) = 0.0D0
      DFDU(14, 2) = 0.0D0
      DFDU(14, 3) = 0.0D0
      DFDU(14, 4) = 0.0D0
      DFDU(14, 5) = 0.0D0
      DFDU(14, 6) = 0.0D0
      DFDU(14, 7) = 0.0D0
      DFDU(14, 8) = 0.0D0
      DFDU(14, 9) = 0.0D0
      DFDU(14,10) = 0.0D0
      DFDU(14,11) = 0.0D0
      DFDU(14,12) = 0.0D0
      DFDU(14,13) = 0.0D0
      DFDU(14,14) = 0.0D0
      DFDU(14,15) = 0.0D0
C
C     F(15)
C
      DFDU(15, 1) = 0.0D0
      DFDU(15, 2) = 0.0D0
      DFDU(15, 3) = 0.0D0
      DFDU(15, 4) = 0.0D0
      DFDU(15, 5) = 0.0D0
      DFDU(15, 6) = 0.0D0
      DFDU(15, 7) = 0.0D0
      DFDU(15, 8) = 0.0D0
      DFDU(15, 9) = 0.0D0
      DFDU(15,10) = 0.0D0
      DFDU(15,11) = 0.0D0
      DFDU(15,12) = 0.0D0
      DFDU(15,13) = 0.0D0
      DFDU(15,14) = 0.0D0
      DFDU(15,15) = 0.0D0

C     Derivtives of F(*) by parameter

      DFDP( 1, 2) = 0.0D0
      DFDP( 2, 2) = 0.0D0
      DFDP( 3, 2) = 0.0D0
      DFDP( 4, 2) = 0.0D0
      DFDP( 5, 2) = 0.0D0
      DFDP( 6, 2) = 0.0D0
      DFDP( 7, 2) = 0.0D0
```

```
      DFDP( 8, 2) = 0.0D0
      DFDP( 9, 2) = 0.0D0
      DFDP(10, 2) = 0.0D0
      DFDP(11, 2) = 0.0D0
      DFDP(12, 2) = 0.0D0
      DFDP(13, 2) = 0.0D0
      DFDP(14, 2) = 0.0D0
      DFDP(15, 2) = 0.0D0

      DFDP( 1, 3) = 0.0D0
      DFDP( 2, 3) = 0.0D0
      DFDP( 3, 3) = 0.0D0
      DFDP( 4, 3) = -U( 6)/2
      DFDP( 5, 3) =  U( 7)/2
      DFDP( 6, 3) =  U( 4)/2
      DFDP( 7, 3) = -U( 5)/2
      DFDP( 8, 3) = -U(10)/2
      DFDP( 9, 3) =  U(11)/2
      DFDP(10, 3) =  U( 8)/2
      DFDP(11, 3) = -U( 9)/2
      DFDP(12, 3) = 0.0D0
      DFDP(13, 3) = 0.0D0
      DFDP(14, 3) = 0.0D0
      DFDP(15, 3) = 0.0D0

      RETURN
      END

C
C &&&&&&&&&&&&&&&&&&&&&&&&&&&&&&&&&&&&&&&&&&&&&&&&&&&&&&&&&&&
C
C
      SUBROUTINE STPNT(NDIM,U,PAR,T)
C     ---------- -----
C
      IMPLICIT DOUBLE PRECISION (A-H,O-Z)
C
      DOUBLE PRECISION k1,k2,k3, NPI, NPI2, mufact
      DIMENSION U(NDIM),PAR(20)
      DIMENSION Z(16)
C

         PI     = 4.0D0*DATAN(1.0D0)
         PAR(1) = 20/PI
         PAR(2) = 0.0D0
         PAR(3) = 0.3D0
```

```
          PAR(4) = 0.3D0
          NPI2   = PI*2.0D0
          k1     = 0.1D0
          k2     = 0.1D0
          k3     = (k1 + k2)/7
          mufact = 2.0*k2*PI

C     Calculate some subexpressions which will be used a lot

          dcnpit = DCOS(0.5*PI*T)
          dstpit = DSIN(0.5*PI*T)

          U( 1)  = (1.0 - DCOS(PI*T))/PI
          U( 2)  = 0.0
          U( 3)  = DSIN(PI*T)/PI

          U( 4)  = 0.0
          U( 5)  = dstpit
          U( 6)  = 0.0
          U( 7)  = dcnpit

          U(12)  = 0.0
          U(14)  = 0.0
          U(13)  = 0.0

          U( 8)  = 0.0
          U( 9)  = mufact*dcnpit
          U(10)  = 0.0
          U(11)  = -mufact*dstpit

          U(15)  = T

      RETURN
      END
C
C
C &&&&&&&&&&&&&&&&&&&&&&&&&&&&&&&&&&&&&&&&&&&&&&&&&&&&&&&&&&&&&&&&&&&&&&&&&
C
C
      SUBROUTINE BCND(NDIM,PAR,ICP,NBC,U0,U1,FB,IJAC,DBC)
C     ---------- ----
C
      IMPLICIT DOUBLE PRECISION (A-H,O-Z)
C
      DOUBLE PRECISION NPI, NPTERM
      DIMENSION PAR(20),ICP(20),U0(NDIM),U1(NDIM),FB(NBC)
```

```
      DIMENSION DBC(NBC,40)
C

c
c  BCs for JAW's Problem - twisting
c

       FB(1)  = U0(1)
       FB(2)  = U0(2)
       FB(3)  = U0(3)

       FB(4)  = U1(1) - 2*PAR(1)/20
       FB(5)  = U1(2)
       FB(6)  = U1(3)

       FB(7)  = U0(4)
       FB(8)  = U0(5)
       FB(9)  = U0(6) - DSIN(PAR(2))
       FB(10) = U0(7) - DCOS(PAR(2))

       FB(11) = U0(4)*U0( 8) + U0(5)*U0( 9) + U0(6)*U0(10) +
     &          U0(7)*U0(11)

       FB(12) = (U1(5)*U1(8) - U1(4)*U1(9) + U1(7)*U1(10) -
     &           U1(6)*U1(11))/2

       FB(13) = 2*(U1(4)*U1(6) + U1(5)*U1(7))
       FB(14) = 2*(U1(5)*U1(6) - U1(4)*U1(7))

       FB(15) = U0(15)

       IF (IJAC.EQ.0) RETURN
C
C FB( 1)
C
      DBC( 1, 1) = 1.0
      DBC( 1, 2) = 0.0
      DBC( 1, 3) = 0.0
      DBC( 1, 4) = 0.0
      DBC( 1, 5) = 0.0
      DBC( 1, 6) = 0.0
      DBC( 1, 7) = 0.0
      DBC( 1, 8) = 0.0
      DBC( 1, 9) = 0.0
      DBC( 1,10) = 0.0
      DBC( 1,11) = 0.0
```

```
      DBC( 1,12) = 0.0
      DBC( 1,13) = 0.0
      DBC( 1,14) = 0.0
      DBC( 1,15) = 0.0
      DBC( 1,16) = 0.0
      DBC( 1,17) = 0.0
      DBC( 1,18) = 0.0
      DBC( 1,19) = 0.0
      DBC( 1,20) = 0.0
      DBC( 1,21) = 0.0
      DBC( 1,22) = 0.0
      DBC( 1,23) = 0.0
      DBC( 1,24) = 0.0
      DBC( 1,25) = 0.0
      DBC( 1,26) = 0.0
      DBC( 1,27) = 0.0
      DBC( 1,28) = 0.0
      DBC( 1,29) = 0.0
      DBC( 1,30) = 0.0
      DBC( 1,31) = 0.0
      DBC( 1,32) = 0.0
C
C FB( 2)
C
      DBC( 2, 1) = 0.0
      DBC( 2, 2) = 1.0
      DBC( 2, 3) = 0.0
      DBC( 2, 4) = 0.0
      DBC( 2, 5) = 0.0
      DBC( 2, 6) = 0.0
      DBC( 2, 7) = 0.0
      DBC( 2, 8) = 0.0
      DBC( 2, 9) = 0.0
      DBC( 2,10) = 0.0
      DBC( 2,11) = 0.0
      DBC( 2,12) = 0.0
      DBC( 2,13) = 0.0
      DBC( 2,14) = 0.0
      DBC( 2,15) = 0.0
      DBC( 2,16) = 0.0
      DBC( 2,17) = 0.0
      DBC( 2,18) = 0.0
      DBC( 2,19) = 0.0
      DBC( 2,20) = 0.0
      DBC( 2,21) = 0.0
      DBC( 2,22) = 0.0
```

```
      DBC( 2,23) = 0.0
      DBC( 2,24) = 0.0
      DBC( 2,25) = 0.0
      DBC( 2,26) = 0.0
      DBC( 2,27) = 0.0
      DBC( 2,28) = 0.0
      DBC( 2,29) = 0.0
      DBC( 2,30) = 0.0
      DBC( 2,31) = 0.0
      DBC( 2,32) = 0.0
C
C FB( 3)
C
      DBC( 3, 1) = 0.0
      DBC( 3, 2) = 0.0
      DBC( 3, 3) = 1.0
      DBC( 3, 4) = 0.0
      DBC( 3, 5) = 0.0
      DBC( 3, 6) = 0.0
      DBC( 3, 7) = 0.0
      DBC( 3, 8) = 0.0
      DBC( 3, 9) = 0.0
      DBC( 3,10) = 0.0
      DBC( 3,11) = 0.0
      DBC( 3,12) = 0.0
      DBC( 3,13) = 0.0
      DBC( 3,14) = 0.0
      DBC( 3,15) = 0.0
      DBC( 3,16) = 0.0
      DBC( 3,17) = 0.0
      DBC( 3,18) = 0.0
      DBC( 3,19) = 0.0
      DBC( 3,20) = 0.0
      DBC( 3,21) = 0.0
      DBC( 3,22) = 0.0
      DBC( 3,23) = 0.0
      DBC( 3,24) = 0.0
      DBC( 3,25) = 0.0
      DBC( 3,26) = 0.0
      DBC( 3,27) = 0.0
      DBC( 3,28) = 0.0
      DBC( 3,29) = 0.0
      DBC( 3,30) = 0.0
      DBC( 3,31) = 0.0
      DBC( 3,32) = 0.0
C
```

```
C FB( 4)
C
      DBC( 4, 1) = 0.0
      DBC( 4, 2) = 0.0
      DBC( 4, 3) = 0.0
      DBC( 4, 4) = 0.0
      DBC( 4, 5) = 0.0
      DBC( 4, 6) = 0.0
      DBC( 4, 7) = 0.0
      DBC( 4, 8) = 0.0
      DBC( 4, 9) = 0.0
      DBC( 4,10) = 0.0
      DBC( 4,11) = 0.0
      DBC( 4,12) = 0.0
      DBC( 4,13) = 0.0
      DBC( 4,14) = 0.0
      DBC( 4,15) = 0.0
      DBC( 4,16) = 1.0
      DBC( 4,17) = 0.0
      DBC( 4,18) = 0.0
      DBC( 4,19) = 0.0
      DBC( 4,20) = 0.0
      DBC( 4,21) = 0.0
      DBC( 4,22) = 0.0
      DBC( 4,23) = 0.0
      DBC( 4,24) = 0.0
      DBC( 4,25) = 0.0
      DBC( 4,26) = 0.0
      DBC( 4,27) = 0.0
      DBC( 4,28) = 0.0
      DBC( 4,29) = 0.0
      DBC( 4,30) = 0.0
      DBC( 4,31) = -0.1
      DBC( 4,32) = 0.0
C
C FB( 5)
C
      DBC( 5, 1) = 0.0
      DBC( 5, 2) = 0.0
      DBC( 5, 3) = 0.0
      DBC( 5, 4) = 0.0
      DBC( 5, 5) = 0.0
      DBC( 5, 6) = 0.0
      DBC( 5, 7) = 0.0
      DBC( 5, 8) = 0.0
      DBC( 5, 9) = 0.0
```

```
      DBC( 5,10) = 0.0
      DBC( 5,11) = 0.0
      DBC( 5,12) = 0.0
      DBC( 5,13) = 0.0
      DBC( 5,14) = 0.0
      DBC( 5,15) = 0.0
      DBC( 5,16) = 0.0
      DBC( 5,17) = 1.0
      DBC( 5,18) = 0.0
      DBC( 5,19) = 0.0
      DBC( 5,20) = 0.0
      DBC( 5,21) = 0.0
      DBC( 5,22) = 0.0
      DBC( 5,23) = 0.0
      DBC( 5,24) = 0.0
      DBC( 5,25) = 0.0
      DBC( 5,26) = 0.0
      DBC( 5,27) = 0.0
      DBC( 5,28) = 0.0
      DBC( 5,29) = 0.0
      DBC( 5,30) = 0.0
      DBC( 5,31) = 0.0
      DBC( 5,32) = 0.0
C
C FB( 6)
C
      DBC( 6, 1) = 0.0
      DBC( 6, 2) = 0.0
      DBC( 6, 3) = 0.0
      DBC( 6, 4) = 0.0
      DBC( 6, 5) = 0.0
      DBC( 6, 6) = 0.0
      DBC( 6, 7) = 0.0
      DBC( 6, 8) = 0.0
      DBC( 6, 9) = 0.0
      DBC( 6,10) = 0.0
      DBC( 6,11) = 0.0
      DBC( 6,12) = 0.0
      DBC( 6,13) = 0.0
      DBC( 6,14) = 0.0
      DBC( 6,15) = 0.0
      DBC( 6,16) = 0.0
      DBC( 6,17) = 0.0
      DBC( 6,18) = 1.0
      DBC( 6,19) = 0.0
      DBC( 6,20) = 0.0
```

```
      DBC( 6,21) = 0.0
      DBC( 6,22) = 0.0
      DBC( 6,23) = 0.0
      DBC( 6,24) = 0.0
      DBC( 6,25) = 0.0
      DBC( 6,26) = 0.0
      DBC( 6,27) = 0.0
      DBC( 6,28) = 0.0
      DBC( 6,29) = 0.0
      DBC( 6,30) = 0.0
      DBC( 6,31) = 0.0
      DBC( 6,32) = 0.0
C
C FB( 7)
C
      DBC( 7, 1) = 0.0
      DBC( 7, 2) = 0.0
      DBC( 7, 3) = 0.0
      DBC( 7, 4) = 1.0
      DBC( 7, 5) = 0.0
      DBC( 7, 6) = 0.0
      DBC( 7, 7) = 0.0
      DBC( 7, 8) = 0.0
      DBC( 7, 9) = 0.0
      DBC( 7,10) = 0.0
      DBC( 7,11) = 0.0
      DBC( 7,12) = 0.0
      DBC( 7,13) = 0.0
      DBC( 7,14) = 0.0
      DBC( 7,15) = 0.0
      DBC( 7,16) = 0.0
      DBC( 7,17) = 0.0
      DBC( 7,18) = 0.0
      DBC( 7,19) = 0.0
      DBC( 7,20) = 0.0
      DBC( 7,21) = 0.0
      DBC( 7,22) = 0.0
      DBC( 7,23) = 0.0
      DBC( 7,24) = 0.0
      DBC( 7,25) = 0.0
      DBC( 7,26) = 0.0
      DBC( 7,27) = 0.0
      DBC( 7,28) = 0.0
      DBC( 7,29) = 0.0
      DBC( 7,30) = 0.0
      DBC( 7,31) = 0.0
```

```
      DBC( 7,32) = 0.0
C
C FB( 8)
C
      DBC( 8, 1) = 0.0
      DBC( 8, 2) = 0.0
      DBC( 8, 3) = 0.0
      DBC( 8, 4) = 0.0
      DBC( 8, 5) = 1.0
      DBC( 8, 6) = 0.0
      DBC( 8, 7) = 0.0
      DBC( 8, 8) = 0.0
      DBC( 8, 9) = 0.0
      DBC( 8,10) = 0.0
      DBC( 8,11) = 0.0
      DBC( 8,12) = 0.0
      DBC( 8,13) = 0.0
      DBC( 8,14) = 0.0
      DBC( 8,15) = 0.0
      DBC( 8,16) = 0.0
      DBC( 8,17) = 0.0
      DBC( 8,18) = 0.0
      DBC( 8,19) = 0.0
      DBC( 8,20) = 0.0
      DBC( 8,21) = 0.0
      DBC( 8,22) = 0.0
      DBC( 8,23) = 0.0
      DBC( 8,24) = 0.0
      DBC( 8,25) = 0.0
      DBC( 8,26) = 0.0
      DBC( 8,27) = 0.0
      DBC( 8,28) = 0.0
      DBC( 8,29) = 0.0
      DBC( 8,30) = 0.0
      DBC( 8,31) = 0.0
      DBC( 8,32) = 0.0
C
C FB( 9)
C
      DBC( 9, 1) = 0.0
      DBC( 9, 2) = 0.0
      DBC( 9, 3) = 0.0
      DBC( 9, 4) = 0.0
      DBC( 9, 5) = 0.0
      DBC( 9, 6) = 1.0
      DBC( 9, 7) = 0.0
```

```
      DBC( 9, 8) = 0.0
      DBC( 9, 9) = 0.0
      DBC( 9,10) = 0.0
      DBC( 9,11) = 0.0
      DBC( 9,12) = 0.0
      DBC( 9,13) = 0.0
      DBC( 9,14) = 0.0
      DBC( 9,15) = 0.0
      DBC( 9,16) = 0.0
      DBC( 9,17) = 0.0
      DBC( 9,18) = 0.0
      DBC( 9,19) = 0.0
      DBC( 9,20) = 0.0
      DBC( 9,21) = 0.0
      DBC( 9,22) = 0.0
      DBC( 9,23) = 0.0
      DBC( 9,24) = 0.0
      DBC( 9,25) = 0.0
      DBC( 9,26) = 0.0
      DBC( 9,27) = 0.0
      DBC( 9,28) = 0.0
      DBC( 9,29) = 0.0
      DBC( 9,30) = 0.0
      DBC( 9,31) = 0.0
      DBC( 9,32) = -DCOS(PAR(2))
C
C FB(10)
C
      DBC(10, 1) = 0.0
      DBC(10, 2) = 0.0
      DBC(10, 3) = 0.0
      DBC(10, 4) = 0.0
      DBC(10, 5) = 0.0
      DBC(10, 6) = 0.0
      DBC(10, 7) = 1.0
      DBC(10, 8) = 0.0
      DBC(10, 9) = 0.0
      DBC(10,10) = 0.0
      DBC(10,11) = 0.0
      DBC(10,12) = 0.0
      DBC(10,13) = 0.0
      DBC(10,14) = 0.0
      DBC(10,15) = 0.0
      DBC(10,16) = 0.0
      DBC(10,17) = 0.0
      DBC(10,18) = 0.0
```

```
      DBC(10,19) = 0.0
      DBC(10,20) = 0.0
      DBC(10,21) = 0.0
      DBC(10,22) = 0.0
      DBC(10,23) = 0.0
      DBC(10,24) = 0.0
      DBC(10,25) = 0.0
      DBC(10,26) = 0.0
      DBC(10,27) = 0.0
      DBC(10,28) = 0.0
      DBC(10,29) = 0.0
      DBC(10,30) = 0.0
      DBC(10,31) = 0.0
      DBC(10,32) = DSIN(PAR(2))
C
C FB(11)
C
      DBC(11, 1) = 0.0
      DBC(11, 2) = 0.0
      DBC(11, 3) = 0.0
      DBC(11, 4) = U0( 8)
      DBC(11, 5) = U0( 9)
      DBC(11, 6) = U0(10)
      DBC(11, 7) = U0(11)
      DBC(11, 8) = U0( 4)
      DBC(11, 9) = U0( 5)
      DBC(11,10) = U0( 6)
      DBC(11,11) = U0( 7)
      DBC(11,12) = 0.0
      DBC(11,13) = 0.0
      DBC(11,14) = 0.0
      DBC(11,15) = 0.0
      DBC(11,16) = 0.0
      DBC(11,17) = 0.0
      DBC(11,18) = 0.0
      DBC(11,19) = 0.0
      DBC(11,20) = 0.0
      DBC(11,21) = 0.0
      DBC(11,22) = 0.0
      DBC(11,23) = 0.0
      DBC(11,24) = 0.0
      DBC(11,25) = 0.0
      DBC(11,26) = 0.0
      DBC(11,27) = 0.0
      DBC(11,28) = 0.0
      DBC(11,29) = 0.0
```

```
      DBC(11,30) = 0.0
      DBC(11,31) = 0.0
      DBC(11,32) = 0.0
C
C FB(12)
C
      DBC(12, 1) = 0.0
      DBC(12, 2) = 0.0
      DBC(12, 3) = 0.0
      DBC(12, 4) = 0.0
      DBC(12, 5) = 0.0
      DBC(12, 6) = 0.0
      DBC(12, 7) = 0.0
      DBC(12, 8) = 0.0
      DBC(12, 9) = 0.0
      DBC(12,10) = 0.0
      DBC(12,11) = 0.0
      DBC(12,12) = 0.0
      DBC(12,13) = 0.0
      DBC(12,14) = 0.0
      DBC(12,15) = 0.0
      DBC(12,16) = 0.0
      DBC(12,17) = 0.0
      DBC(12,18) = 0.0
      DBC(12,19) = -U1( 9)/2
      DBC(12,20) =  U1( 8)/2
      DBC(12,21) = -U1(11)/2
      DBC(12,22) =  U1(10)/2
      DBC(12,23) =  U1( 5)/2
      DBC(12,24) = -U1( 4)/2
      DBC(12,25) =  U1( 7)/2
      DBC(12,26) = -U1( 6)/2
      DBC(12,27) = 0.0
      DBC(12,28) = 0.0
      DBC(12,29) = 0.0
      DBC(12,30) = 0.0
      DBC(12,31) = 0.0
      DBC(12,32) = 0.0
C
C FB(13)
C
      DBC(13, 1) = 0.0
      DBC(13, 2) = 0.0
      DBC(13, 3) = 0.0
      DBC(13, 4) = 0.0
      DBC(13, 5) = 0.0
```

```
      DBC(13, 6) = 0.0
      DBC(13, 7) = 0.0
      DBC(13, 8) = 0.0
      DBC(13, 9) = 0.0
      DBC(13,10) = 0.0
      DBC(13,11) = 0.0
      DBC(13,12) = 0.0
      DBC(13,13) = 0.0
      DBC(13,14) = 0.0
      DBC(13,15) = 0.0
      DBC(13,16) = 0.0
      DBC(13,17) = 0.0
      DBC(13,18) = 0.0
      DBC(13,19) = 2*U1(6)
      DBC(13,20) = 2*U1(7)
      DBC(13,21) = 2*U1(4)
      DBC(13,22) = 2*U1(5)
      DBC(13,23) = 0.0
      DBC(13,24) = 0.0
      DBC(13,25) = 0.0
      DBC(13,26) = 0.0
      DBC(13,27) = 0.0
      DBC(13,28) = 0.0
      DBC(13,29) = 0.0
      DBC(13,30) = 0.0
      DBC(13,31) = 0.0
      DBC(13,32) = 0.0
C
C FB(14)
C
      DBC(14, 1) = 0.0
      DBC(14, 2) = 0.0
      DBC(14, 3) = 0.0
      DBC(14, 4) = 0.0
      DBC(14, 5) = 0.0
      DBC(14, 6) = 0.0
      DBC(14, 7) = 0.0
      DBC(14, 8) = 0.0
      DBC(14, 9) = 0.0
      DBC(14,10) = 0.0
      DBC(14,11) = 0.0
      DBC(14,12) = 0.0
      DBC(14,13) = 0.0
      DBC(14,14) = 0.0
      DBC(14,15) = 0.0
      DBC(14,16) = 0.0
```

```
      DBC(14,17) = 0.0
      DBC(14,18) = 0.0
      DBC(14,19) = -2*U1(7)
      DBC(14,20) =  2*U1(6)
      DBC(14,21) =  2*U1(5)
      DBC(14,22) = -2*U1(4)
      DBC(14,23) = 0.0
      DBC(14,24) = 0.0
      DBC(14,25) = 0.0
      DBC(14,26) = 0.0
      DBC(14,27) = 0.0
      DBC(14,28) = 0.0
      DBC(14,29) = 0.0
      DBC(14,30) = 0.0
      DBC(14,31) = 0.0
      DBC(14,32) = 0.0
C
C FB(15)
C
      DBC(15, 1) = 0.0
      DBC(15, 2) = 0.0
      DBC(15, 3) = 0.0
      DBC(15, 4) = 0.0
      DBC(15, 5) = 0.0
      DBC(15, 6) = 0.0
      DBC(15, 7) = 0.0
      DBC(15, 8) = 0.0
      DBC(15, 9) = 0.0
      DBC(15,10) = 0.0
      DBC(15,11) = 0.0
      DBC(15,12) = 0.0
      DBC(15,13) = 0.0
      DBC(15,14) = 0.0
      DBC(15,15) = 1.0
      DBC(15,16) = 0.0
      DBC(15,17) = 0.0
      DBC(15,18) = 0.0
      DBC(15,19) = 0.0
      DBC(15,20) = 0.0
      DBC(15,21) = 0.0
      DBC(15,22) = 0.0
      DBC(15,23) = 0.0
      DBC(15,24) = 0.0
      DBC(15,25) = 0.0
      DBC(15,26) = 0.0
      DBC(15,27) = 0.0
```

```
      DBC(15,28) = 0.0
      DBC(15,29) = 0.0
      DBC(15,30) = 0.0
      DBC(15,31) = 0.0
      DBC(15,32) = 0.0

      RETURN
      END
C
C
C &&&&&&&&&&&&&&&&&&&&&&&&&&&&&&&&&&&&&&&&&&&&&&&&&&&&&&&&&&&&&&&&
C
C
      SUBROUTINE ICND(NDIM,PAR,ICP,NINT,U,UOLD,UDOT,UPOLD,F,
     *                IJAC,DINT)
C
      IMPLICIT DOUBLE PRECISION (A-H,O-Z)
CSGLE IMPLICIT REAL (A-H,O-Z)
C
C ( THIS PROBLEM HAS NO INTEGRAL CONSTRAINTS  )
C
      RETURN
      END
C
C
C &&&&&&&&&&&&&&&&&&&&&&&&&&&&&&&&&&&&&&&&&&&&&&&&&&&&&&&&&&&&&&&&
C
C
      SUBROUTINE FOPT(NDIM,U,ICP,PAR,IJAC,FS,DFDU,DFDP)
C
      RETURN
      END
```

A.1.2 AUTO Input File

```
15 4 6 1                     NDIM,IPS,IRS,ILP
1 2                          NICP,(ICP(I),I=1,NICP)
30 4 3 2 1 0 15 0            NTST,NCOL,IADS,ISP,ISW,IPLT,NBC,NINT
1000 -8.0 8.0 -50.0 50.0     NMX,RL0,RL1,A0,A1
1000 10 4 8 7 3 0            NPR,MXBF,IID,ITMX,ITNW,NWTN,JAC
1.0E-7 1.0E-7 1.0E-5         EPSL,EPSU,EPSS
0.01 .00001 0.1 1            DS,DSMIN,DSMAX,IADS
0                            NTHL,(/,I,THL(I)),I=1,NTHL)
0                            NTHU,(/,I,THU(I)),I=1,NTHU)
4                            NUZR,(/,I,PAR(I)),I=1,NUZR)
```

```
  2   0.00
  2   3.14
  2   4.71
  2   6.28
```

A.2 9^{th} Order System with 3 Integral Constraints

A.2.1 Software

```
C------------------------------------------------------------
C------------------------------------------------------------
C  AUTRING : A Semicircle with Bifurcations.
C------------------------------------------------------------
C------------------------------------------------------------

      DOUBLE PRECISION FUNCTION smu1(s)
      IMPLICIT DOUBLE PRECISION (A-H,O-Z)
      COMMON /BLBCN/ NDIM,IPS,IRS,ILP,ICP(20),PAR(20)
      uhat1 = 0.0D0
      smu1 = PAR(6)*uhat1
      END

      DOUBLE PRECISION FUNCTION smu2(s)
      IMPLICIT DOUBLE PRECISION (A-H,O-Z)
      COMMON /BLBCN/ NDIM,IPS,IRS,ILP,ICP(20),PAR(20)
      uhat2 = 0.0D0
      smu2 = PAR(6)*uhat2
      END

      DOUBLE PRECISION FUNCTION smu3(s)
      IMPLICIT DOUBLE PRECISION (A-H,O-Z)
      COMMON /BLBCN/ NDIM,IPS,IRS,ILP,ICP(20),PAR(20)
      smu3 = 0.0D0
      END

      SUBROUTINE FUNC(NDIM,U,ICP,PAR,IJAC,F,DFDU,DFDP)
C     ---------- ----

      IMPLICIT DOUBLE PRECISION (A-H,O-Z)
      DOUBLE PRECISION I1,I2,I3

      DIMENSION U(NDIM),PAR(20),F(NDIM),DFDU(NDIM,NDIM)
      DIMENSION d3qn(4), DFDP(NDIM,20)
      DOUBLE PRECISION m(3), k(3), mu(3), kappa, alpha, beta
```

```fortran
      DOUBLE PRECISION fact1, fact2, fact3

      kappa = 0.0D0
      alpha = 0.0D0
      beta  = 0.0D0

C     Calculate some subexpressions which will be used a lot

      mu(1) = 0.0
      mu(2) = PAR(6)
      mu(3) = beta

      m(1) = (U(4)*U(5) + U(3)*U(6) - U(2)*U(7) - U(1)*U(8))/2
      m(2) = (-U(3)*U(5) + U(4)*U(6) + U(1)*U(7) - U(2)*U(8))/2
      m(3) = (U(2)*U(5) - U(1)*U(6) + U(4)*U(7) - U(3)*U(8))/2

      d3qn(1) =  -2.0D0*(U(3)*PAR(2) - U(4)*PAR(3) - U(1)*PAR(4))
      d3qn(2) =  -2.0D0*(U(4)*PAR(2) + U(3)*PAR(3) - U(2)*PAR(4))
      d3qn(3) =  -2.0D0*(U(1)*PAR(2) + U(2)*PAR(3) + U(3)*PAR(4))
      d3qn(4) =  -2.0D0*(U(2)*PAR(2) - U(1)*PAR(3) + U(4)*PAR(4))

      k(1) = 0.1D0
      k(2) = 0.1D0
      k(3) = k(1)*par(7)

      a = (m(1)/k(1) + mu(1))/2
      b = (m(2)/k(2) + mu(2))/2
      c = (m(3)/k(3) + mu(3))/2

c     Now calculate the right hand sides

      F(1) =  a*U(4) - b*U(3) + c*U(2)
      F(2) =  a*U(3) + b*U(4) - c*U(1)
      F(3) = -a*U(2) + b*U(1) + c*U(4)
      F(4) = -a*U(1) - b*U(2) - c*U(3)

      F(5) =  a*U(8) - b*U(7) + c*U(6) + d3qn(1)
      F(6) =  a*U(7) + b*U(8) - c*U(5) + d3qn(2)
      F(7) = -a*U(6) + b*U(5) + c*U(8) + d3qn(3)
      F(8) = -a*U(5) - b*U(6) - c*U(7) + d3qn(4)

      F(9) = 1.0D0

      IF(IJAC.EQ.0) RETURN
C
      fact1 = 1/(4*k(1))
```

```
      fact2 = 1/(4*k(2))
      fact3 = 1/(4*k(3))
C
      DFDU(1,1)=   -fact1*U(4)*U(8)-fact2*U(3)*U(7)-
     *              fact3*U(2)*U(6)
      DFDU(1,2)=  c-fact1*U(4)*U(7)+fact2*U(3)*U(8)+
     *              fact3*U(2)*U(5)
      DFDU(1,3)= -b+fact1*U(4)*U(6)+fact2*U(3)*U(5)-
     *              fact3*U(2)*U(8)
      DFDU(1,4)=  a+fact1*U(4)*U(5)-fact2*U(3)*U(6)+
     *              fact3*U(2)*U(7)
      DFDU(1,5)=  fact1*U(4)*U(4)+fact2*U(3)*U(3)+
     *              fact3*U(2)*U(2)
      DFDU(1,6)=  fact1*U(3)*U(4)-fact2*U(4)*U(3)-
     *              fact3*U(1)*U(2)
      DFDU(1,7)= -fact1*U(2)*U(4)-fact2*U(1)*U(3)+
     *              fact3*U(4)*U(2)
      DFDU(1,8)= -fact1*U(1)*U(4)+fact2*U(2)*U(3)-
     *              fact3*U(3)*U(2)
      DFDU(1,9) = 0.0D0
C
      DFDU(2,1)= -c-fact1*U(3)*U(8)+fact2*U(4)*U(7)+
     *              fact3*U(1)*U(6)
      DFDU(2,2)=   -fact1*U(3)*U(7)-fact2*U(4)*U(8)-
     *              fact3*U(1)*U(5)
      DFDU(2,3)=  a+fact1*U(3)*U(6)-fact2*U(4)*U(5)+
     *              fact3*U(1)*U(8)
      DFDU(2,4)=  b+fact1*U(3)*U(5)+fact2*U(4)*U(6)-
     *              fact3*U(1)*U(7)
      DFDU(2,5)=  fact1*U(4)*U(3)-fact2*U(3)*U(4)-
     *              fact3*U(2)*U(1)
      DFDU(2,6)=  fact1*U(3)*U(3)+fact2*U(4)*U(4)+
     *              fact3*U(1)*U(1)
      DFDU(2,7)= -fact1*U(2)*U(3)+fact2*U(1)*U(4)-
     *              fact3*U(4)*U(1)
      DFDU(2,8)= -fact1*U(1)*U(3)-fact2*U(2)*U(4)+
     *              fact3*U(3)*U(1)
      DFDU(2,9) = 0.0D0
C
      DFDU(3,1)=  b+fact1*U(2)*U(8)+fact2*U(1)*U(7)-
     *              fact3*U(4)*U(6)
      DFDU(3,2)= -a+fact1*U(2)*U(7)-fact2*U(1)*U(8)+
     *              fact3*U(4)*U(5)
      DFDU(3,3)=   -fact1*U(2)*U(6)-fact2*U(1)*U(5)-
     *              fact3*U(4)*U(8)
      DFDU(3,4)=  c-fact1*U(2)*U(5)+fact2*U(1)*U(6)+
```

```
     *              fact3*U(4)*U(7)
      DFDU(3,5)= -fact1*U(4)*U(2)-fact2*U(3)*U(1)+
     *              fact3*U(2)*U(4)
      DFDU(3,6)= -fact1*U(3)*U(2)+fact2*U(4)*U(1)-
     *              fact3*U(1)*U(4)
      DFDU(3,7)=  fact1*U(2)*U(2)+fact2*U(1)*U(1)+
     *              fact3*U(4)*U(4)
      DFDU(3,8)=  fact1*U(1)*U(2)-fact2*U(2)*U(1)-
     *              fact3*U(3)*U(4)
      DFDU(3,9) = 0.0D0
C
      DFDU(4,1)= -a+fact1*U(1)*U(8)-fact2*U(2)*U(7)+
     *              fact3*U(3)*U(6)
      DFDU(4,2)= -b+fact1*U(1)*U(7)+fact2*U(2)*U(8)-
     *              fact3*U(3)*U(5)
      DFDU(4,3)= -c-fact1*U(1)*U(6)+fact2*U(2)*U(5)+
     *              fact3*U(3)*U(8)
      DFDU(4,4)=   -fact1*U(1)*U(5)-fact2*U(2)*U(6)-
     *              fact3*U(3)*U(7)
      DFDU(4,5)= -fact1*U(4)*U(1)+fact2*U(3)*U(2)-
     *              fact3*U(2)*U(3)
      DFDU(4,6)= -fact1*U(3)*U(1)-fact2*U(4)*U(2)+
     *              fact3*U(1)*U(3)
      DFDU(4,7)=  fact1*U(2)*U(1)-fact2*U(1)*U(2)-
     *              fact3*U(4)*U(3)
      DFDU(4,8)=  fact1*U(1)*U(1)+fact2*U(2)*U(2)+
     *              fact3*U(3)*U(3)
      DFDU(4,9) = 0.0D0
C
      DFDU(5,1)=  2*PAR(4) - fact1*U(8)*U(8) - fact2*U(7)*U(7) -
     *            fact3*U(6)*U(6)
      DFDU(5,2)=          - fact1*U(7)*U(8) + fact2*U(8)*U(7) +
     *            fact3*U(5)*U(6)
      DFDU(5,3)= -2*PAR(2) + fact1*U(6)*U(8) + fact2*U(5)*U(7) -
     *            fact3*U(8)*U(6)
      DFDU(5,4)=  2*PAR(3) + fact1*U(5)*U(8) - fact2*U(6)*U(7) +
     *            fact3*U(7)*U(6)
      DFDU(5,5)=    fact1*U(4)*U(8)+fact2*U(3)*U(7)+
     *              fact3*U(2)*U(6)
      DFDU(5,6)=  c+fact1*U(3)*U(8)-fact2*U(4)*U(7)-
     *              fact3*U(1)*U(6)
      DFDU(5,7)= -b-fact1*U(2)*U(8)-fact2*U(1)*U(7)+
     *              fact3*U(4)*U(6)
      DFDU(5,8)=  a-fact1*U(1)*U(8)+fact2*U(2)*U(7)-
     *              fact3*U(3)*U(6)
      DFDU(5,9) = 0.0D0
```

```
C
      DFDU(6,1)=           - fact1*U(8)*U(7) + fact2*U(7)*U(8) +
     *            fact3*U(6)*U(5)
      DFDU(6,2)=  2*PAR(4) - fact1*U(7)*U(7) - fact2*U(8)*U(8) -
     *            fact3*U(5)*U(5)
      DFDU(6,3)= -2*PAR(3) + fact1*U(6)*U(7) - fact2*U(5)*U(8) +
     *            fact3*U(8)*U(5)
      DFDU(6,4)= -2*PAR(2) + fact1*U(5)*U(7) + fact2*U(6)*U(8) -
     *            fact3*U(7)*U(5)
      DFDU(6,5)= -c+fact1*U(4)*U(7)-fact2*U(3)*U(8)-
     *              fact3*U(2)*U(5)
      DFDU(6,6)=    fact1*U(3)*U(7)+fact2*U(4)*U(8)+
     *              fact3*U(1)*U(5)
      DFDU(6,7)=  a-fact1*U(2)*U(7)+fact2*U(1)*U(8)-
     *              fact3*U(4)*U(5)
      DFDU(6,8)=  b-fact1*U(1)*U(7)-fact2*U(2)*U(8)+
     *              fact3*U(3)*U(5)
      DFDU(6,9) = 0.0D0
C
      DFDU(7,1)= -2*PAR(2) + fact1*U(8)*U(6) + fact2*U(7)*U(5) -
     *            fact3*U(6)*U(8)
      DFDU(7,2)= -2*PAR(3) + fact1*U(7)*U(6) - fact2*U(8)*U(5) +
     *            fact3*U(5)*U(8)
      DFDU(7,3)= -2*PAR(4) - fact1*U(6)*U(6) - fact2*U(5)*U(5) -
     *            fact3*U(8)*U(8)
      DFDU(7,4)=           - fact1*U(5)*U(6) + fact2*U(6)*U(5) +
     *            fact3*U(7)*U(8)
      DFDU(7,5)=  b-fact1*U(4)*U(6)-fact2*U(3)*U(5)+
     *              fact3*U(2)*U(8)
      DFDU(7,6)= -a-fact1*U(3)*U(6)+fact2*U(4)*U(5)-
     *              fact3*U(1)*U(8)
      DFDU(7,7)=    fact1*U(2)*U(6)+fact2*U(1)*U(5)+
     *              fact3*U(4)*U(8)
      DFDU(7,8)=  c+fact1*U(1)*U(6)-fact2*U(2)*U(5)-
     *              fact3*U(3)*U(8)
      DFDU(7,9) = 0.0D0
C
      DFDU(8,1)=  2*PAR(3) + fact1*U(8)*U(5) - fact2*U(7)*U(6) +
     *            fact3*U(6)*U(7)
      DFDU(8,2)= -2*PAR(2) + fact1*U(7)*U(5) + fact2*U(8)*U(6) -
     *            fact3*U(5)*U(7)
      DFDU(8,3)=           - fact1*U(6)*U(5) + fact2*U(5)*U(6) +
     *            fact3*U(8)*U(7)
      DFDU(8,4)= -2*PAR(4) - fact1*U(5)*U(5) - fact2*U(6)*U(6) -
     *            fact3*U(7)*U(7)
      DFDU(8,5)= -a-fact1*U(4)*U(5)+fact2*U(3)*U(6)-
```

```
     *              fact3*U(2)*U(7)
      DFDU(8,6)= -b-fact1*U(3)*U(5)-fact2*U(4)*U(6)+
     *              fact3*U(1)*U(7)
      DFDU(8,7)= -c+fact1*U(2)*U(5)-fact2*U(1)*U(6)-
     *              fact3*U(4)*U(7)
      DFDU(8,8)=    fact1*U(1)*U(5)+fact2*U(2)*U(6)+
     *              fact3*U(3)*U(7)
      DFDU(8,9) = 0.0D0
C
      DFDU(9,1) = 0.0D0
      DFDU(9,2) = 0.0D0
      DFDU(9,3) = 0.0D0
      DFDU(9,4) = 0.0D0
      DFDU(9,5) = 0.0D0
      DFDU(9,6) = 0.0D0
      DFDU(9,7) = 0.0D0
      DFDU(9,8) = 0.0D0
      DFDU(9,9) = 0.0D0
C
C     Derivatives wrt parameters
C
      DFDP(1,1) = 0.0D0
      DFDP(2,1) = 0.0D0
      DFDP(3,1) = 0.0D0
      DFDP(4,1) = 0.0D0
      DFDP(5,1) = 0.0D0
      DFDP(6,1) = 0.0D0
      DFDP(7,1) = 0.0D0
      DFDP(8,1) = 0.0D0
      DFDP(9,1) = 0.0D0
C
      DFDP(1,2) = 0.0D0
      DFDP(2,2) = 0.0D0
      DFDP(3,2) = 0.0D0
      DFDP(4,2) = 0.0D0
      DFDP(5,2) = -2*U(3)
      DFDP(6,2) = -2*U(4)
      DFDP(7,2) = -2*U(1)
      DFDP(8,2) = -2*U(2)
      DFDP(9,2) = 0.0D0
C
      DFDP(1,3) = 0.0D0
      DFDP(2,3) = 0.0D0
      DFDP(3,3) = 0.0D0
      DFDP(4,3) = 0.0D0
      DFDP(5,3) =  2*U(4)
```

```
      DFDP(6,3) = -2*U(3)
      DFDP(7,3) = -2*U(2)
      DFDP(8,3) =  2*U(1)
      DFDP(9,3) = 0.0D0
C
      DFDP(1,4) = 0.0D0
      DFDP(2,4) = 0.0D0
      DFDP(3,4) = 0.0D0
      DFDP(4,4) = 0.0D0
      DFDP(5,4) =  2*U(1)
      DFDP(6,4) =  2*U(2)
      DFDP(7,4) = -2*U(3)
      DFDP(8,4) = -2*U(4)
      DFDP(9,4) = 0.0D0
C
      DFDP(1,5) = 0.0D0
      DFDP(2,5) = 0.0D0
      DFDP(3,5) = 0.0D0
      DFDP(4,5) = 0.0D0
      DFDP(5,5) = 0.0D0
      DFDP(6,5) = 0.0D0
      DFDP(7,5) = 0.0D0
      DFDP(8,5) = 0.0D0
      DFDP(9,5) = 0.0D0
C

      RETURN
      END

C
C &&&&&&&&&&&&&&&&&&&&&&&&&&&&&&&&&&&&&&&&&&&&&&&&&&&&&&&&&&
C
C
      SUBROUTINE STPNT(NDIM,U,PAR,T)
C     ---------- -----
C
      IMPLICIT DOUBLE PRECISION (A-H,O-Z)
C
      DOUBLE PRECISION k1,k2,k3, NPI, NPI2, mufact
      DIMENSION U(NDIM),PAR(20)
      DIMENSION Z(16)
C

         PI     = 4.0D0*DATAN(1.0D0)
         PAR(1) = 20/PI
         PAR(2) = 0.0D0
```

```
         PAR(3) = 0.0D0
         PAR(4) = 0.0D0
         PAR(5) = 0.0D0
         PAR(6) = 0.3D0
         PAR(7) = 2.0/7.0
         NPI2   = PI*2.0D0
         k1     = 0.1D0
         k2     = 0.1D0
         k3     = (k1 + k2)/7
         mufact = 2.0*k2*PI

C     Calculate some subexpressions which will be used a lot

         dcnpit = DCOS(0.5*PI*T)
         dstpit = DSIN(0.5*PI*T)

         U(1)  =  0.0
         U(2)  =  dstpit
         U(3)  =  0.0
         U(4)  =  dcnpit

         U(5)  =  0.0
         U(6)  =  mufact*dcnpit
         U(7)  =  0.0
         U(8)  = -mufact*dstpit

         U(9)  = T

      RETURN
      END
C
C
C &&&&&&&&&&&&&&&&&&&&&&&&&&&&&&&&&&&&&&&&&&&&&&&&&&&&&&&&&&&&
C
C
      SUBROUTINE BCND(NDIM,PAR,ICP,NBC,U0,U1,FB,IJAC,DBC)
C     ---------- ----
C
      IMPLICIT DOUBLE PRECISION (A-H,O-Z)
C
      DOUBLE PRECISION NPI, NPTERM
      DIMENSION PAR(20),ICP(20),U0(NDIM),U1(NDIM),FB(NBC)
      DIMENSION DBC(NBC,20)
C

c
```

```
c  BCs for JAW's Problem - Sliding L
c

          FB(1) = U0(1)
          FB(2) = U0(2)
          FB(3) = U0(3) - DSIN(PAR(5))
          FB(4) = U0(4) - DCOS(PAR(5))

          FB(5) = U0(1)*U0(5) + U0(2)*U0(6) + U0(3)*U0(7) +
     &             U0(4)*U0(8)

          FB(6) = (U1(2)*U1(5) - U1(1)*U1(6) + U1(4)*U1(7) -
     &             U1(3)*U1(8))/2

          FB(7) = 2*(U1(1)*U1(3) + U1(2)*U1(4))
          FB(8) = 2*(U1(2)*U1(3) - U1(1)*U1(4))

          FB(9) = U0(9)

       IF (IJAC.EQ.0) RETURN
C
C     Derivatives of BCs
C
      DBC(1, 1) = 1.0
      DBC(1, 2) = 0.0
      DBC(1, 3) = 0.0
      DBC(1, 4) = 0.0
      DBC(1, 5) = 0.0
      DBC(1, 6) = 0.0
      DBC(1, 7) = 0.0
      DBC(1, 8) = 0.0
      DBC(1, 9) = 0.0
      DBC(1,10) = 0.0
      DBC(1,11) = 0.0
      DBC(1,12) = 0.0
      DBC(1,13) = 0.0
      DBC(1,14) = 0.0
      DBC(1,15) = 0.0
      DBC(1,16) = 0.0
      DBC(1,17) = 0.0
      DBC(1,18) = 0.0
      DBC(1,19) = 0.0
      DBC(1,20) = 0.0
      DBC(1,21) = 0.0
      DBC(1,22) = 0.0
      DBC(1,23) = 0.0
```

```
C
      DBC(2, 1) = 0.0
      DBC(2, 2) = 1.0
      DBC(2, 3) = 0.0
      DBC(2, 4) = 0.0
      DBC(2, 5) = 0.0
      DBC(2, 6) = 0.0
      DBC(2, 7) = 0.0
      DBC(2, 8) = 0.0
      DBC(2, 9) = 0.0
      DBC(2,10) = 0.0
      DBC(2,11) = 0.0
      DBC(2,12) = 0.0
      DBC(2,13) = 0.0
      DBC(2,14) = 0.0
      DBC(2,15) = 0.0
      DBC(2,16) = 0.0
      DBC(2,17) = 0.0
      DBC(2,18) = 0.0
      DBC(2,19) = 0.0
      DBC(2,20) = 0.0
      DBC(2,21) = 0.0
      DBC(2,22) = 0.0
      DBC(2,23) = 0.0
C
      DBC(3, 1) = 0.0
      DBC(3, 2) = 0.0
      DBC(3, 3) = 1.0
      DBC(3, 4) = 0.0
      DBC(3, 5) = 0.0
      DBC(3, 6) = 0.0
      DBC(3, 7) = 0.0
      DBC(3, 8) = 0.0
      DBC(3, 9) = 0.0
      DBC(3,10) = 0.0
      DBC(3,11) = 0.0
      DBC(3,12) = 0.0
      DBC(3,13) = 0.0
      DBC(3,14) = 0.0
      DBC(3,15) = 0.0
      DBC(3,16) = 0.0
      DBC(3,17) = 0.0
      DBC(3,18) = 0.0
      DBC(3,19) = 0.0
      DBC(3,20) = 0.0
      DBC(3,21) = 0.0
```

```
      DBC(3,22) = 0.0
      DBC(3,23) = -DCOS(PAR(5))
C
      DBC(4, 1) = 0.0
      DBC(4, 2) = 0.0
      DBC(4, 3) = 0.0
      DBC(4, 4) = 1.0
      DBC(4, 5) = 0.0
      DBC(4, 6) = 0.0
      DBC(4, 7) = 0.0
      DBC(4, 8) = 0.0
      DBC(4, 9) = 0.0
      DBC(4,10) = 0.0
      DBC(4,11) = 0.0
      DBC(4,12) = 0.0
      DBC(4,13) = 0.0
      DBC(4,14) = 0.0
      DBC(4,15) = 0.0
      DBC(4,16) = 0.0
      DBC(4,17) = 0.0
      DBC(4,18) = 0.0
      DBC(4,19) = 0.0
      DBC(4,20) = 0.0
      DBC(4,21) = 0.0
      DBC(4,22) = 0.0
      DBC(4,23) = DSIN(PAR(5))
C
      DBC(5, 1) = U0(5)
      DBC(5, 2) = U0(6)
      DBC(5, 3) = U0(7)
      DBC(5, 4) = U0(8)
      DBC(5, 5) = U0(1)
      DBC(5, 6) = U0(2)
      DBC(5, 7) = U0(3)
      DBC(5, 8) = U0(4)
      DBC(5, 9) = 0.0
      DBC(5,10) = 0.0
      DBC(5,11) = 0.0
      DBC(5,12) = 0.0
      DBC(5,13) = 0.0
      DBC(5,14) = 0.0
      DBC(5,15) = 0.0
      DBC(5,16) = 0.0
      DBC(5,17) = 0.0
      DBC(5,18) = 0.0
      DBC(5,19) = 0.0
```

```
      DBC(5,20) = 0.0
      DBC(5,21) = 0.0
      DBC(5,22) = 0.0
      DBC(5,23) = 0.0
C
      DBC(6, 1) = 0.0
      DBC(6, 2) = 0.0
      DBC(6, 3) = 0.0
      DBC(6, 4) = 0.0
      DBC(6, 5) = 0.0
      DBC(6, 6) = 0.0
      DBC(6, 7) = 0.0
      DBC(6, 8) = 0.0
      DBC(6, 9) = 0.0
      DBC(6,10) = -U1(6)/2
      DBC(6,11) =  U1(5)/2
      DBC(6,12) = -U1(8)/2
      DBC(6,13) =  U1(7)/2
      DBC(6,14) =  U1(2)/2
      DBC(6,15) = -U1(1)/2
      DBC(6,16) =  U1(4)/2
      DBC(6,17) = -U1(3)/2
      DBC(6,18) = 0.0
      DBC(6,19) = 0.0
      DBC(6,20) = 0.0
      DBC(6,21) = 0.0
      DBC(6,22) = 0.0
      DBC(6,23) = 0.0
C
      DBC(7, 1) = 0.0
      DBC(7, 2) = 0.0
      DBC(7, 3) = 0.0
      DBC(7, 4) = 0.0
      DBC(7, 5) = 0.0
      DBC(7, 6) = 0.0
      DBC(7, 7) = 0.0
      DBC(7, 8) = 0.0
      DBC(7, 9) = 0.0
      DBC(7,10) = 2*U1(3)
      DBC(7,11) = 2*U1(4)
      DBC(7,12) = 2*U1(1)
      DBC(7,13) = 2*U1(2)
      DBC(7,14) = 0.0
      DBC(7,15) = 0.0
      DBC(7,16) = 0.0
      DBC(7,17) = 0.0
```

```
      DBC(7,18) = 0.0
      DBC(7,19) = 0.0
      DBC(7,20) = 0.0
      DBC(7,21) = 0.0
      DBC(7,22) = 0.0
      DBC(7,23) = 0.0
C
      DBC(8, 1) = 0.0
      DBC(8, 2) = 0.0
      DBC(8, 3) = 0.0
      DBC(8, 4) = 0.0
      DBC(8, 5) = 0.0
      DBC(8, 6) = 0.0
      DBC(8, 7) = 0.0
      DBC(8, 8) = 0.0
      DBC(8, 9) = 0.0
      DBC(8,10) = -2*U1(4)
      DBC(8,11) =  2*U1(3)
      DBC(8,12) =  2*U1(2)
      DBC(8,13) = -2*U1(1)
      DBC(8,14) = 0.0
      DBC(8,15) = 0.0
      DBC(8,16) = 0.0
      DBC(8,17) = 0.0
      DBC(8,18) = 0.0
      DBC(8,19) = 0.0
      DBC(8,20) = 0.0
      DBC(8,21) = 0.0
      DBC(8,22) = 0.0
      DBC(8,23) = 0.0
C
      DBC(9, 1) = 0.0
      DBC(9, 2) = 0.0
      DBC(9, 3) = 0.0
      DBC(9, 4) = 0.0
      DBC(9, 5) = 0.0
      DBC(9, 6) = 0.0
      DBC(9, 7) = 0.0
      DBC(9, 8) = 0.0
      DBC(9, 9) = 1.0
      DBC(9,10) = 0.0
      DBC(9,11) = 0.0
      DBC(9,12) = 0.0
      DBC(9,13) = 0.0
      DBC(9,14) = 0.0
      DBC(9,15) = 0.0
```

```
      DBC(9,16) = 0.0
      DBC(9,17) = 0.0
      DBC(9,18) = 0.0
      DBC(9,19) = 0.0
      DBC(9,20) = 0.0
      DBC(9,21) = 0.0
      DBC(9,22) = 0.0
      DBC(9,23) = 0.0
C

      RETURN
      END
C
C
C &&&&&&&&&&&&&&&&&&&&&&&&&&&&&&&&&&&&&&&&&&&&&&&&&&&&&&&&&&&
C
C
      SUBROUTINE ICND(NDIM,PAR,ICP,NINT,U,UOLD,UDOT,UPOLD,F,
     *                IJAC,DINT)
C
      IMPLICIT DOUBLE PRECISION (A-H,O-Z)
      DIMENSION F(NINT), U(NDIM), PAR(20), DINT(NINT,*)

C
C

      F(1) = 2*(U(1)*U(3) + U(2)*U(4)) - 2*PAR(1)/20
      F(2) = 2*(U(2)*U(3) - U(1)*U(4))
      F(3) = U(4)*U(4) + U(3)*U(3) - U(2)*U(2) - U(1)*U(1)

      IF (IJAC.EQ.0) RETURN
C
C     Derivatives of Integral Conditions
C
      DINT(1, 1) = 2*U(3)
      DINT(1, 2) = 2*U(4)
      DINT(1, 3) = 2*U(1)
      DINT(1, 4) = 2*U(2)
      DINT(1, 5) = 0.0
      DINT(1, 6) = 0.0
      DINT(1, 7) = 0.0
      DINT(1, 8) = 0.0
      DINT(1, 9) = 0.0
      DINT(1,10) = -0.1
      DINT(1,11) = 0.0
      DINT(1,12) = 0.0
```

```
      DINT(1,13) = 0.0
      DINT(1,14) = 0.0
C
      DINT(2, 1) = -2*U(4)
      DINT(2, 2) =  2*U(3)
      DINT(2, 3) =  2*U(2)
      DINT(2, 4) = -2*U(1)
      DINT(2, 5) = 0.0
      DINT(2, 6) = 0.0
      DINT(2, 7) = 0.0
      DINT(2, 8) = 0.0
      DINT(2, 9) = 0.0
      DINT(2,10) = 0.0
      DINT(2,11) = 0.0
      DINT(2,12) = 0.0
      DINT(2,13) = 0.0
      DINT(2,14) = 0.0
C
      DINT(3, 1) = -2*U(1)
      DINT(3, 2) = -2*U(2)
      DINT(3, 3) =  2*U(3)
      DINT(3, 4) =  2*U(4)
      DINT(3, 5) = 0.0
      DINT(3, 6) = 0.0
      DINT(3, 7) = 0.0
      DINT(3, 8) = 0.0
      DINT(3, 9) = 0.0
      DINT(3,10) = 0.0
      DINT(3,11) = 0.0
      DINT(3,12) = 0.0
      DINT(3,13) = 0.0
      DINT(3,14) = 0.0
C

      RETURN
      END
C
C
C &&&&&&&&&&&&&&&&&&&&&&&&&&&&&&&&&&&&&&&&&&&&&&&&&&&&&&&&&&&
C
C
      SUBROUTINE FOPT(NDIM,U,ICP,PAR,IJAC,FS,DFDU,DFDP)
C
      RETURN
      END
```

A.2.2 AUTO Input File

```
9 4 6 1                       NDIM,IPS,IRS,ILP
4 5 2 3 4                     NICP,(ICP(I),I=1,NICP)
30 4 3 2 1 0 9 3              NTST,NCOL,IAD,ISP,ISW,IPLT,NBC,NINT
6000 -8.0 8.0 -50.0 50.0      NMX,RL0,RL1,A0,A1
1000 10 2 8 7 7 1             NPR,MXBF,IID,ITMX,ITNW,NWTN,JAC
1.0E-7 1.0E-7 1.0E-5          EPSL,EPSU,EPSS
0.01 .00001 0.1 1             DS,DSMIN,DSMAX,IADS
0                             NTHL,(/,I,THL(I)),I=1,NTHL)
0                             NTHU,(/,I,THU(I)),I=1,NTHU)
4                             NUZR,(/,I,PAR(I)),I=1,NUZR)
   5   0.00
   5   3.14
   5   4.71
   5   6.28
```

Appendix B

Full Sized Twisting Diagrams

In this Appendix we give the full-sized versions of all the Twisting Diagrams displayed in Figure 3.27. Each of the figures plots Twist Angle vs Torque, and covers the full range of $\hat{u}_2$ employed in this study.

For ease of comparison, the end of each figure caption contains a pointer to the location in Figure 3.27 occupied by the large figure. Accordingly, pointer (1,1) refers to the upper left hand corner diagram in Figure 3.27, while pointer (1,2) refers to the diagram directly to the right of diagram (1,1), and pointer (2,1) refers to the diagram directly beneath diagram (1,1).

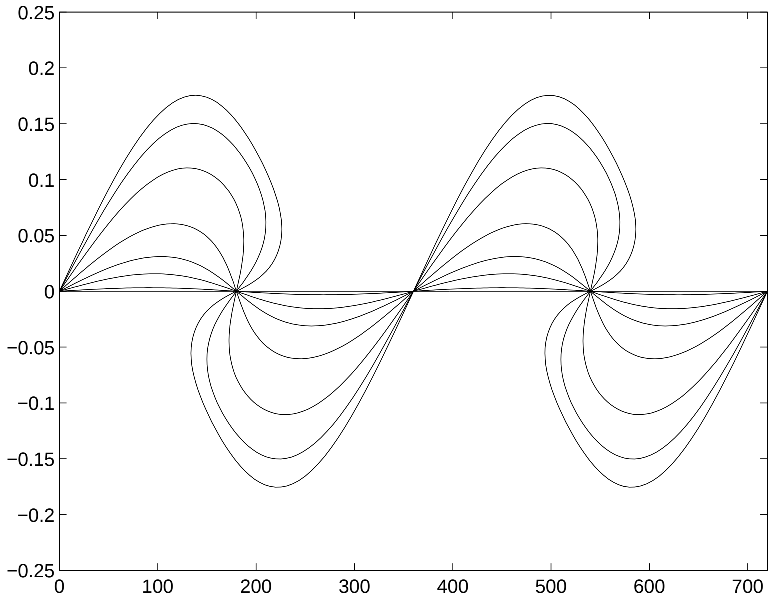

Figure B.1: Twist Angle vs m_3 for $K_3/K_1 = 0.4$, $\rho = 0.80$ (1,1)

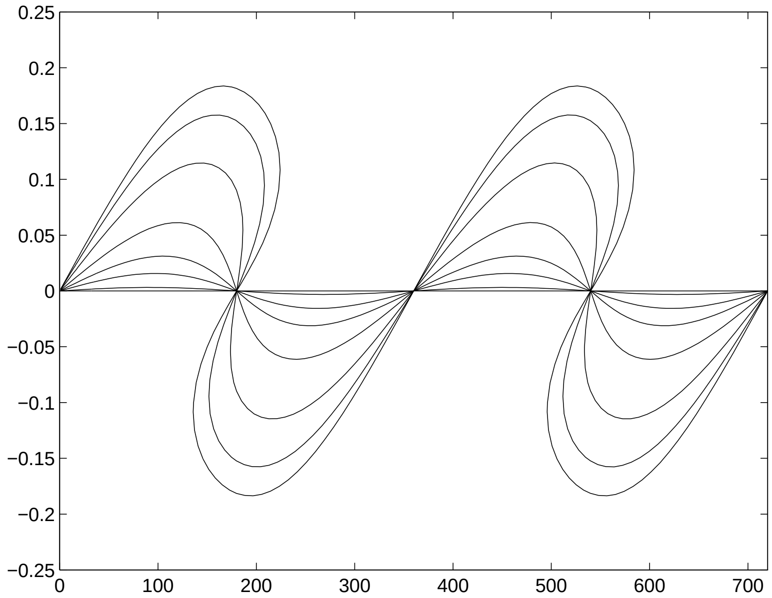

Figure B.2: Twist Angle vs m_3 for $K_3/K_1 = 0.4$, $\rho = 2/\pi$ (1,2)

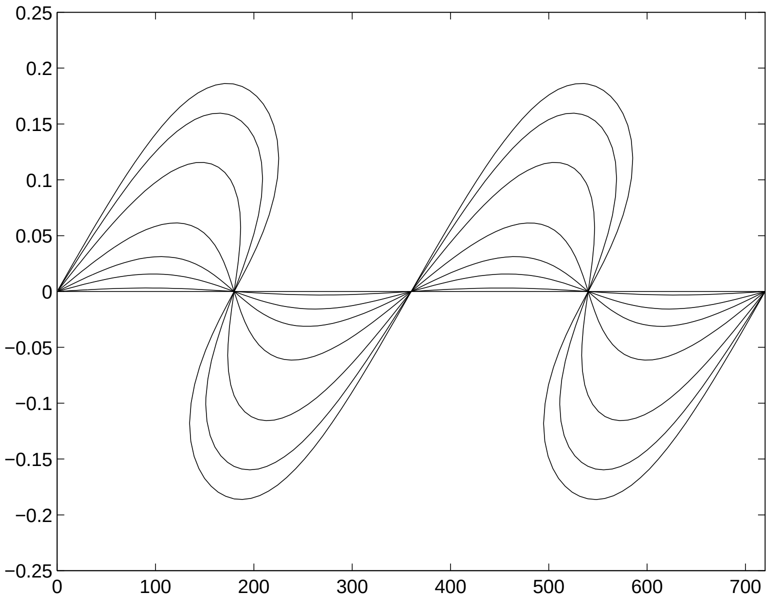

Figure B.3: Twist Angle vs m_3 for $K_3/K_1 = 0.4$, $\rho = 0.60$ (1,3)

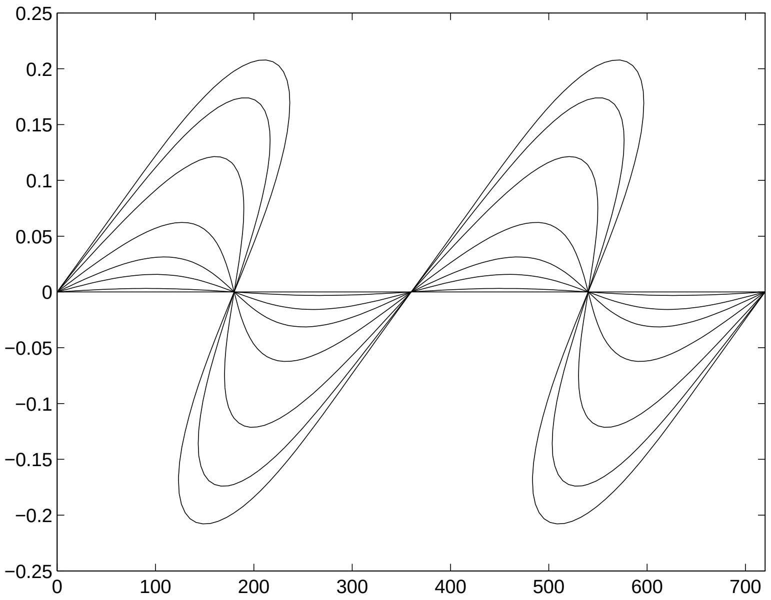

Figure B.4: Twist Angle vs m_3 for $K_3/K_1 = 0.4$, $\rho = 0.40$ (1,4)

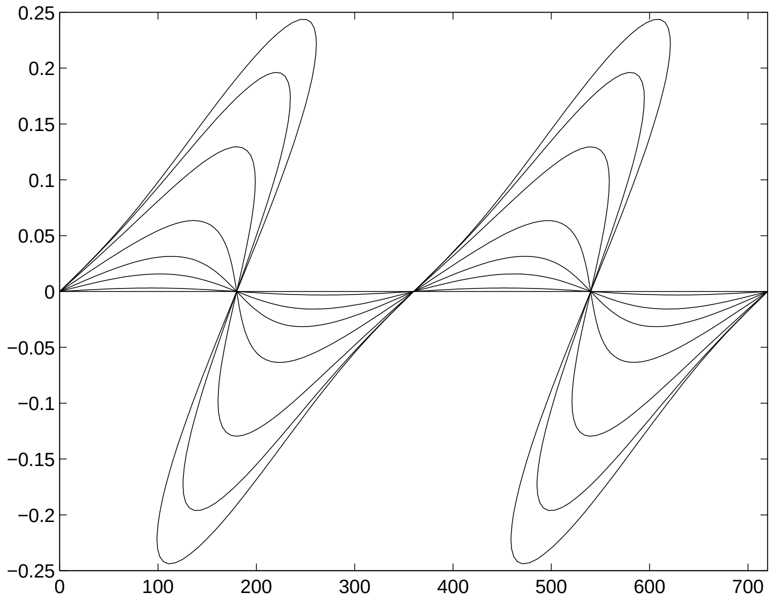

Figure B.5: Twist Angle vs m_3 for $K_3/K_1 = 0.4$, $\rho = 0.20$ (1,5)

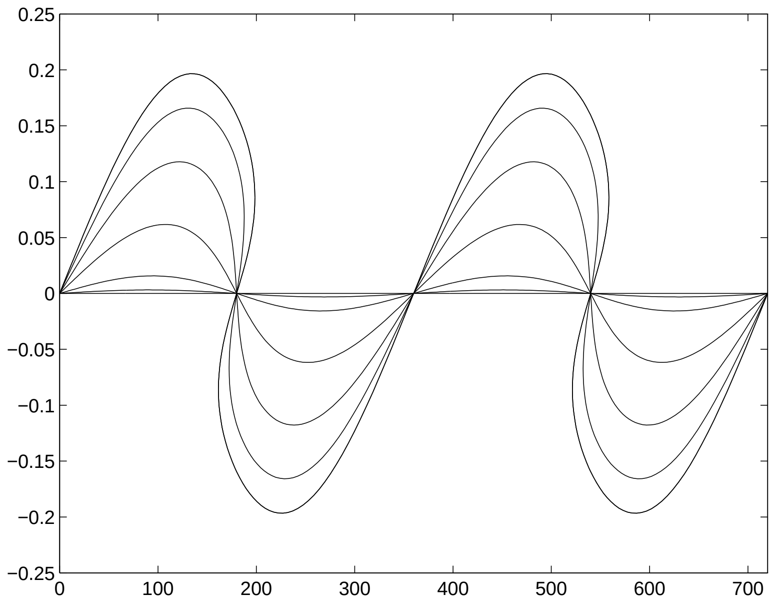

Figure B.6: Twist Angle vs m_3 for $K_3/K_1 = 0.6$, $\rho = 0.80$ (2,1)

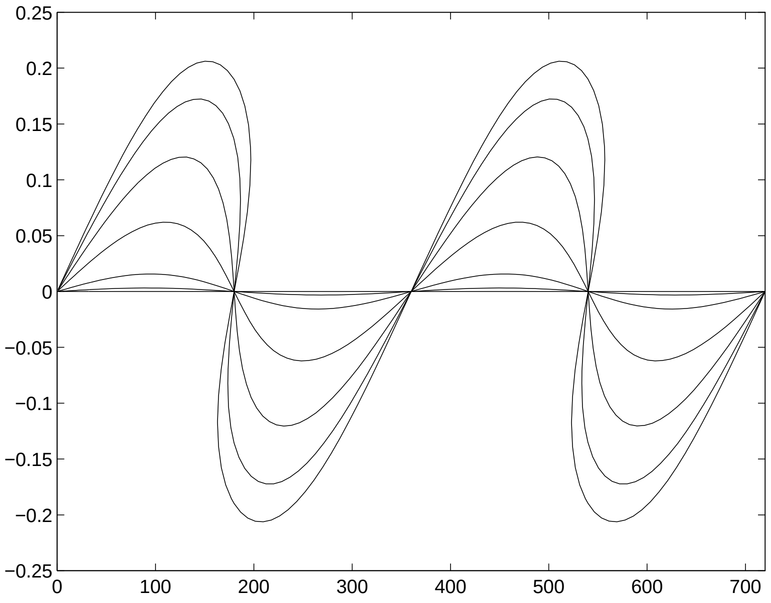

Figure B.7: Twist Angle vs m_3 for $K_3/K_1 = 0.6$, $\rho = 2/\pi$ (2,2)

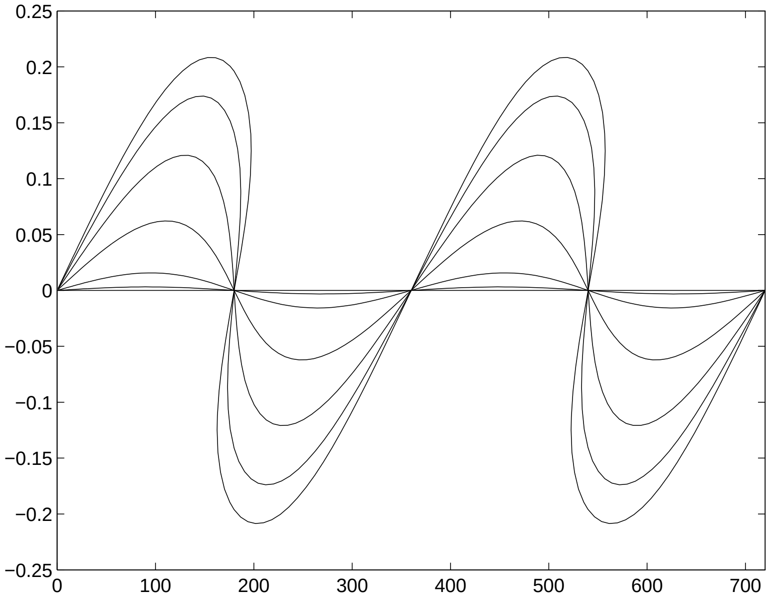

Figure B.8: Twist Angle vs m_3 for $K_3/K_1 = 0.6$, $\rho = 0.60$ (2,3)

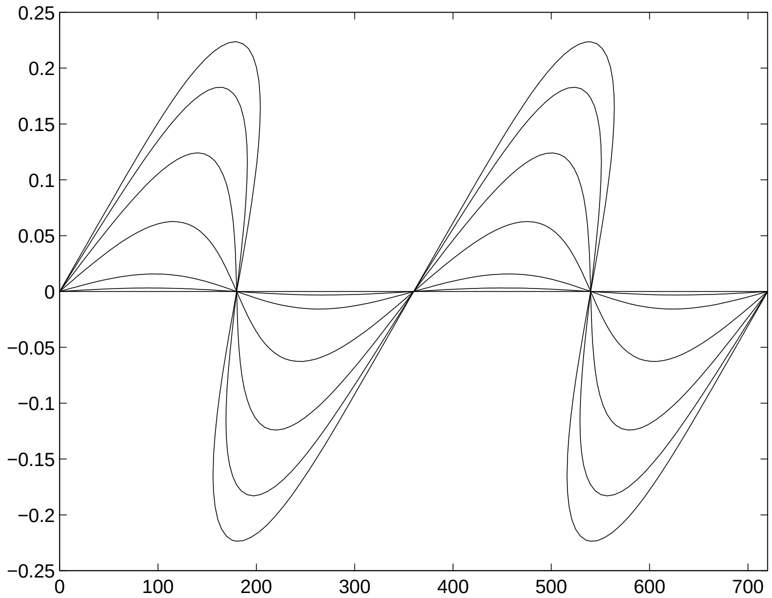

Figure B.9: Twist Angle vs m_3 for $K_3/K_1 = 0.6$, $\rho = 0.40$ (2,4)

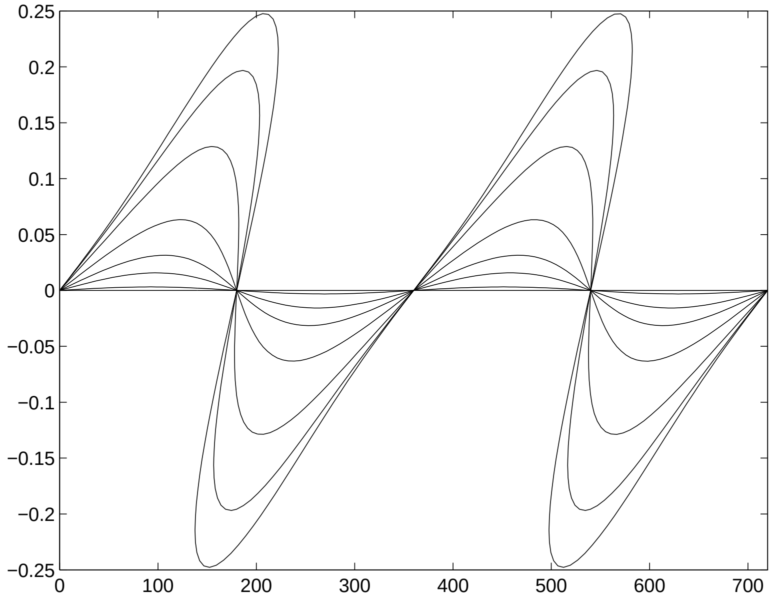

Figure B.10: Twist Angle vs m_3 for $K_3/K_1 = 0.6$, $\rho = 0.20$ (2,5)

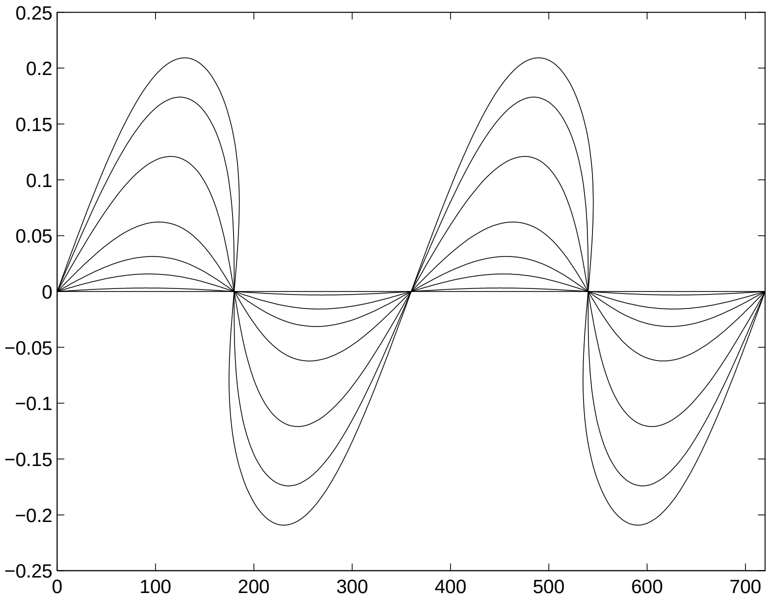

Figure B.11: Twist Angle vs m_3 for $K_3/K_1 = 0.8$, $\rho = 0.80$ (3,1)

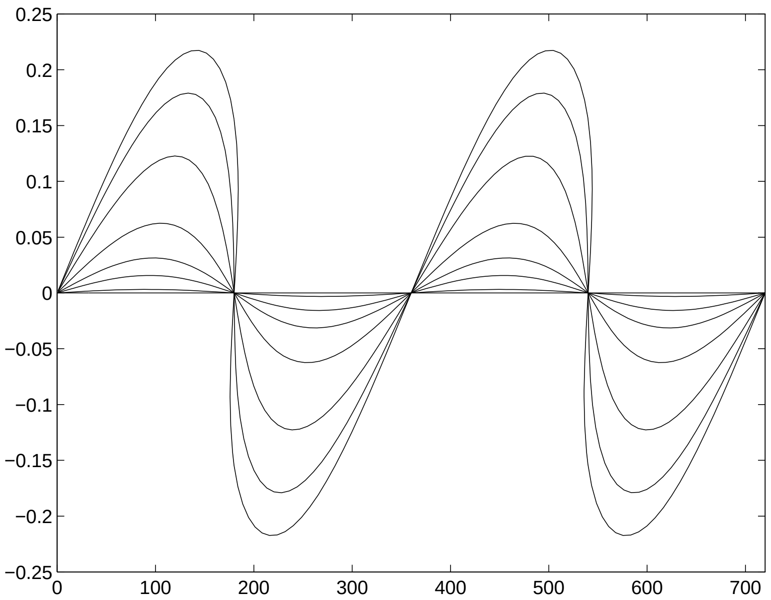

Figure B.12: Twist Angle vs m_3 for $K_3/K_1 = 0.8$, $\rho = 2/\pi$ (3,2)

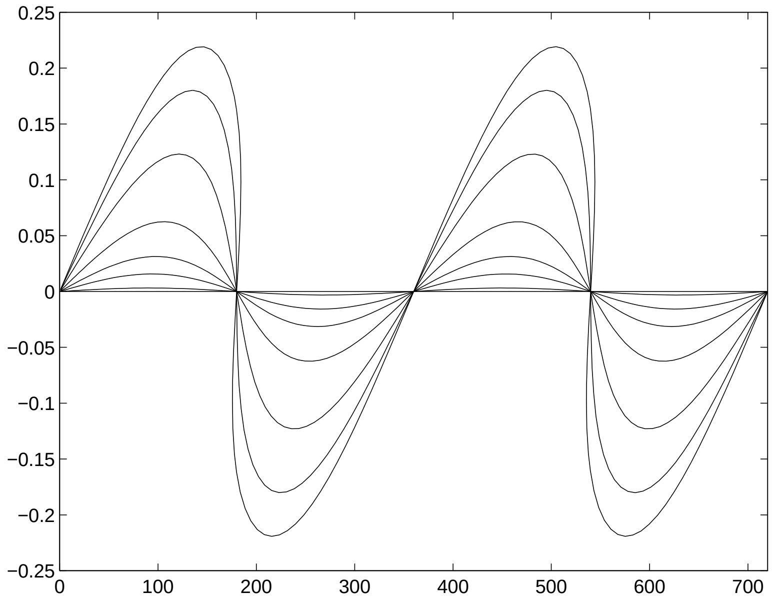

Figure B.13: Twist Angle vs m_3 for $K_3/K_1 = 0.8$, $\rho = 0.60$ (3,3)

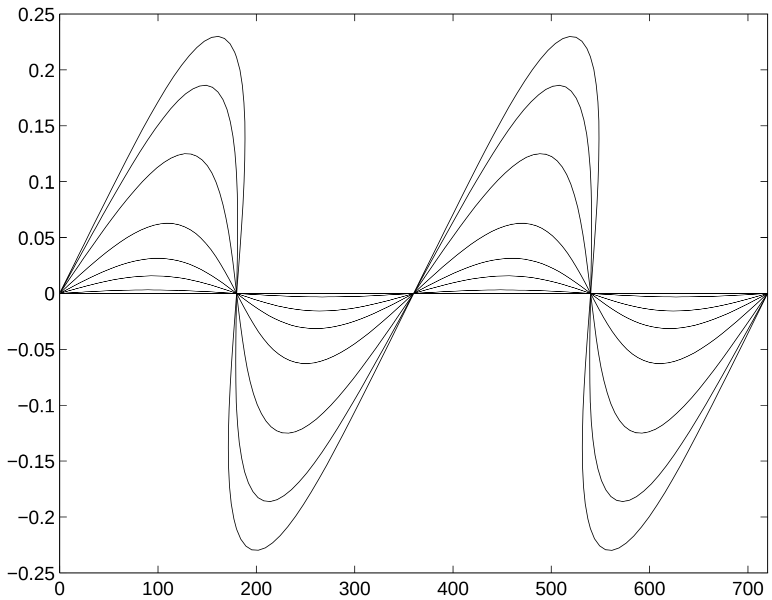

Figure B.14: Twist Angle vs m_3 for $K_3/K_1 = 0.8$, $\rho = 0.40$ (3,4)

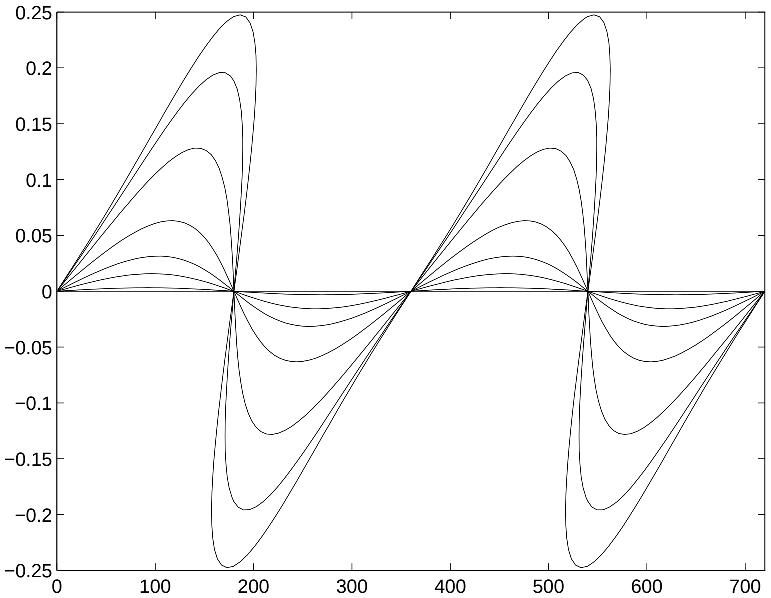

Figure B.15: Twist Angle vs m_3 for $K_3/K_1 = 0.8$, $\rho = 0.20$ (3,5)

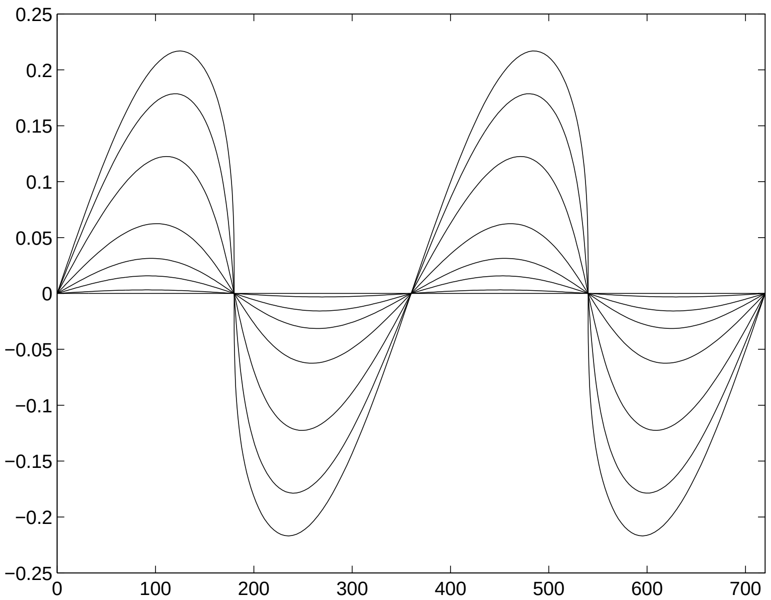

Figure B.16: Twist Angle vs m_3 for $K_3/K_1 = 1.0$, $\rho = 0.80$ (4,1)

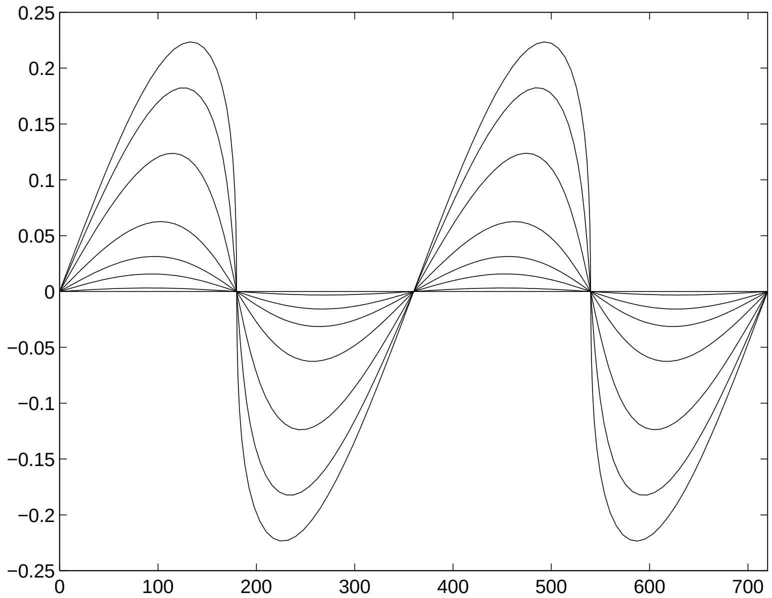

Figure B.17: Twist Angle vs m_3 for $K_3/K_1 = 1.0$, $\rho = 2/\pi$ (4,2)

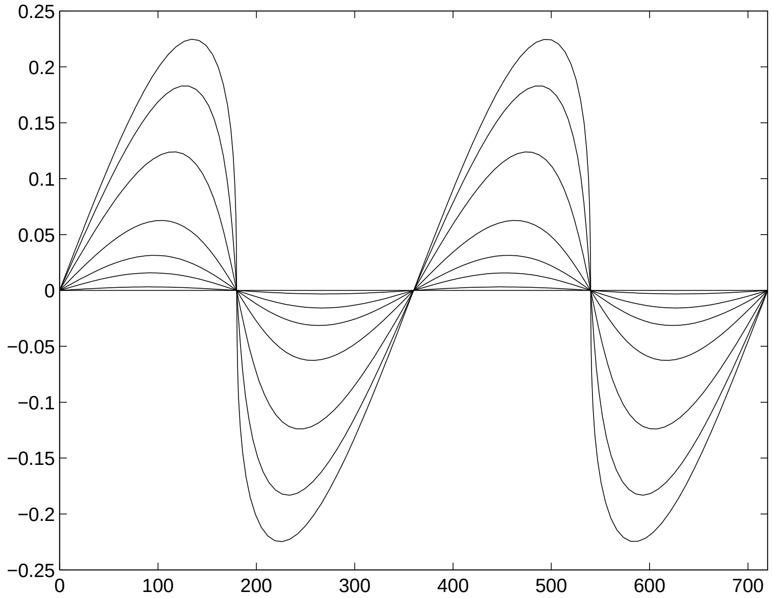

Figure B.18: Twist Angle vs m_3 for $K_3/K_1 = 1.0$, $\rho = 0.60$ (4,3)

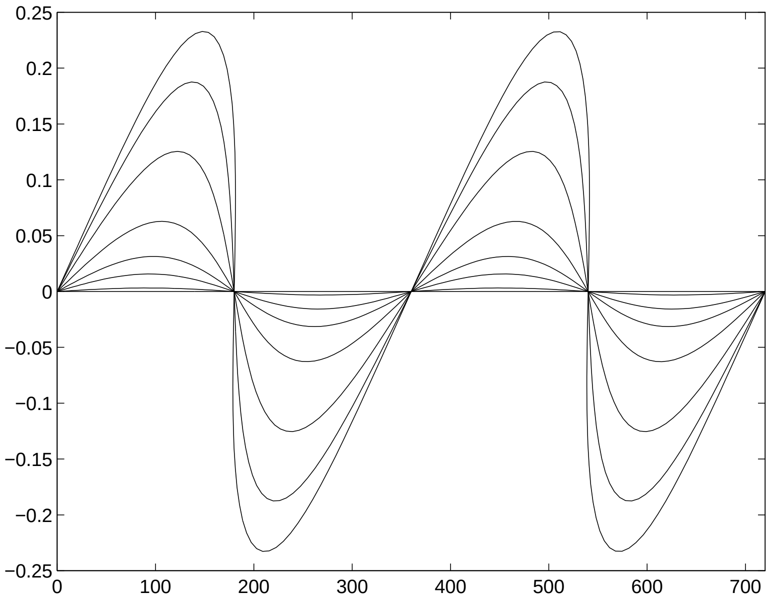

Figure B.19: Twist Angle vs m_3 for $K_3/K_1 = 1.0$, $\rho = 0.40$ (4,4)

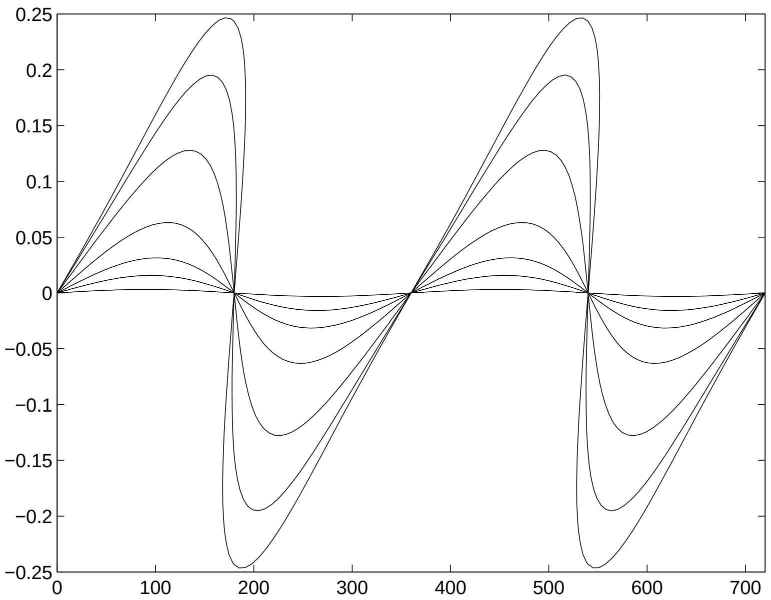

Figure B.20: Twist Angle vs m_3 for $K_3/K_1 = 1.0$, $\rho = 0.20$ (4,5)

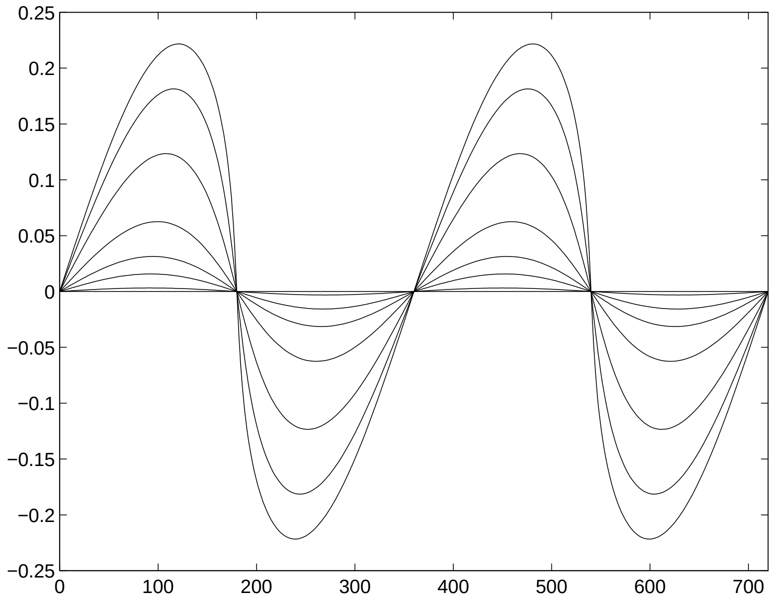

Figure B.21: Twist Angle vs m_3 for $K_3/K_1 = 1.2$, $\rho = 0.80$ (5,1)

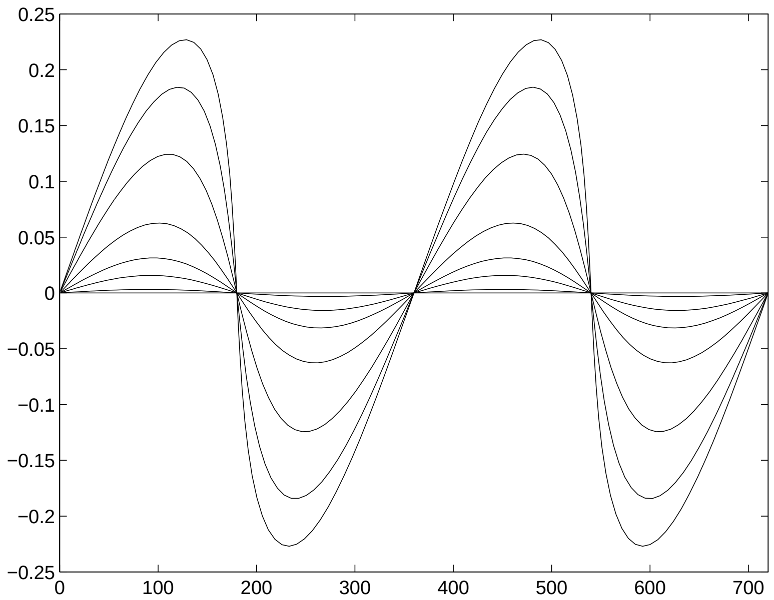

Figure B.22: Twist Angle vs m_3 for $K_3/K_1 = 1.2$, $\rho = 2/\pi$ (5,2)

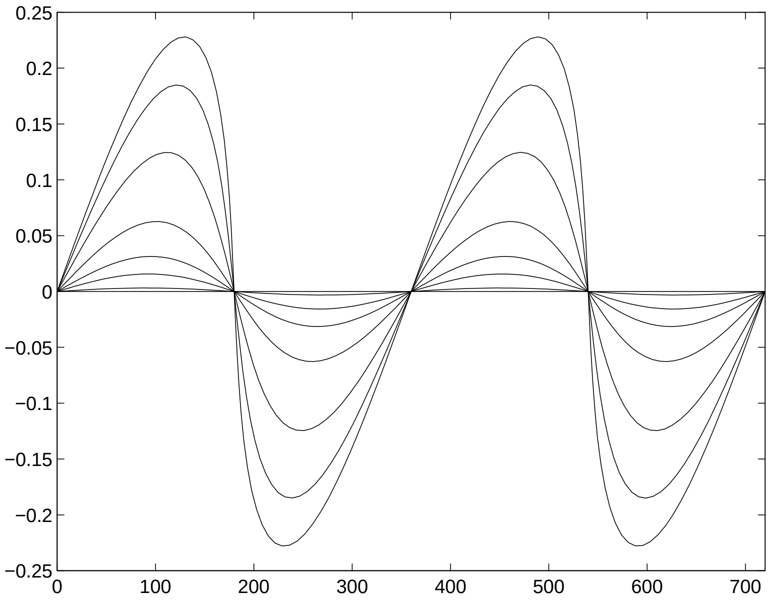

Figure B.23: Twist Angle vs m_3 for $K_3/K_1 = 1.2$, $\rho = 0.60$ (5,3)

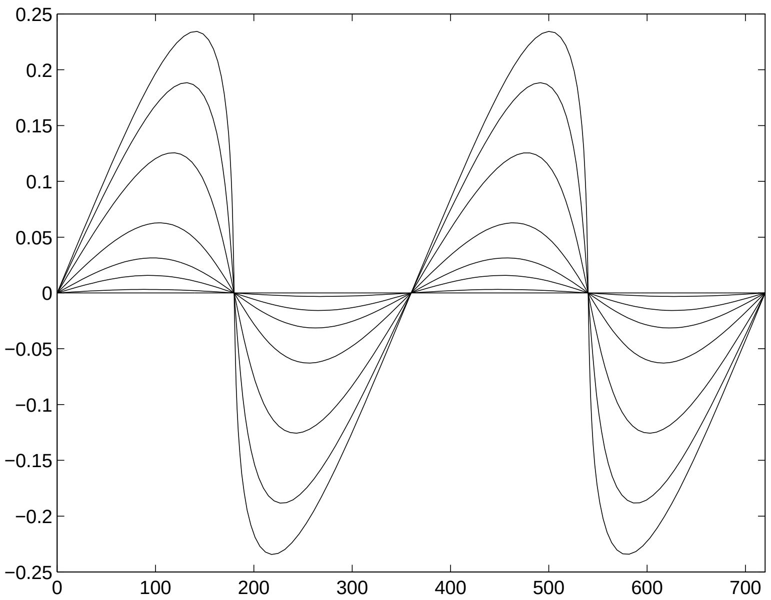

Figure B.24: Twist Angle vs m_3 for $K_3/K_1 = 1.2$, $\rho = 0.40$ (5,4)

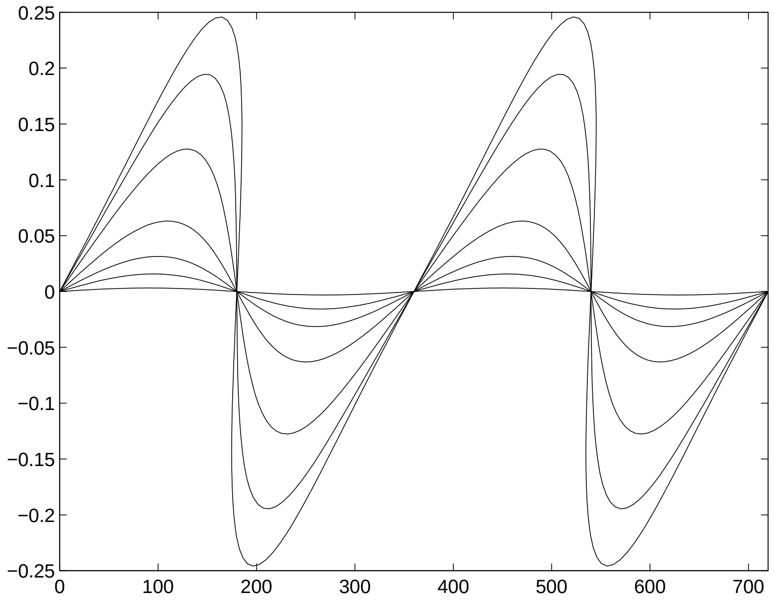

Figure B.25: Twist Angle vs m_3 for $K_3/K_1 = 1.2$, $\rho = 0.20$ (5,5)

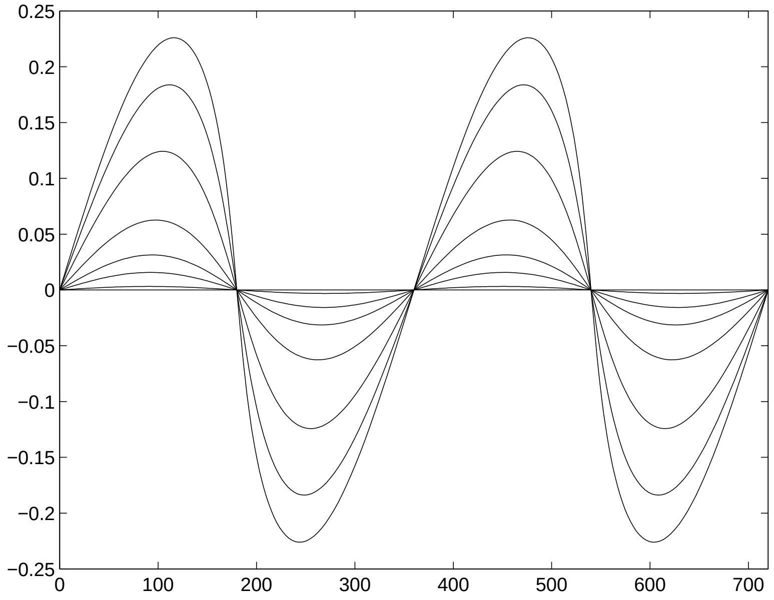

Figure B.26: Twist Angle vs m_3 for $K_3/K_1 = 1.4$, $\rho = 0.80$ (6,1)

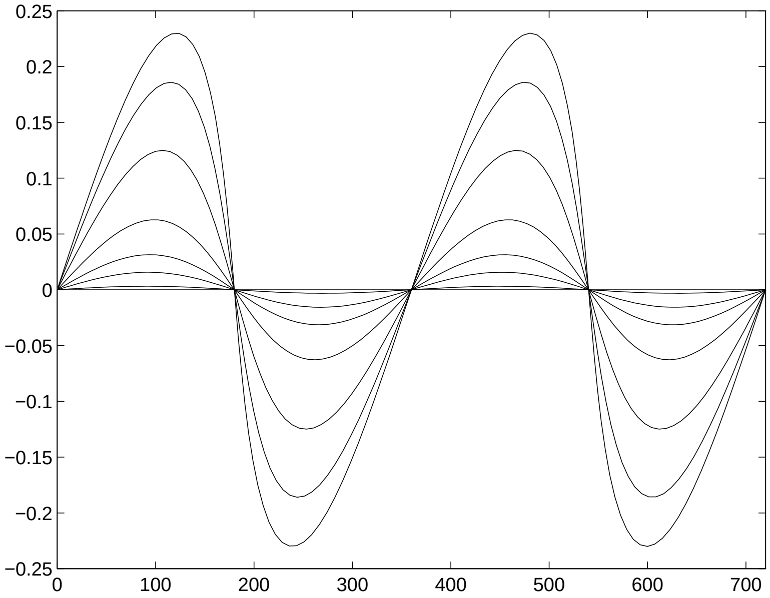

Figure B.27: Twist Angle vs m_3 for $K_3/K_1 = 1.4$, $\rho = 2/\pi$ (6,2)

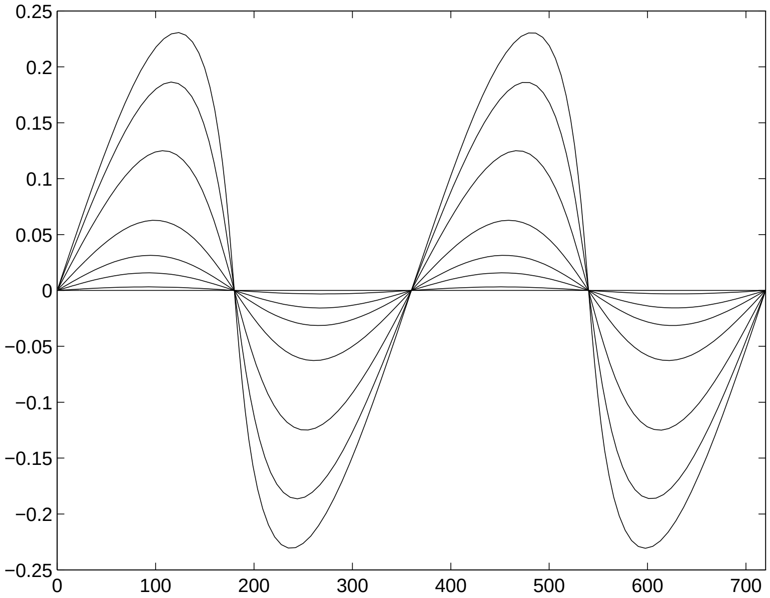

Figure B.28: Twist Angle vs m_3 for $K_3/K_1 = 1.4$, $\rho = 0.60$ (6,3)

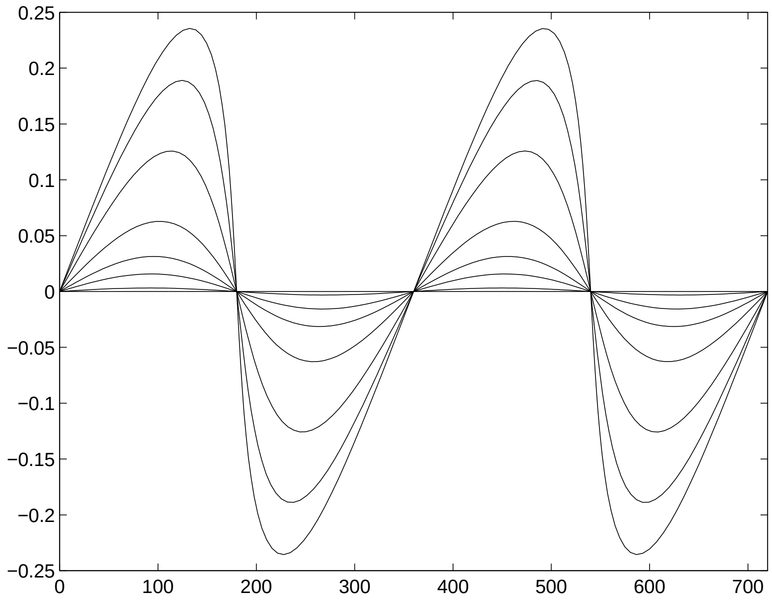

Figure B.29: Twist Angle vs m_3 for $K_3/K_1 = 1.4$, $\rho = 0.40$ (6,4)

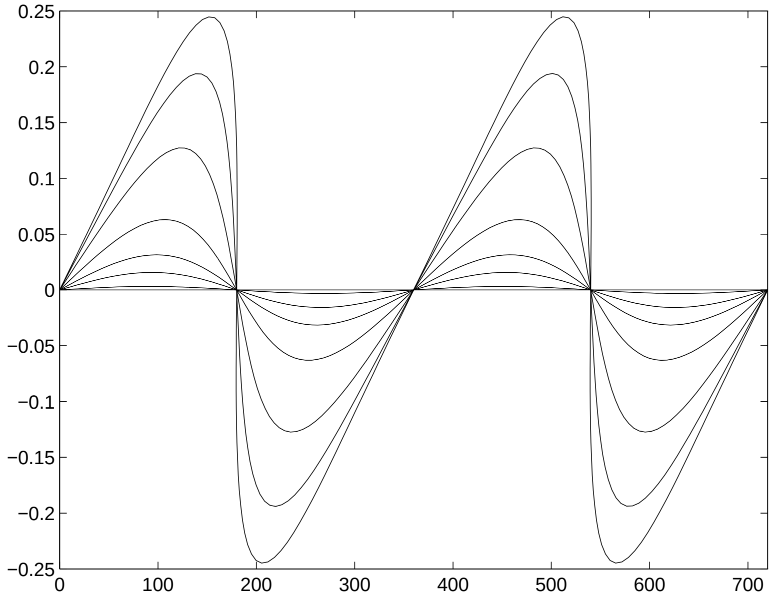

Figure B.30: Twist Angle vs m_3 for $K_3/K_1 = 1.4$, $\rho = 0.20$ (6,5)

Bibliography

[1] S.S. Antman, *Nonlinear Problems of Elasticity*, (Springer–Verlag, 1994).

[2] U. Ascher, J. Christiansen & R.D. Russell, *Collocation software for boundary value ODE's*, *ACM TOMS 7*, No. 2, 209, (1981).

[3] W.J. Beyn & E.J. Doedel, *Stability and multiplicity of solutions to discretizations of nonlinear ordinary differential equations*, *SIAM J. Sci. Stat. Compt. 2*, No. 1, (1981), pp. 107–120.

[4] R. Bulirsch, J. Stoer & P. Deuflhard, *Numerical solution of nonlinear two point boundary value problems*, *Numer. Math. Handbook Series Approx.*, (1976).

[5] D.J. Dichmann, *Hamiltonian Dynamics of an Elastica and Stability of Solitary Waves*, *Ph. D. thesis, University of Maryland*, (1994).

[6] E. Doedel, *AUTO 86 User Manual*, *Caltech, Dept. Applied Mathematics*, (1986).

[7] E.J. Doedel, H.B. Keller & J.P. Kernevez, *Numerical analysis and control of bifurcation problems (I) Bifurcation in finite dimensions*, *International Journal of Bifurcation and Chaos*, Vol. 1, No. 3, (1991), pp. 493–520.

[8] E.J. Doedel, H.B. Keller & J.P. Kernevez, *Numerical analysis and control of bifurcation problems (II) Bifurcation in infinite dimensions*, *International Journal of Bifurcation and Chaos*, Vol. 1, No. 4, (1991), pp. 745–772.

[9] G. Domokos & R. Paffenroth, Case study: Visualization for Boundary Value Problems in *IEEE Visualization '94 Conference Proceedings*, Ed. R. D. Bergeron and A. E. Kaufman (IEEE Computer Society Press, 1994) pp. 345–348

[10] J. Douglas Jr. & T. Dupont, *Collocation methods for parabolic equations in a single space variable*, *Lecture Notes in Mathematics*, 385, (Springer–Verlag, 1974).

[11] H. Goldstein, *Classical Mechanics*, Second Edition, (Addison–Wesley, 1981).

[12] T. R. Kane, P. W. Likins & D. A. Levinson, *Spacecraft Dynamics*, (McGraw–Hill, 1983).

[13] Li, Y. & J.H. Maddocks. On the Computation of Equilibria of Elastic Rods, PART I: Integrals, Symmetry, and a Hamiltonian Formulation. In preparation.

[14] A.E.H. Love, *A Treatise on the Mathematical Theory of Elasticity*, (Dover, 1944).

[15] P.M. Prenter, *Splines and Variational Methods*, (John Wiley & Sons, 1975).

[16] R. Weiss, *The application of implicit Runge–Kutta and collocation methods to boundary problems*, *Math. Comp.*, **28**, (1974), pp. 449–464.